



# ESA Climate Change Initiative (CCI+) Essential Climate Variable (ECV)

## Greenland\_Ice\_Sheet\_cci+ (GIS\_cci+)

### Product Validation and Intercomparison Report (PVIR)


Prime & Science Lead: René Forsberg  
DTU Space, Copenhagen, Denmark  
[rf@space.dtu.dk](mailto:rf@space.dtu.dk)

Technical Officer: Marcus Engdahl  
ESA ESRIN, Frascati, Italy  
[Marcus.Engdahl@esa.int](mailto:Marcus.Engdahl@esa.int)

Consortium:  
Asiaq Greenland Survey (ASIAQ)  
DTU-Space, Department of Geodynamics (DTU-S)  
DTU-Space, Department of Microwaves and Remote Sensing (DTU-N)  
Danish Meteorological Institute (DMI)  
ENVIRONMENTAL EARTH OBSERVATION IT GmbH (ENVEO)  
Science [&] Technology AS (S&T)  
Technische Universität Dresden (TUDr)  
The Geological Survey of Denmark and Greenland (GEUS)  
The Niels Bohr Institute (NBI)  
University of Leeds, School of Earth and Environment (UL)



## Signatures page

Prepared by	Anne Solgaard		Date: 2022.05.05
Issued by	Daniele Fantin, Project Manager, S&T		Date: 2022.05.05
Checked by	Rene' Forsberg Science Leader, DTU-S		Date: 2022.05.05
Approved by	Marcus Engdahl ESA Technical Officer		Date:

## Table of Contents

<b>1</b>	<b>Change Log .....</b>	<b>5</b>
<b>2</b>	<b>Acronyms and Abbreviations .....</b>	<b>6</b>
<b>3</b>	<b>Introduction.....</b>	<b>8</b>
1.1	Purpose and Scope .....	8
1.2	Document Structure .....	8
1.3	Applicable and Reference Documents.....	8
<b>4</b>	<b>Surface elevation change (SEC) .....</b>	<b>10</b>
4.1	2.1 Sources and selection of independent validation data .....	10
4.1.1	2.1.1 Validation data errors and biases .....	10
2.2	Validation procedure .....	11
2.3	Validation procedure outcome .....	12
2.4	Recommendations for products improvement.....	12
<b>3</b>	<b>Ice Velocity (IV).....</b>	<b>13</b>
3.1	Radar IV .....	13
3.1.1	Offset Tracking Product .....	13
3.1.1.1	Sources and selection of independent validation data .....	13
3.1.1.2	Validation procedure .....	15
3.1.1.3	Validation procedure outcome .....	15
3.1.1.4	Recommendations for products improvement .....	19
3.1.1.5	Acknowledgments of data contributors for IV validation .....	20
3.1.2	InSAR Product .....	20
3.2	Optical IV .....	23
3.2.1	Sources and selection of independent validation data.....	23
3.2.2	Validation procedure.....	23
3.2.3	Validation procedure Outcome .....	23
3.2.4	Recommendations for products improvement .....	26
3.2.5	Optical IV – SAR IV product intercomparison – version 2.....	26
<b>4</b>	<b>Gravimetry Mass Balance (GMB) .....</b>	<b>30</b>
4.1	(Inter-) comparison procedure .....	30
4.2	(Inter-) comparison procedure outcome.....	30
4.3	Recommendations for products improvement.....	33
<b>5</b>	<b>Mass Flow Rate and Ice Discharge (MFID) .....</b>	<b>35</b>
5.1	Sources and selection of independent validation data .....	35
5.2	Validation procedure .....	35
5.3	Validation procedure outcome .....	35
5.4	Recommendations for products improvement.....	35
<b>6</b>	<b>Supraglacial Lakes .....</b>	<b>45</b>
6.1	Sources and selection of independent validation data .....	45
6.2	Validation procedure .....	46
6.3	Validation procedure outcome .....	46
6.4	Recommendations for products improvement.....	47
<b>7</b>	<b>Calving Front Location (CFL).....</b>	<b>48</b>



7.1	Sources and selection of independent validation data .....	48
7.2	Validation procedure .....	49
7.3	Validation procedure outcome .....	50
7.3.1	Hagen Brae .....	51
7.3.2	Humboldt Gletsjer .....	52
7.3.3	Jakobshavn Isbrae .....	53
7.3.4	Upernavik A.....	54
7.3.5	Upernavik E.....	55
7.3.6	Upernavik F.....	56
7.3.7	Zachariae Isstroem .....	57
7.3.8	Overview and summary .....	58
7.4	Recommendations for products improvement.....	59
<b>8</b>	<b>References.....</b>	<b>60</b>



# 1 Change Log

Issue	Author	Affected Section	Change	Status
0.5	S&T	All	Document Creation	
1.0	GEUS + All	All	Input on ECV validation and intercomparison	
2.0	GEUS + All	All	Version 2 Update	
3.0	ENVEO	Chapter 7	Validation CFL	

## 2 Acronyms and Abbreviations

Acronyms	Explanation
<b>ATBD</b>	Algorithm Theoretical Basis Document
<b>C3S</b>	Copernicus Climate Change Service
<b>CCI</b>	Climate Change Initiative
<b>CFL</b>	Calving Front Location
<b>CS2</b>	CryoSat-2
<b>CSR</b>	Center for Space Research, University of Austin
<b>DEM</b>	Digital Elevation Model
<b>DInSAR</b>	Differential Interferometric Synthetic Aperture Radar
<b>DMI</b>	Danish Meteorological Institute
<b>DTU-N</b>	DTU Microwaves and Remote Sensing Group
<b>DTU-S</b>	DTU Geodynamics Group
<b>E3UB</b>	End-to-End ECV Uncertainty Budget
<b>ECV</b>	Essential Climate Variable
<b>ENU</b>	East North Up
<b>ENVEO</b>	ENVironmental Earth Observation GmbH
<b>EO</b>	Earth Observation
<b>ESA</b>	European Space Agency
<b>GCOS</b>	Global Climate Observation System
<b>GCP</b>	Ground Control Point
<b>GEUS</b>	Geological Survey of Denmark and Greenland
<b>GFZ</b>	Deutsche GeoForschungsZentrum
<b>GIA</b>	Glacial Isostatic Adjustment
<b>GIS</b>	Greenland Ice Sheet
<b>GLL</b>	Grounding Line Location
<b>GMB</b>	Gravimetry Mass Balance
<b>GRACE(-FO)</b>	The Gravity Recovery and Climate Experiment (Follow On)
<b>IMBIE</b>	Ice Sheet Mass Balance Inter-Comparison Exercise
<b>InSAR</b>	Interferometric Synthetic Aperture Radar
<b>IPP</b>	Interferometric Post-Processing
<b>IV</b>	Ice Velocity
<b>JPL</b>	NASA Jet Propulsion Laboratory
<b>MAI</b>	Multiple Aperture Interferometry
<b>MEaSURES</b>	Making Earth System Data Records for Use in Research Environments (NASA)
<b>MFID</b>	Mass Flow Rate and Ice Discharge
<b>NBI</b>	Niels Bohr Institute, University of Copenhagen
<b>NEGIS</b>	North East Greenland Ice Stream
<b>PROMICE</b>	Danish Program for Monitoring of the Greenland Ice Sheet
<b>RA</b>	Radar Altimetry



<b>RMS</b>	Root Mean Square
<b>S&amp;T</b>	Science and Technology AS
<b>S2</b>	Sentinel-2
<b>SAR</b>	Synthetic Aperture Radar
<b>SEC</b>	Surface Elevation Change
<b>SLR</b>	Satellite Laser Ranging
<b>SMB</b>	Surface Mass Balance
<b>SOW</b>	Statement of Work
<b>TEC</b>	Total Electron Content
<b>TOA</b>	Top of Atmosphere
<b>TPROP</b>	Technical Proposal
<b>TUDr</b>	Technische Universität Dresden
<b>UL</b>	University of Leeds
<b>URD</b>	User Requirement Document

### 3 Introduction

#### 1.1 Purpose and Scope

This document contains the Product Validation and Inter-comparison Report (PVIR) version 2 for the Greenland\_Ice\_Sheet\_cci+ (GIS\_cci+) project for CCI+ Phase 2, in accordance with contract and SoW [AD1 and AD2].

This document describes the results of the validation and intercomparison activities described in the Product Validation Plan for the Greenland\_Ice\_Sheet\_cci (GIS\_cci) project for CCI+ Phase 1 [RD1] for the four types of data products:

- Surface elevation Change;
- Ice Velocity;
- Gravimetry Mass Balance;
- Mass Flow Rate and Ice Discharge;

As well as the research objects:

- Supraglacial Lakes
- Calving Front Locations

The ice velocity product based on InSAR as well as the Calving Front Location product have been added in this version of the document. The results of the validation and inter-comparison activities provide input for reviewing the product specifications and algorithms.

#### 1.2 Document Structure

This document is structured as follows:

Chapter 1 contains an introduction to the document.

Chapter 2 – 7: A chapter for each ECV and the research objects. The IV chapter is split into radar IV including both offset tracking and InSAR based products, and optical IV. Each chapter contains section describing the validation data sets, validation procedure and outcome and recommendations for product improvement.

Chapter 8 contains a reference list.

#### 1.3 Applicable and Reference Documents

**Table 1-1: List of Applicable Documents**

No	Doc. Id	Doc. Title	Date	Issue/ Revision/ Version
AD1	ESA/Contract No. 4000126023/19/I-NB, and its Appendix 1	CCI+ PHASE 1 - NEW R&D ON CCI ECVS, for Greenland_Ice Sheet_cci	2019.04.01	
AD2	ESA-CCI-EOPS-PRGM-SOW-18-0118 Appendix 2 to contract.	Climate Change Initiative Extension (CCI+) Phase 1, New R&D on CCI ECVs Statement of Work	2018.05.31	Issue 1 Revision 6
AD3	ST-DTU-ESA-GISCCI-PVP-001	Product Validation Plan for the Ice_Sheets_cci project of ESA's Climate Change Initiative	2012.08.21	
AD4	ST-DTU-ESA-GISCCI-PVIR-001	Greenland_Ice_Sheet_cci Product Validation and Intercomparison Report	2018.07.25	
AD5	ST-DTU-ESA-GISCCI-PSD-001	_Product Specification Document for the Ice_Sheets_cci project of ESA's Climate Change Initiative	2016.06.20	Version 2.2





**Table 1-2: List of Reference Documents**

No	Doc. Id	Doc. Title	Date	Issue/ Revision/ Version
RD1	ST-DTU-ESA-GISCCI+-PVP-001	Greenland_Ice_Sheet_cci+ Product Validation Plan	2019.07.02	
RD2	ST-DTU-ESA-GISCCI+-ATBD-001	Greenland_Ice_Sheet_cci+ Algorithm Theoretical Basis Document (ATBD) for CCI+ Phase 1	2020.02.02	

**Note:** If not provided, the reference applies to the latest released Issue/Revision/Version

## 4 Surface elevation change (SEC)

The validation strategies are described in section 6.1 of the “Product Validation Plan for the Ice\_Sheets\_cci project of ESA’s Climate Change Initiative” [AD3], however the described round robin will be omitted. Hence, the main validation efforts will focus on:

- Comparison of temporally consistent airborne elevation changes with satellite altimeter elevation changes.
- Comparison of elevation changes derived from different sensors (e.g. radar vs. laser).

The SEC validation will be based upon the following metrics:

- RMSE (with respect to independent validation data)
- Temporal/spatial coverage and density of observations.

This chapter gives a complete report of the activities carried out to assess the quality of the SEC products. In section 2.1 the sources of independent validation data considered for the SEC product validation, can be found, section 2.2 describes the validation procedure undertaken for the final SEC product, section 2.3 gives the results of the preformed validation, before the recommendation for future improvements are described in section 2.4.

### 4.1 2.1 Sources and selection of independent validation data

The main source of validation data for the SEC-product are elevation change derived from repeat airborne laser scanning. Due to the significantly smaller horizontal and vertical errors associated with laser data compared to radar data (Brenner et al., 2007), the SEC trends are validated against elevation change trends derived from airborne laser-scanner data after being averaged at similar grid resolution as the SEC product. Here, two different observational platforms and data products are used:

1. NASA’s Operation IceBridge (Krabill, 2014) Airborne Topographic Mapper (ATM). The ATM data are acquired seasonally in the months April to June, and on a nearly yearly basis starting in 1993. The ATM instrument is mounted on-board an aircraft, usually the NASA DC-8 or P3-B, and typically flown at an altitude of 450 m. Given a 30-degree swath width, the laser pulses illuminate an approximately 250 m wide path on the ground. Each pulse has a footprint diameter of 1 to 3 m. The elevation change trends used in the validation are generated from the IceBridge ATM L1B Elevation and Return Strength (version 2) product (Krabill, 2010), and the surface elevation change is available at the National Snow and Ice Data center as a Level-4 data product.
2. DTU airborne laser scanning (ALS) conducted as part of the Programme for Monitoring of the Greenland Ice Sheet (PROMICE) or ESA’s CryoSat Validation Experiment (CryoVEx) campaigns (Blair and Hofton, 2012; Geological Survey of Denmark and Greenland, 2015; Sørensen et al., 2018; Skourup, 2011). The DTU ALS system measures surface elevation measurements from scanning the surface in an approximately 200m wide swath, and surface elevation change have been derived from all available repeat flight paths. In contrast to the ATM dataset the ALS data also contain surface elevation change records from autumn campaigns.

An advantage of using airborne campaigns is that they most often are targeted at areas of the ice sheet which undergoes significant surface changes, both in time and space and thereby are multiple repeats available over especially the ice margin, where the largest SEC occurs and the radar altimeter observations is most challenged. Additionally, the long time series of airborne observations also ensures that we have a representative sampling over the more stable interior of the ice sheet.

#### 4.1.1 2.1.1 Validation data errors and biases

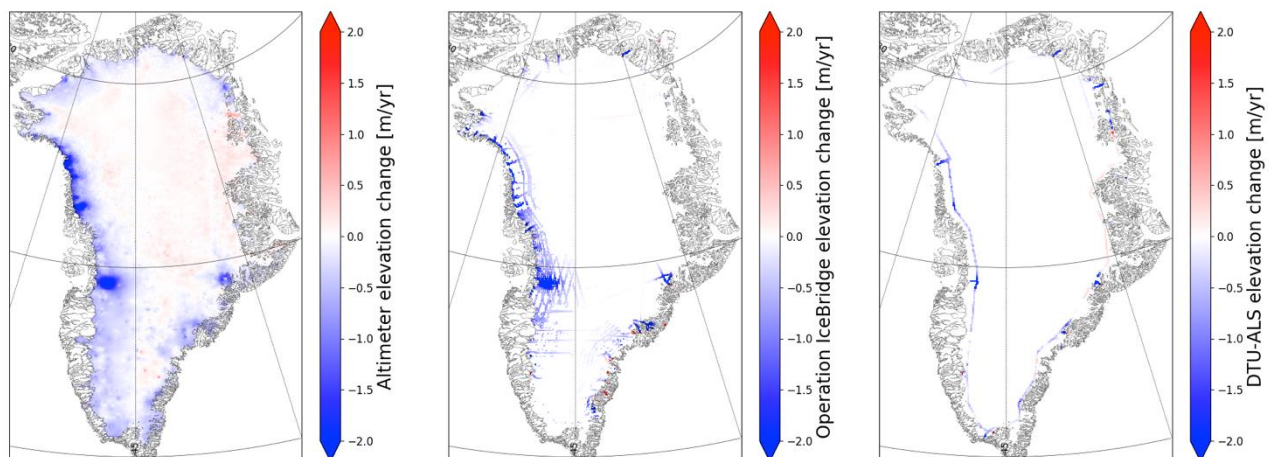
Errors in airborne laser scanning arise from several sources, such as errors in the pitch, roll, and yaw of the aircraft and instrument, as well as multi-path effects. The latter arises when the direct path of the signal is

blocked, thus increasing the travel time of the respective laser pulse and decreasing the resulting elevation estimate. The effect of the aircraft inertial navigation system pitch cancels when averaging and smoothing the observations, while the roll induces a cross-track error. Krabill et al, (2002) considered repeat ATM flights in 1993/1998 and 1994/1999 and found the effects to produce SEC errors up to 1 cm/yr. Atmospheric errors are on the same order of magnitude, and thus vertical errors are typically less than 10 cm.

The validation data uncertainty is also associated with errors from the surface roughness in the area in which the trend is derived, particularly along the ice margin where significant changes may occur within the 200 m distance used for overlapping trajectories. Furthermore, a low number of estimation points reduce the accuracy of the generated trend.

## 2.2 Validation procedure

As the validation data (ATM/ALS) and the SEC-product have different spatial resolution (250 x 250 m vs. 5 x 5 km), the first step in the validation procedure is to average the validation data at the native posting of the SEC posting. This is done by assessing the median value of observations within a given grid cell. Then this median value is subtracted from the radar SEC estimate, and the mean, median and standard deviation (STD) hereof are computed. So are the minimum and maximum differences. Most often, the median is more informative of the product performance, as both data set are subject to outliers and the coarser resolution of radar-SEC product induces larger negative biases at outlet glaciers. The radar-SEC product consists of



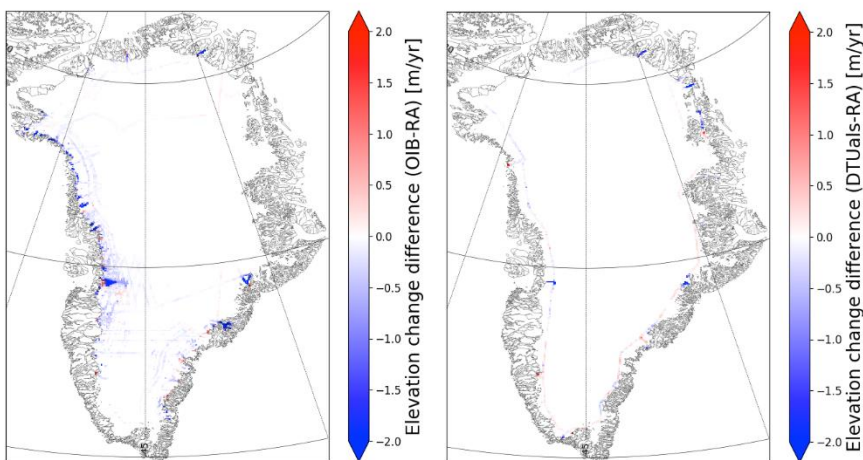
trends generated from combining all available ESA radar observation from 1992 to present and as five-year running means. The current 24 available SEC estimates are validated against the available validation data spanning the same time-windows. The region the ice sheet evaluated in each of the validation reports will differ from year to year due to differences in the flight paths from year to year of the airborne data. Figure 2-1 shows the spatial distribution of the available data from 2011 flights which approximately repeated the observations made in 2007.

## 2.3 Validation procedure outcome

The combination all available validation data (ATM/ALS) and the SEC-product produces a validation report

	Operation IceBridge	DTU ALS	unit
number of data points	4411	1427	-
Mean difference	-0.28	-0.1	m pr. year
Median difference	-0.08	0.01	m pr. year
Standard deviation	0.88	0.67	m pr. year
Max. difference	6.84	5.55	m pr. year
Min. difference	-9.59	-7.82	m pr. year

for 19 of the 24 five-year running means in the SEC product, an example of the validation reports is shown in Figure 2-2. This report is typical for the time-slices but contains more data than the average example as both 2007 and 2011 had a lot of activity in Operation IceBridge and PROMICE. As observed with the different medians between the two validation data sets, the main bias between the airborne data and the SEC-product originates at the outlet glaciers. This may be attributed to slope-induced errors in radar data (Brenner et al. 1983; Roemer et al. 2007), which relocate the measurements up-slope from nadir and cause surface depressions such as the bottom of troughs and narrow valleys to be missed. The result is a very limited number of radar measurements inside the glacier trunks. Despite this, both the mean and STD are low relative to the min and max



offsets, showing that radar data are indeed capable of resolving SEC even at the margin of the ice sheet.

## 2.4 Recommendations for products improvement

One possibility for improving the SEC accuracy could be the use of a different retracker for the radar data. A number of studies have shown that such observations need to be adjusted for all three waveform parameters, i.e. the backscatter coefficient, leading edge width, and trailing edge slope, to ensure the highest accuracy (e.g. Khvorostovsky, 2012; Legresy et al, 2005, Simonsen and Sørensen 2017). However, as shown by Simonsen and Sørensen (2017) waveform corrections still leave a bias between the laser and radar estimated SEC, suggesting that a more surface-sensitive retracker could improve the laser-radar intercomparison. Another approach could be to implement waveform deconvolution to isolate surface elevation change (Slater et al 2019). Further research is needed to derive true surface elevation change from radar altimetry, but the implementation of the shaper waveform in SAR and SARIn seems a promising technological advance in retrieving this goal (McMillan et al. 2019).

The novel swath processing of the Cryosat-2 should be implemented to enhance the resolution of the radar observations and gain more information about the spatial pattern of the elevation change happening in the high sloping areas. Work will be ongoing to estimate adaptability of the method.

Another product improvement could be to increase the temporal resolution of the SEC. Although we are currently producing multi-year-trends because this suppresses the weather signal and isolates the climate signal, there might be users that would appreciate a higher temporal resolution.

## 3 Ice Velocity (IV)

### 3.1 Radar IV

For version 1 of this document, the ice velocity (IV) product validation and intercomparison in this chapter provided an update of previous validation efforts, incorporating reprocessed velocity maps (version 1.3) derived from SAR offset tracking (OT) and new and/or updated external validation datasets (see section 3.1.1). For version 2 of the document we added a detailed validation of a new Greenland-wide ice velocity map derived from InSAR processing (see section 3.1.2). The InSAR product is a key improvement for IV, developed within GIS CCI+, providing improved accuracy, particularly in the slow-moving interior of the ice sheet, and a higher resolution.

#### 3.1.1 Offset Tracking Product

The assessment is done for the annually-averaged ice-sheet wide OT velocity maps as well as for the individual track maps (based on 6/12-day repeats) produced in the Greenland Ice Sheet CCI project and derived from Sentinel-1 (S1) SAR data. The individual track IV maps are the source data for the monthly and annually averaged maps. The quality assessment includes detailed validation with contemporaneous in-situ GPS data at various sites across the ice sheet. The products are also evaluated, on a pixel-by-pixel basis, against publicly available datasets covering the Greenland Ice Sheet. This product intercomparison provides a good level of quality assurance, in particular in areas where little change is to be expected. Additionally, we report on the performance of the algorithm in stable terrain, i.e. where no velocity is expected. This provides a good overall indication of the bias introduced in the end-to-end velocity processing chain including co-registration of images, velocity retrieval, etc.

##### 3.1.1.1 Sources and selection of independent validation data

For in-situ validation, we use GPS data acquired by field teams of the Danish Programme for Monitoring of the Greenland Ice Sheet (PROMICE; Fausto and Van As, 2019; Fausto et al, 2021) and available through the PROMICE Data Portal (<https://promice.org/PromiceDataPortal/>). The GPS instruments are attached to Automatic Weather Stations (AWS) operated by GEUS in collaboration with DTU Space and Asiaq. The version 3 data set provides hourly, daily and monthly average positions. Figure 3-1 shows the locations of the GPS sites used for validation.

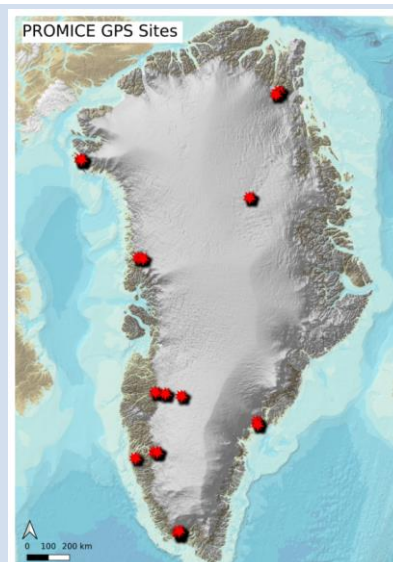


**Figure 3-1: Locations of the PROMICE AWS stations equipped with GPS and used for validation.**



For the product intercomparisons we utilize two different products created as part of the NASA 'Making Earth System Data Records for Use in Research Environments' (MEaSUREs) project: 1) annual Greenland wide IV map based on multi-mission SAR satellites; 2) IV maps covering main outlet glaciers and based on higher resolution TerraSAR-X (TSX) and TanDEM-X (TDX) data.

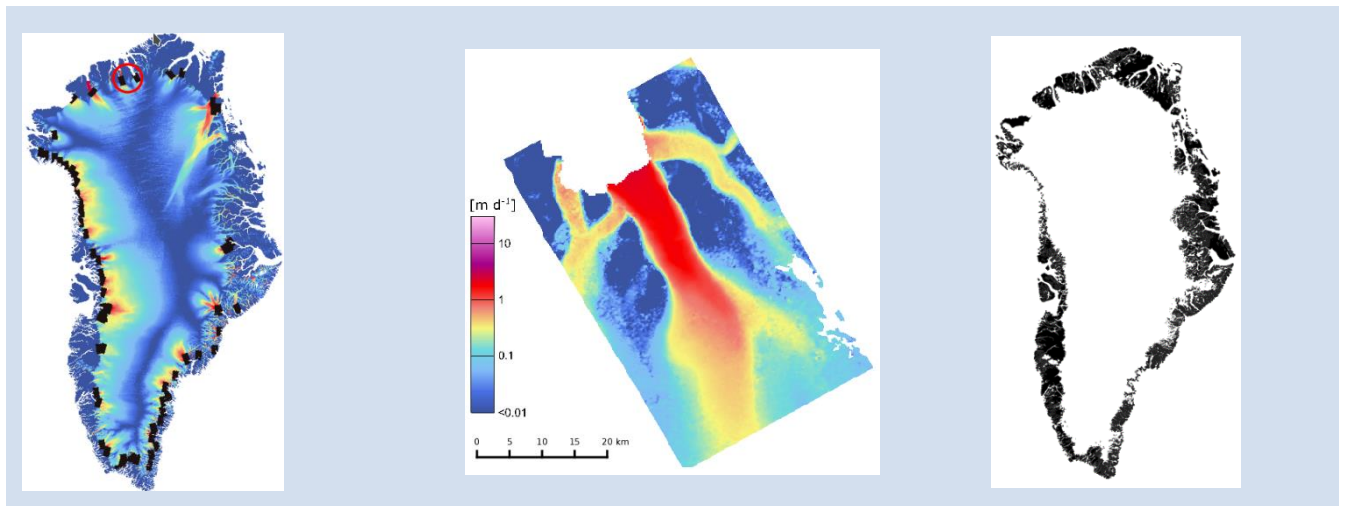


**Figure 3-2: Sentinel-1 IV mosaic showing locations of MEaSUREs TerraSAR-X/TanDEM-X derived IV maps used for product inter-comparison in black (left). The IV data sets cover the margins of Greenland and include most of the major outlet glaciers. The red circle indicates the location of C.H. Ostenfeld Glacier shown as example (middle). Right: shapefile showing ice-free terrain in Greenland and used for the stable terrain test (Rastner et al., 2012, updated 2018).**

The MEaSUREs annual Greenland-wide data set covers selected years since 2000 up to 2018 and is provided at 200 m and 500 m. The IV maps are based on multiple SAR satellites including: ALOS, RADARSAT-1, SENTINEL-1A and -1B, TDX and TSX. From 2014 onwards the maps are mostly based on Sentinel-1 data, supplemented with TSX and TDX data for coastal outlets. The annual maps run from September to May largely overlapping with the CCI products which run from October to September. We use version 2 of the data set, available through the NSIDC data portal (data set ID: NSIDC-0478, Joughin et al., 2015, updated 2018).

The MEaSUREs TSX/TDX-based data set consists of a collection of IV maps covering most of the major outlet glaciers from January 2009 to December 2019 (Figure 3-2, left and middle). The ice velocity is retrieved from repeat pass images (1 to 3 cycles with 11-day repeats) applying a combination of conventional InSAR and speckle tracking techniques (Joughin, 2002). Here we use release V3.0 of the data set, available through the NSIDC data portal (data set ID: NSIDC-0481, Joughin et al., 2020). Data files are delivered in GeoTIFF format at 100m grid spacing in North Polar Stereographic projection (EPSG: 3413). Separate files are provided for the x and y velocity components (in m/yr) along with corresponding (pseudo-)error estimates for both velocity components.

For the analysis of stable terrain, the moving ice is masked out using a polygon shapefile of the ice sheet and peripheral glacier outlines produced by Rastner et al (2012, updated 2018). The outlines are derived semi-automatically from Landsat-5 and Landsat-7, using a band ratio approach (red/SWIR) with scene specific thresholds and manual correction of debris cover, seasonal snow, shadow, water (outside of glaciers), sea ice and icebergs. By inverting the ice sheet/glacier shapefile and combining with an ocean mask a land mask file is created as depicted in Figure 3-2 (right).

### 3.1.1.2 Validation procedure

We use four different validation/intercomparison procedures, e.g. for GPS, product intercomparison and stable terrain analysis:

1. GPS: We use the monthly average positions provided in version 3 of the PROMICE AWS data set to calculate the local monthly averaged velocity magnitude, which is assigned to the station position. The monthly values are used to calculate yearly averages for Oct-Sept corresponding to the respective ice velocity map. For each monthly position, the corresponding pixel value in the Sentinel-1 IV map is selected and finally also averaged over a year. In this way there is one corresponding value for each station representing the annual mean IV. These are used to calculate the validation statistics and to create the scatter plots.
2. MEaSURES Greenland Ice Sheet Velocity Map: As a pre-processing step, the 200m IV maps are converted to m/d, resampled to a 250 m grid spacing and the separate V<sub>x</sub> and V<sub>y</sub> velocity files are merged into a 2-bands GeoTIFF to match the native Sentinel-1 IV maps geometry and format. The intercomparison is done on both the x and y velocity components separately on a pixel-by-pixel basis (ignoring the vertical component of velocity).
3. MEaSURES TSX/TDX-based IV maps: Pre-processing is similar as described above. As glacier velocity can fluctuate significantly over short time periods, in particular on the downstream section of large outlet glaciers, we only compare datasets derived from single Sentinel-1 SAR repeat pass pairs (6/12-days) and with a maximum time difference of 2 days between the respective start dates (master). We inter compare both x and y velocity components separately on a pixel-by-pixel basis.
4. Stable terrain analysis: The results for the ice covered (moving) area are separated from ice-free (stable) ground. The masking is done using a polygon of the rock outlines.

As a measure of quality, we provide, statistics on the mean and the root mean square error (RMSE) of the residuals (defined here as Sentinel-1 IV minus GPS/MEaSURES IV).

### 3.1.1.3 Validation procedure outcome

Figure 3-3 shows the results of the intercomparison of the annual Sentinel-1 Greenland Ice Sheet velocity with in-situ GPS measurements for 2014/15, 2015/16 and 2016/17 (v1.3). The figures show an excellent agreement between the GPS and Sentinel-1 surface velocity. For 2014/15 a total number of 15 stations could be used, with a mean difference <1 cm/d and an RMSE of 4.5 cm/d. In 2015/16 22 stations could be used showing a mean difference of 1.2 cm/d and an RMSE of 2 cm/d. In 2016/17 also 22 stations could be used with a mean difference of 1.1 cm/d and an RMSE of 3 cm/d. The observed differences can partly be attributed to uncertainties inherent to both methods including differences in spatial sampling: the GPS measures a point location, while the feature tracking procedure averages an area of which the size is based on the window size used for image correlation.

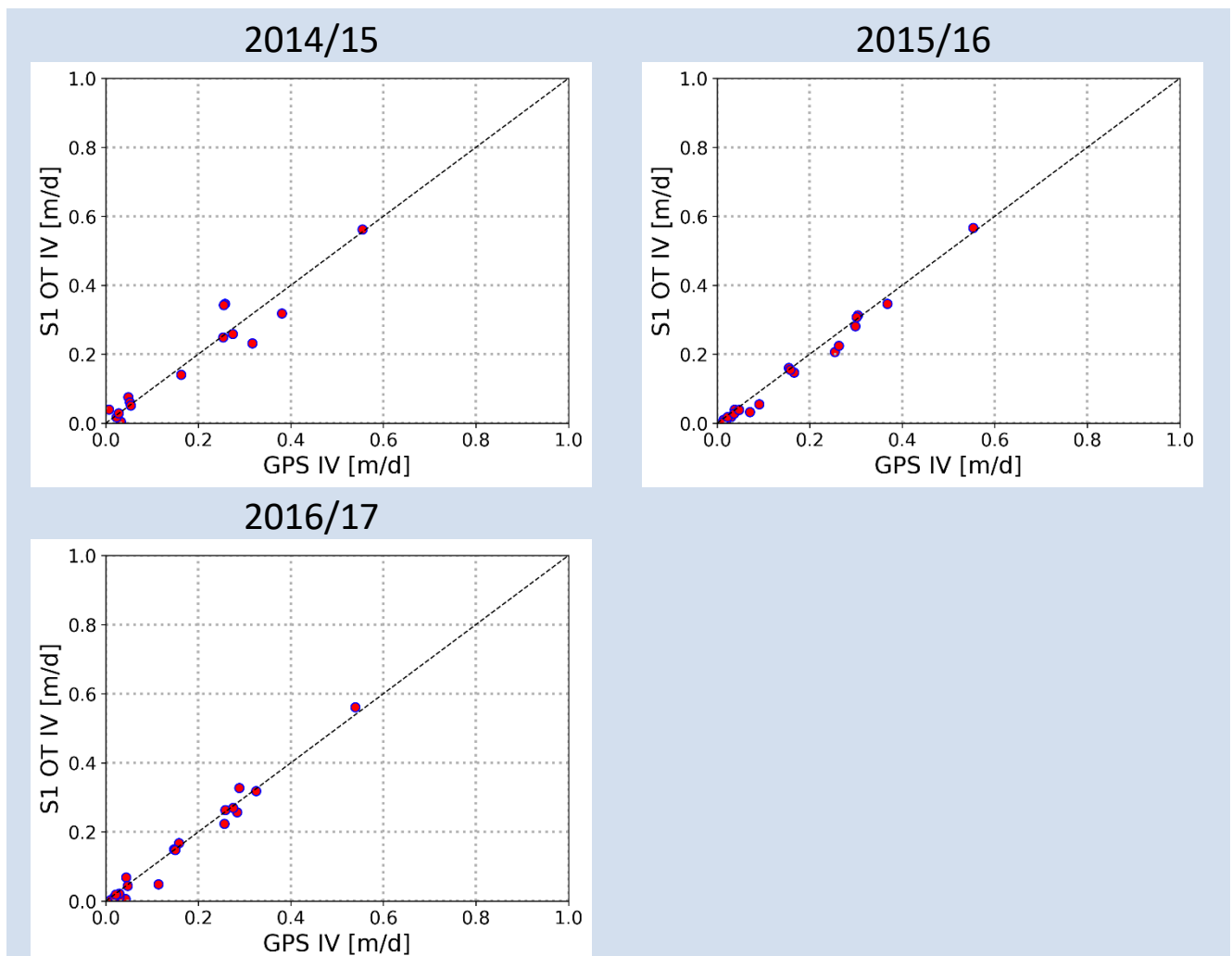


**Figure 3-3: Scatter plots of GPS and Sentinel-1 ice velocity for 2014/15, 2015/16 and 2016/17.**

Excluding the TSX/TDX derived IV maps that do not fall within the desired temporal range (max time difference 2 days in comparison to S1 IV maps) leaves a total number of 123, 230 and 376 suitable TSX/TDX IV maps for product intercomparison for respectively 2014/15, 2015/16 and 2016/17. For each TSX/TDX derived IV map multiple intercomparisons are possible as an area can be overlapped by different S1 tracks over the 2-day time range. In total 168 (2014/15), 312 (2015/16) and 1231 (2016/17) Sentinel-1 maps fulfil the 2-day criterium and also have an overlap. For these maps, the residuals and their statistics are calculated (Figure 3-4). The overall mean bias between the data sets is well below 1 cm/d with an RMSE in the range of 15-20 cm/d for both x and y velocity components.



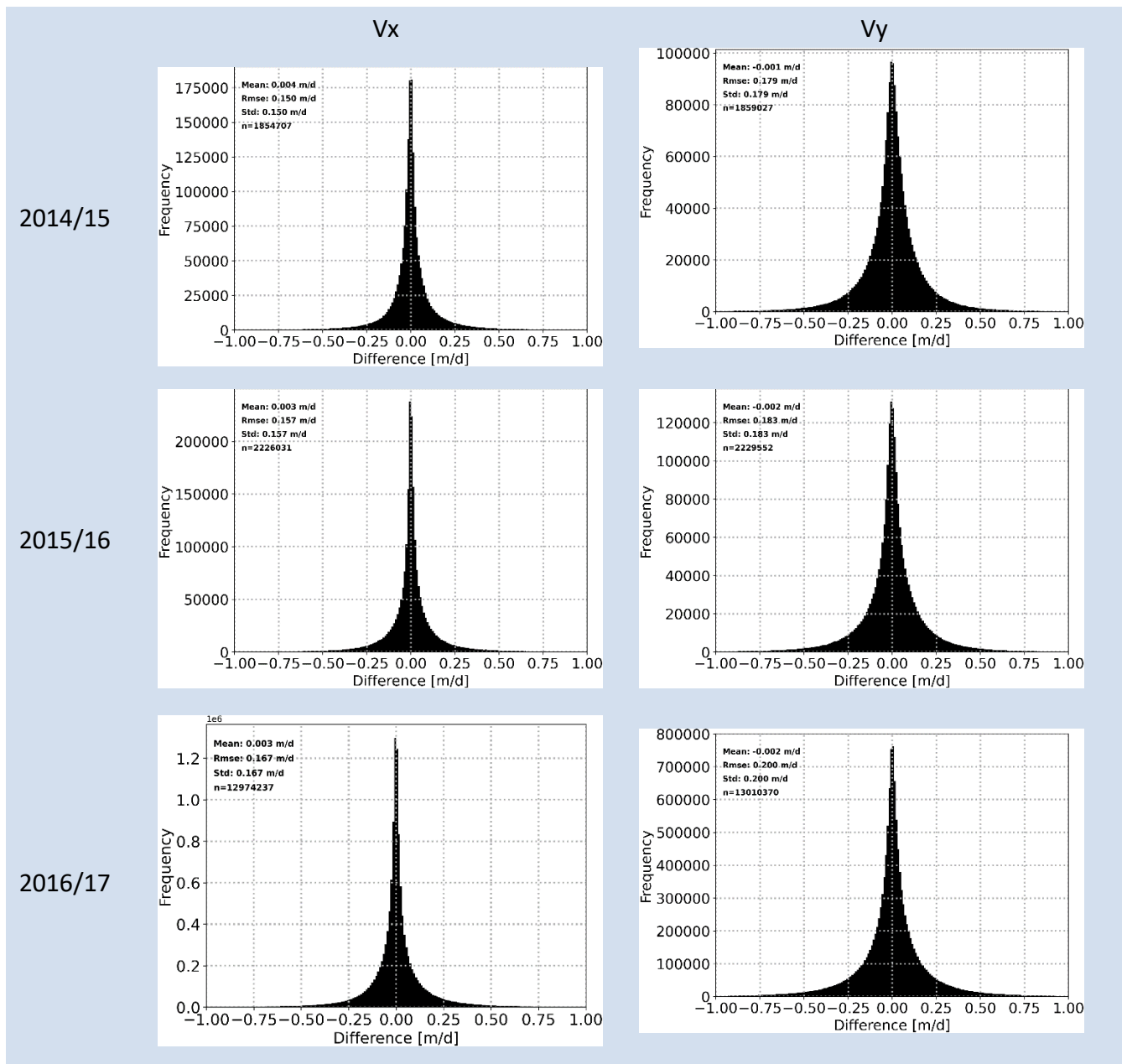


**Figure 3-4: Histograms of Vx (left) and Vy (right) residuals of the intercomparison with MEaSURES TerraSAR-X derived IV maps (selected outlet glaciers) acquired within 2 days of Sentinel-1 derived single track IV maps in 2014/15 (top), 2015/16 (middle), 2016/17 (bottom).**

Figure 3-5 shows the intercomparison results of the GIS CCI annual ice sheet wide IV maps of 2014/15, 2015/16 and 2016/17 with the MEaSURES IV maps for the same years. Based on a sample size of >30 million pixels for each map comparison, the overall mean bias between the two data sets is less than 2 mm/d with an RMSE in the range of 3 to 6 cm/d for both x and y velocity components.

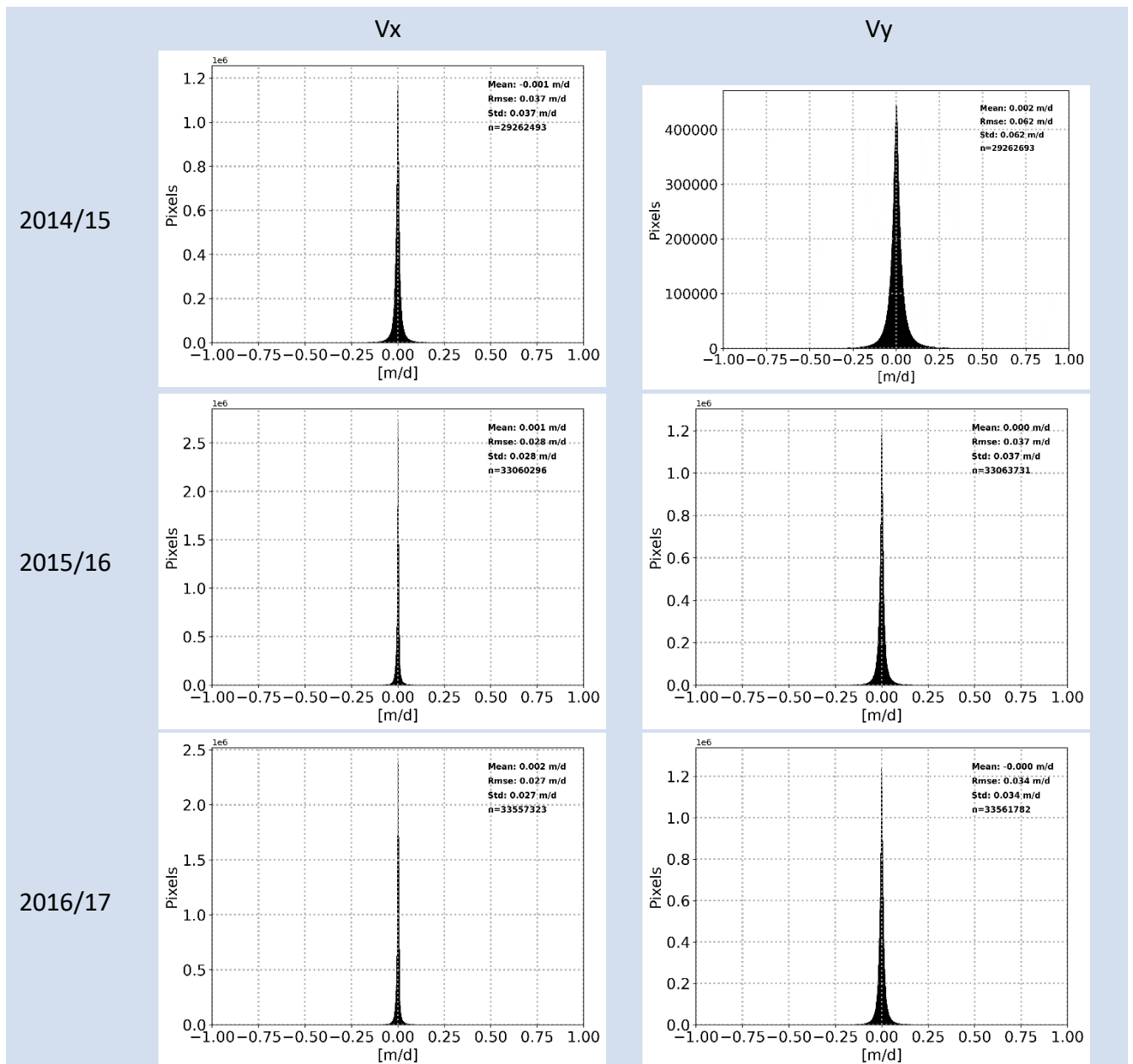


**Figure 3-5: Histograms of Vx (left) and Vy (right) residuals of the intercomparison between the CCI Greenland Ice Sheet velocity maps (v1.3) and MEaSURES in 2014/15 (top), 2015/16 (middle), 2016/17 (bottom).**

Differences between the products have a variety of causes, among others the different native resolution of the SAR data (e.g. TSX vs. Sentinel-1), different temporal range, different processing settings used for IV retrieval (e.g. matching window, correlation threshold), differences in post processing (e.g. outlier removal, gap filling), different land/ocean and lay-over masks or short term velocity fluctuations. In general, higher resolution satellite data better captures the ice velocity, in particular in shear zones, where the velocity gradient can be high. The drawback often being that much smaller regions are covered.

Figure 3-6 shows the results of the stable terrain test as scatterplots of easting versus northing velocity for all maps, including the 2019/20 winter mapping campaign (CCI v1.3). Based on more than 1.2 million pixels

the outcome of the stable ground test indicates for all products a mean of <1 cm/d and an RMSE < 2 cm/d for both easting and northing velocity components.

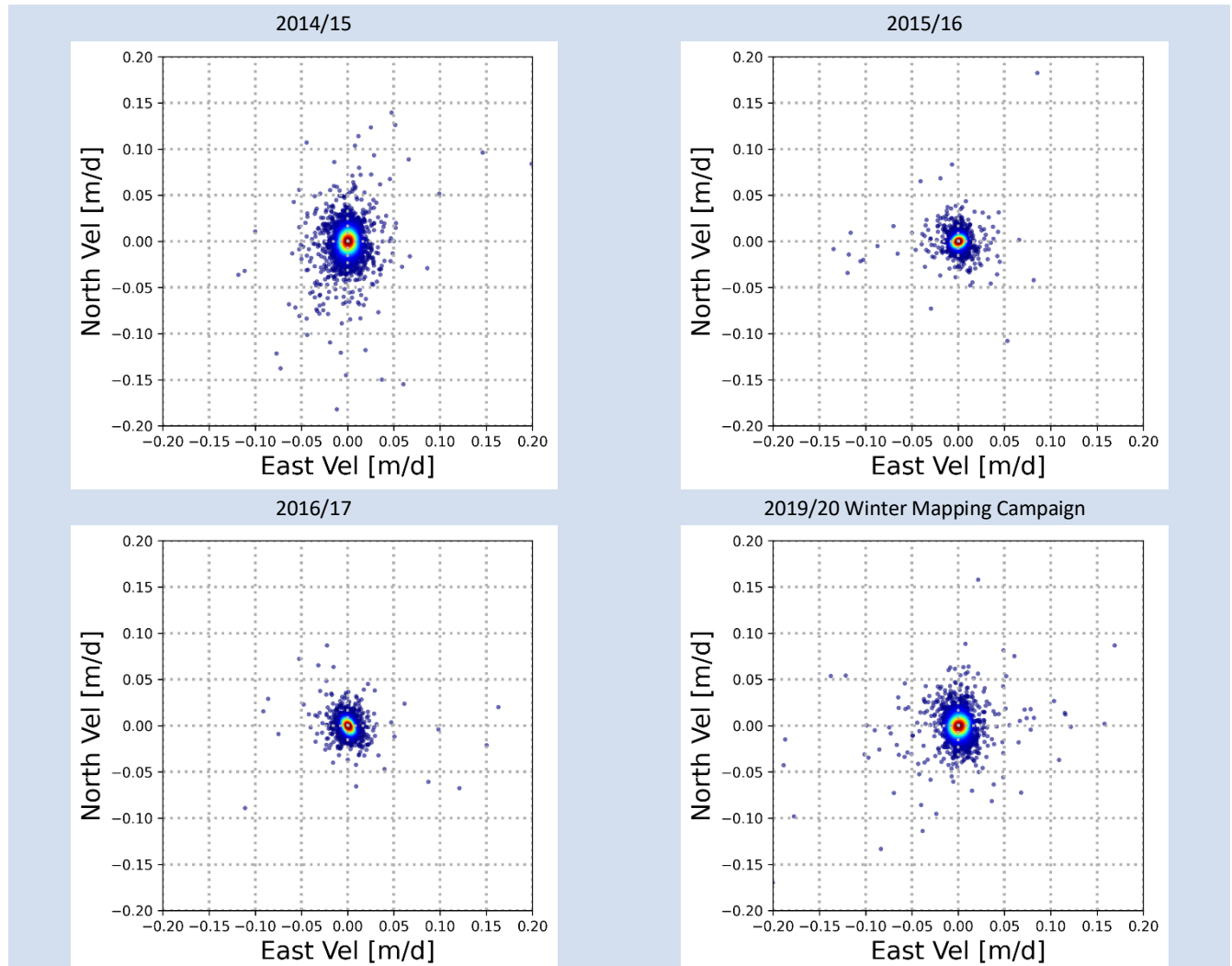


**Figure 3-6: Results of the stable rock test for the different CCI+ velocity products. The scatter plots show easting velocity versus northing velocity with colour coding blue to red indicating point density from low to high.**

#### 3.1.1.4 Recommendations for products improvement

Table 3.3 provides a statistical overview of all validation and intercomparison results. The current IV products perform very well. The accuracy requirements for IV as described in the User Requirements Document (URD) of the Ice Sheets CCI project (Hvidberg, et al, 2012), identified through an extensive user survey within the glaciology community, lists a minimum accuracy of 30-100 m/y (0.08-0.27 m/d) with an optimum accuracy of 10-30 m/y (0.03-0.08 m/d). The results of our quality assessments fall well within this range. A key product improvement for IV is the InSAR processing developed within the CCI+ project and which is included in version 2 of the document (see section 3.1.2). The InSAR product significantly improves the accuracy of the ice velocity, in particular in slower moving terrain.

**Table 3-1: Summary of intercomparison results (values in m/d).**

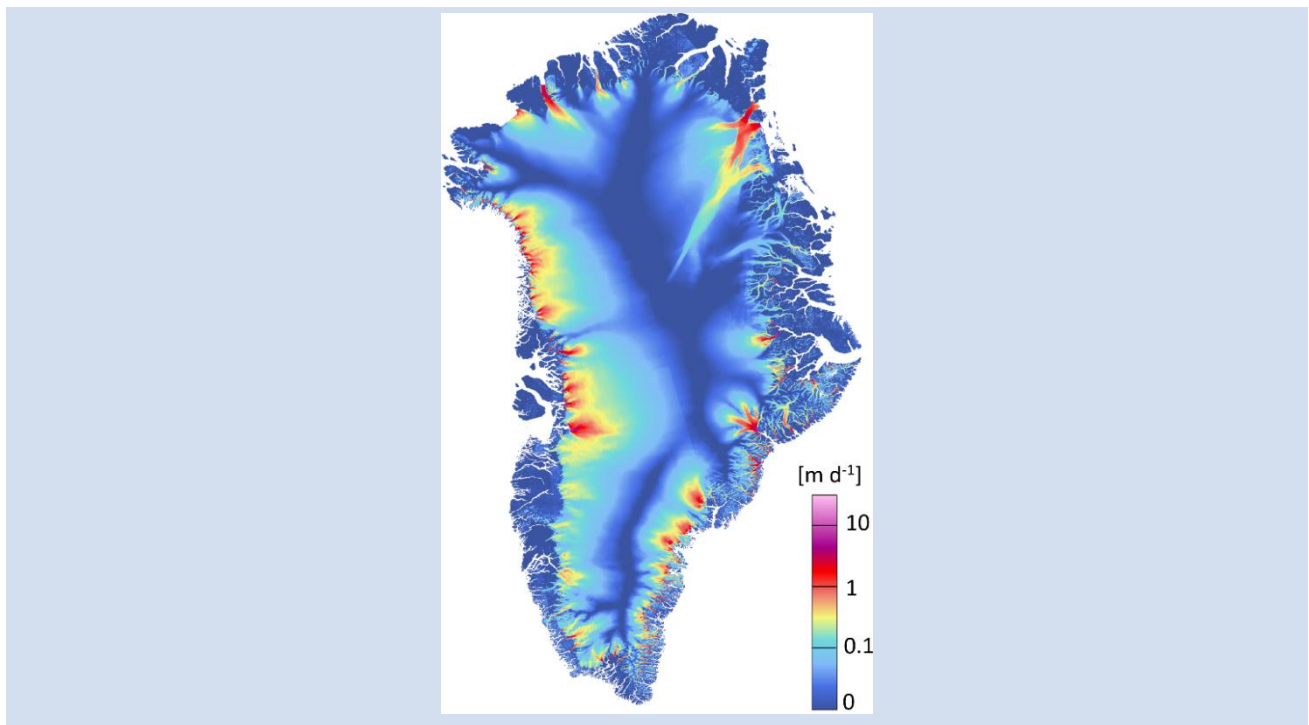
Product	Reference/Test	Pixels	$d_{Mag}$	$RMSE_{Mag}$	$d_E$	$RMSE_E$	$d_N$	$RMSE_N$
2014/15	GPS	15	0.00	0.05	-	-	-	-
	MEaSURES TSX/TDX	1.8 M	-	-	0.00	0.15	0.00	0.18
	MEaSURES S1 (ice sheet)	29 M	-	-	0.00	0.04	0.00	0.06
	Stable Terrain	5 M	-	-	0.00	0.01	0.00	0.02
2015/16	GPS	22	0.01	0.02	-	-	-	-
	MEaSURES TSX/TDX	2.2 M	-	-	0.00	0.16	0.00	0.18
	MEaSURES S1 (ice sheet)	33 M	-	-	0.00	0.03	0.00	0.04
	Stable Terrain	5 M	-	-	0.00	0.01	0.00	0.01
2016/17	GPS	22	0.01	0.03	-	-	-	-
	MEaSURES TSX/TDX	13 M	-	-	0.00	0.17	0.00	0.20
	MEaSURES S1 (ice sheet)	34 M	-	-	0.00	0.03	0.00	0.03
	Stable Terrain	5 M	-	-	0.00	0.01	0.00	0.01
2019/20 winter mapping campaign	Stable Terrain	5 M	-	-	0.00	0.02	0.00	0.01

### 3.1.1.5 Acknowledgments of data contributors for IV validation

Data from the Programme for Monitoring of the Greenland Ice Sheet (PROMICE) and the Greenland Analogue Project (GAP) were provided by the Geological Survey of Denmark and Greenland (GEUS) at <http://www.promice.dk>. Data from the NASA Making Earth System Data Records for Use in Research Environments (MEaSURES) Program were provided by the National Snow and Ice Data Center (NSIDC) at <https://nsidc.org/data/measures>.

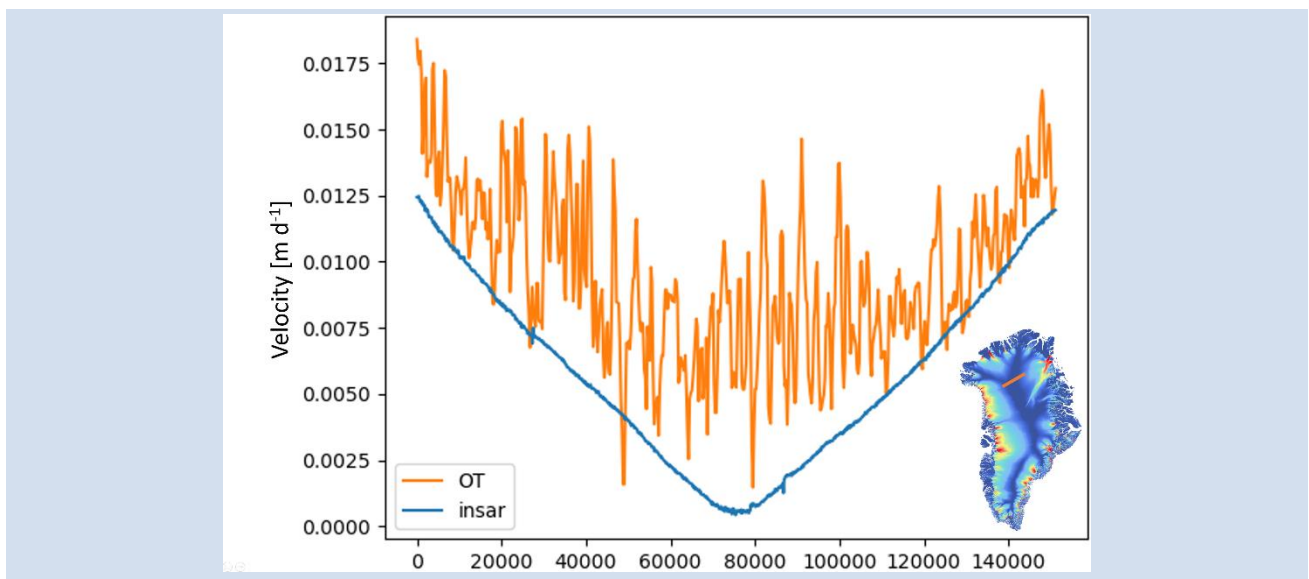
### 3.1.2 InSAR Product

Figure 3-7 shows the Greenland Ice Sheet wide InSAR velocity (magnitude) map. The data product is generated from Sentinel-1 data acquired during the winter campaigns of 2018/2019, 2019/2020 and 2020/2021. The velocity field is derived by combining InSAR results from overlapping ascending and descending orbits. It includes both horizontal components of the velocity, in North and East direction, and is generated at 100 m resolution, providing the most accurate and detailed icesheet-wide flow velocity map of Greenland to date.



**Figure 3-7: Greenland ice sheet wide velocity map, 100 m pixel spacing, combining SAR interferometry and offset tracking, using Sentinel-1A and 1B SAR data with 6 days repeat for the period 2018-2021.**

To assess the quality of the InSAR IV map, we compared the velocity with the multi-annual OT velocity map along profiles in regions without temporal changes. Figure 3-8 shows an example profile across the ice divide in the central part of northern Greenland. The combined IV product is much less affected by ionospheric streaks and is significantly closer to no-motion at the ice divide, as can be expected.



**Figure 3-8: Intercomparison of ice velocity from multi-annual offset tracking (OT; orange) and from the combined InSAR IV map (blue) along a profile in the center of the ice sheet (orange line in the inset).**



Additionally, we show results from an intercomparison of the 2018-2021 InSAR and 2019-2020 OT derived ice velocity maps with a GPS strain network located on the Northeast Greenland Ice Stream (NEGIS) and surveyed repeatedly over the years 2015-2019 (Hvidberg et al., 2020). The network consists of 63 stakes covering the entire width of the ice stream including both shear margins with velocities ranging from  $\sim 0.02$ - $0.16 \text{ m d}^{-1}$  (Figure 3-9). For each stake position, the corresponding pixel value from the ice velocity maps is selected and used to calculate validation statistics. Figure 3-10 shows a scatterplot of the InSAR and OT ice velocity maps versus the GPS derived velocities for all locations. The GPS intercomparison shows excellent agreement with mean differences of only  $\sim 1 \text{ mm d}^{-1}$  and an RMSE of  $2 \text{ mm d}^{-1}$  for the InSAR map. For the OT map the mean difference is  $2 \text{ mm d}^{-1}$  with an RMSE of  $3 \text{ mm d}^{-1}$ .

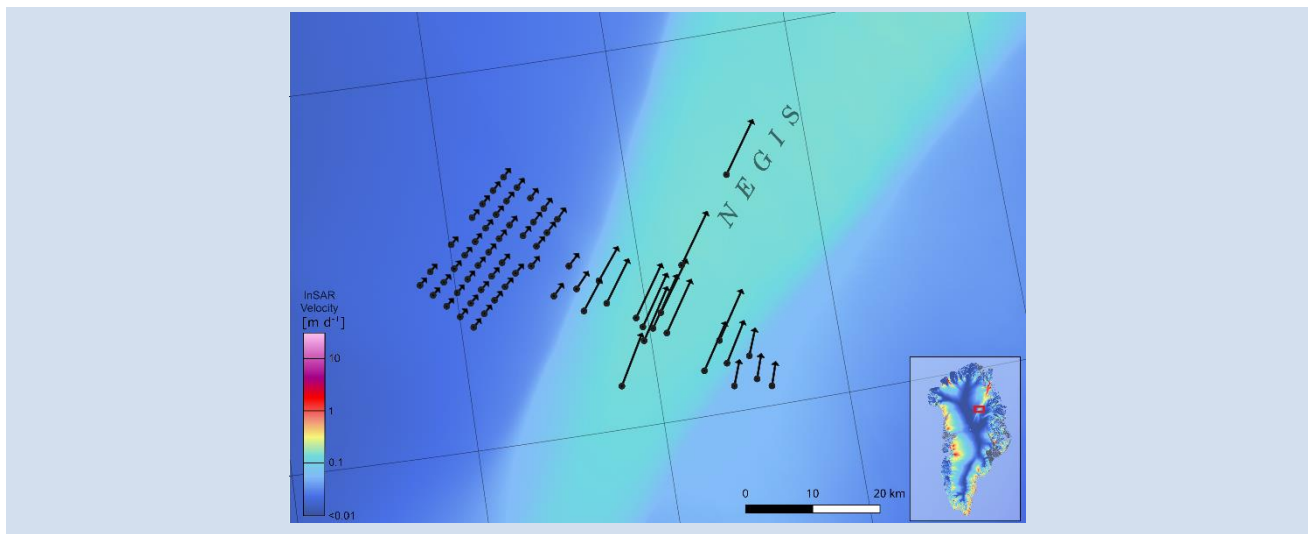


**Figure 3-9: Location of GPS net (Hvidberg et al. 2020) on NEGIS (inset shows location in Greenland). Vectors show ice flow direction and are proportional to velocity magnitude. Background S-1 InSAR velocity map.**

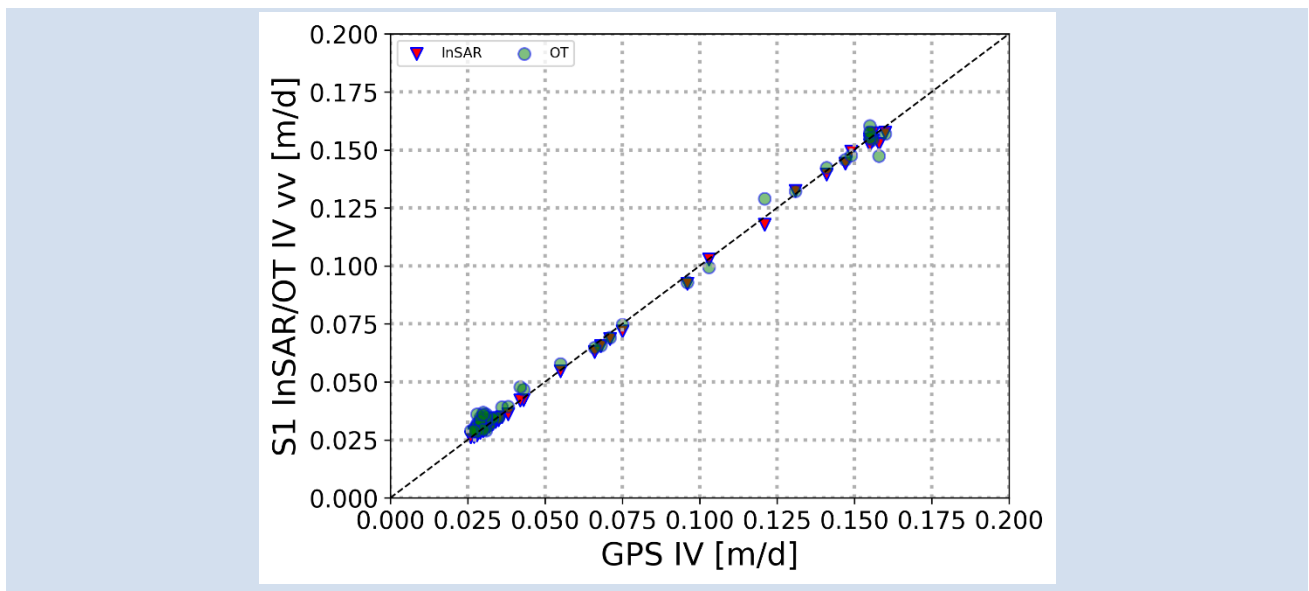


**Figure 3-10: Scatterplot showing InSAR (triangles) and Offset Tracking (OT; circles) versus GPS velocity magnitude (GPS data: Hvidberg et al. 2020).**



## 3.2 Optical IV

### 3.2.1 Sources and selection of independent validation data

In order to validate the Sentinel-2 based optical IV products both in situ data and IV derived from other EO sources were considered. The main source of in situ data is the GPS data gathered by the Promice weather stations, however these stations are located on the ice sheet or relatively slow-moving ice rather than on the fast-flowing outlet glaciers. Since the optical IV products are focussed on the fast-flowing outlet glaciers, relevant in situ data is not available to our knowledge. The main alternative EO data source to derive IV from are SAR measurements. Both Promice and Enveo have produced SAR based products from Sentinel-1 with good spatial temporal coverage allowing for a comparison with the Sentinel-2 optical based IV. Therefore, the two main sources that were selected for an independent validation are:

- 1) Promice Sentinel-1 (SAR) based IV
- 2) Enveo Sentinel-1 (SAR) based IV

### 3.2.2 Validation procedure

For the validation it was decided to compare monthly products, because these products could be derived for all three IV datasets. In the case of Enveo monthly products can be downloaded directly. The Promice IV data products have a time span of 24 days with 50% temporal overlap to the next product. By merging two products roughly monthly products can be derived. For the optical IV a timespan of a month often is long enough to have sufficient cloud free imagery to derive an IV product. Based on the available data for all sources 3 monthly products for different outlet glaciers during the 2019 summer season were selected:

- 1) Jakboshavn august 2019
- 2) Petermann july 2019
- 3) Upernavik july 2019

The three different IV datasets (S&T, Enveo and Promice) come at different resolutions and grids. To allow for a direct comparison the S&T and Promice datasets are re-gridded to 250m resolution to match the resolution and grid of the Enveo dataset. The IV magnitude of the reference products is subtracted from optical IV to derive IV offset maps.

### 3.2.3 Validation procedure Outcome

The overall trend in IV is similar to the one observed in the SAR based products of both Enveo and Promice (see figure Figure 3-11). In regions of low ice flow velocity, typically speeds are higher in the optical product. This is likely due to the limitations within the co-registration process. Furthermore, it should be noted that post processing steps, such as interpolation, smoothing and filtering, likely vary for the different datasets

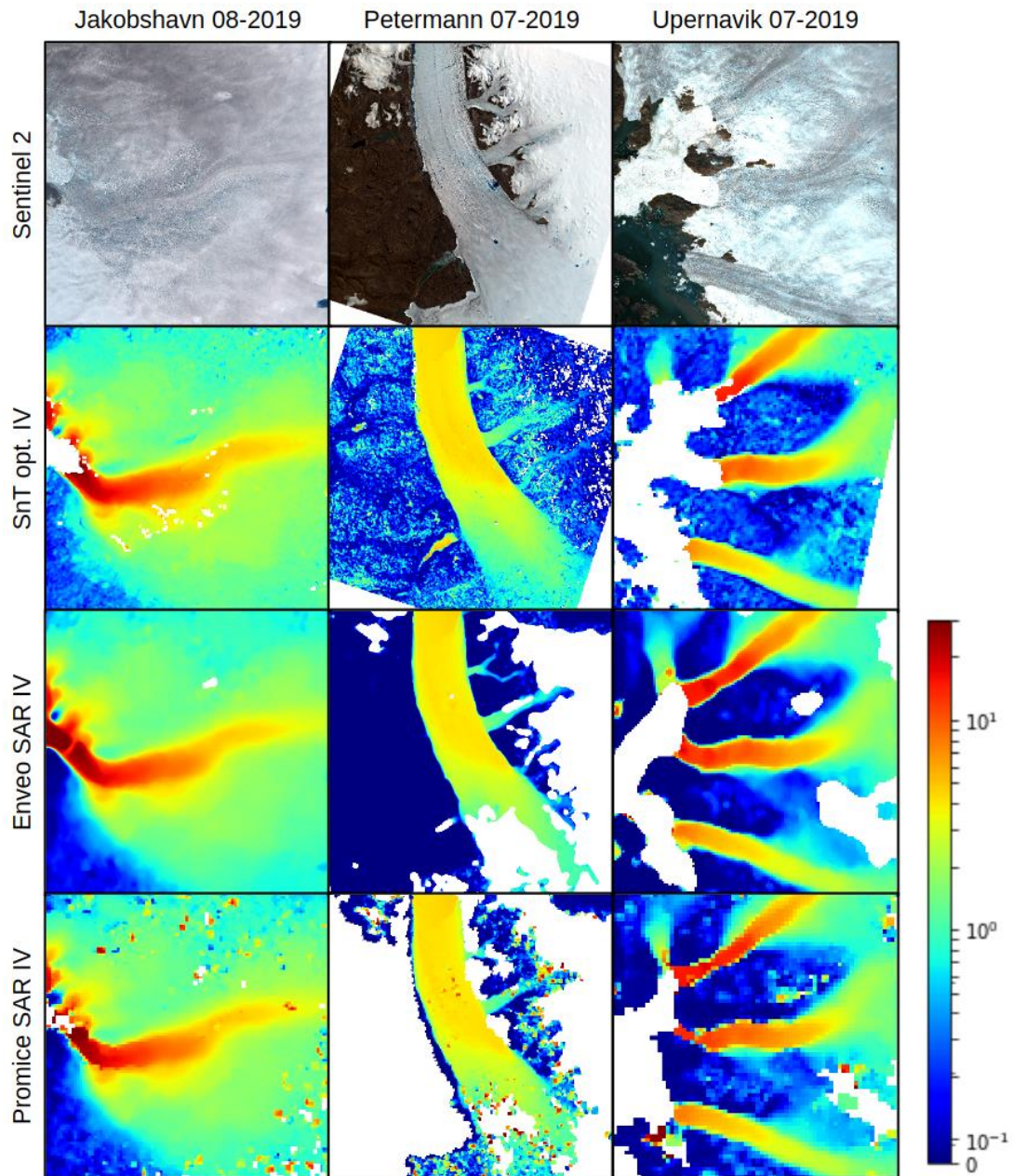


**Figure 3-11: The overall trend in IV is similar to the one observed in the SAR based products of both Enveo and Promice**



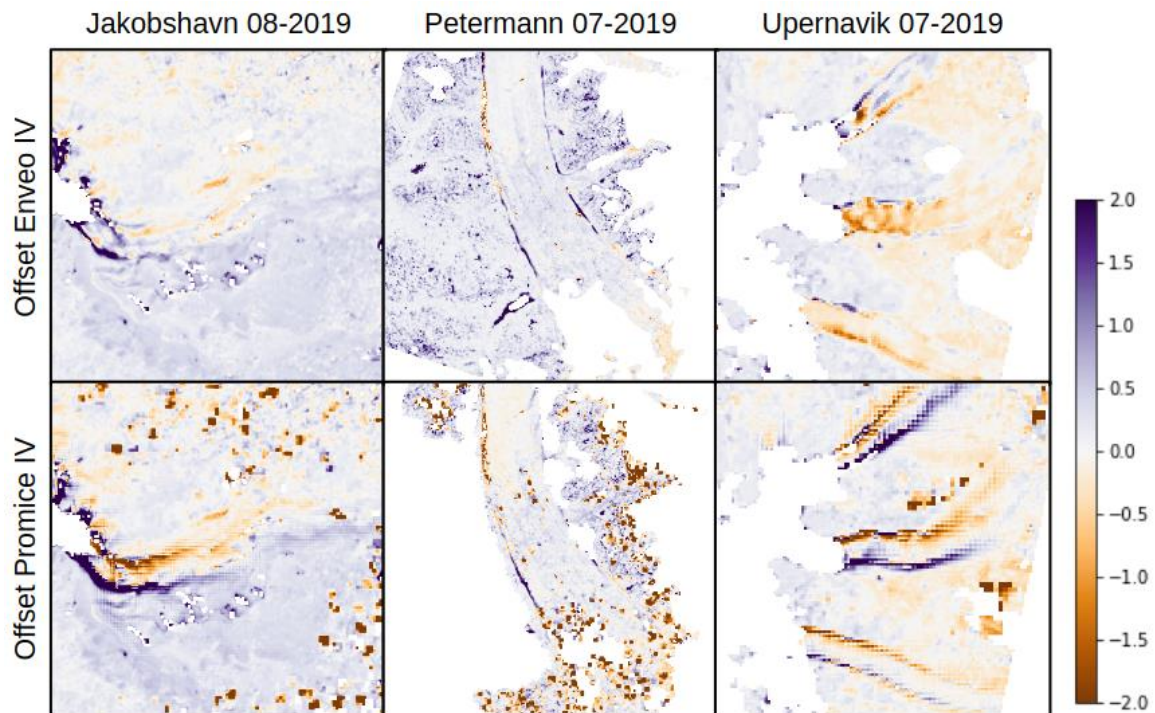


**Figure 3-12: the IV offsets between the S&T optical products compared to the Enveo and Promice SAR products**

Figure 3-12 shows the IV offsets between the S&T optical products compared to the Enveo and Promice SAR products. Speeds are generally the same order of magnitude, with maximum offsets at around 2m/day. Large offsets can be due to artefacts in the data, this is especially the case for the Promice dataset. In addition, large offsets can be observed along the margins of the fast-flowing ice, this is at least partly due to interpolation errors, keeping in mind that the initial resolution of the Promice dataset is 500m. In the offset images it can also be seen that optical based IV is slightly higher in areas of slow-moving ice, this is likely due to the co-registration issue described above. For the fast-flowing ice in Petermann IV is higher whilst for Upernavik speeds of the fast-flowing ice are slightly lower. These offsets could be due to many limitations within the optical and SAR methods. For the optical main error sources are imperfect pixel matching, co-registration, and a lack of a complete time series due to cloud cover. Furthermore, the IV maps are generated from a time series of imagery and Sentinel-2 and Sentinel-1 don't match perfectly in time. The histograms in Figure 3-13 show the difference for the offsets in the low IV ( $< 0.4$ ) and high IV ( $> 4$ ) more clearly.

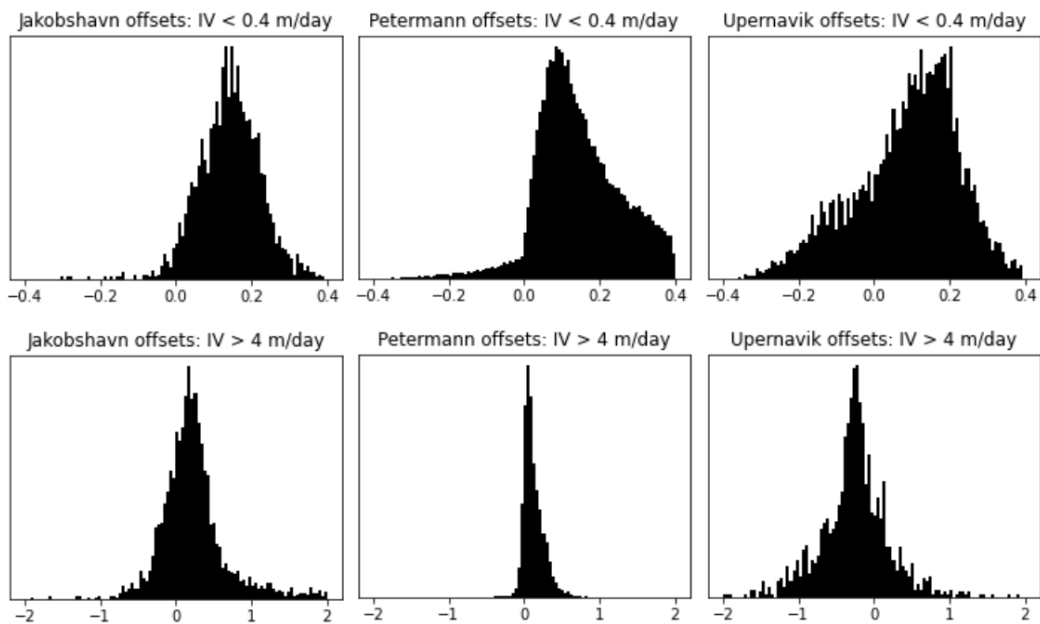


**Figure 3-13: the difference for the offsets in the low IV (< 0.4) and high IV (> 4).**

### 3.2.4 Recommendations for products improvement

The basis of the optical IV algorithm is the matching of pixels to determine a shift. Together with the time difference between two images this allows to derive IV. Improvements to the feature tracking algorithm which does the matching will therefore directly impact results. Possible improvements are exploiting multiple bands and increasing storage of pixel from 8 to 16 bit. Both are ways to exploit more information that is present in the Sentinel-2 imagery. Additionally, co-registration could maybe be improved, currently only a single x/y shift is found and used for correction. However, more complex warping effects are present in the data especially in areas with a lot of topography. Finally, some manual work is still required to run the whole processing chain, such as checking the selection of cloud free scenes. Improvements to cloud masking could automate this step.

### 3.2.5 Optical IV – SAR IV product intercomparison – version 2

For Version 2 of the Product Validation and Intercomparison Report we report on an intercomparison of two newly generated optical IV datasets, derived from Sentinel-2, with contemporaneous velocity maps derived from Sentinel-1 SAR offset tracking (processed by ENVEO). The two datasets cover the 79 Fjord Glacier in north-east Greenland (2019/05/01 - 2019/06/14) and the Jakobshavn Glacier in west Greenland (2019/05/02 - 2019/08/30) (Figure 3-14) and have a grid spacing of 100 m. For the intercomparison all available Sentinel-1 single-track (6-day repeat) IV maps generated within the time frame and covering the spatial extent of the respective optical IV products were averaged and resampled to the same grid extent and size (100 m) to produce two comparable products based on SAR OT. Both horizontal velocity components (easting, northing) are then compared on a pixel-by-pixel basis for which we provide the statistics, histograms and difference maps. Gaps in either of the two datasets, as well as differences larger than of 1 m d<sup>-1</sup>, are excluded from the calculations.

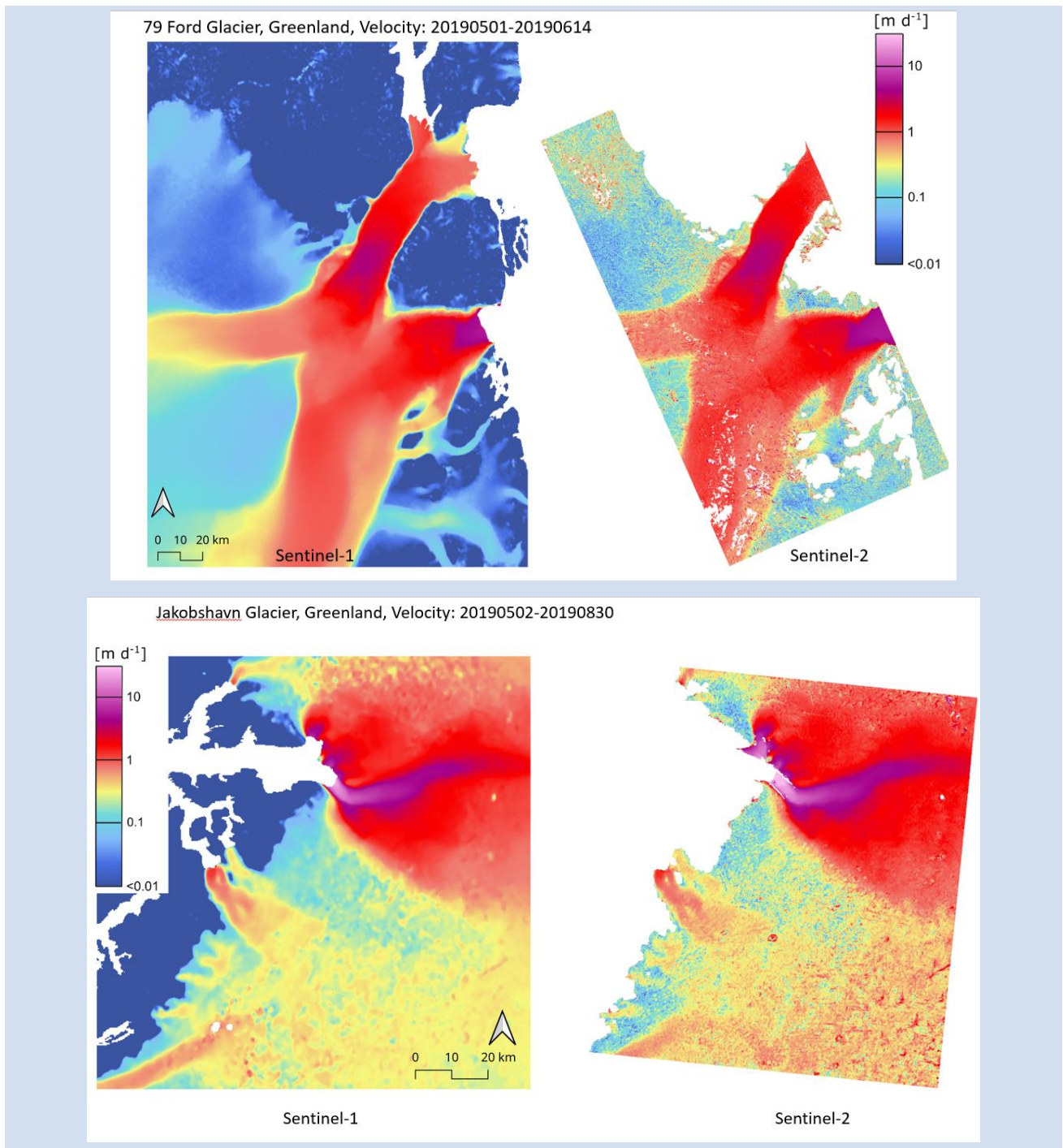


**Figure 3-14: Top: ice velocity maps of 79-Fjord Glacier derived from Sentinel-1 SAR (left) and Sentinel-2 optical images (right) averaged over the period 1/5/2019-14/6/2019. Bottom: ice velocity maps of Jakobshavn Glacier derived from Sentinel-1 SAR (left) and Sentinel-2 optical images (right) averaged over the period 2/5/2019-30/8/2019.**



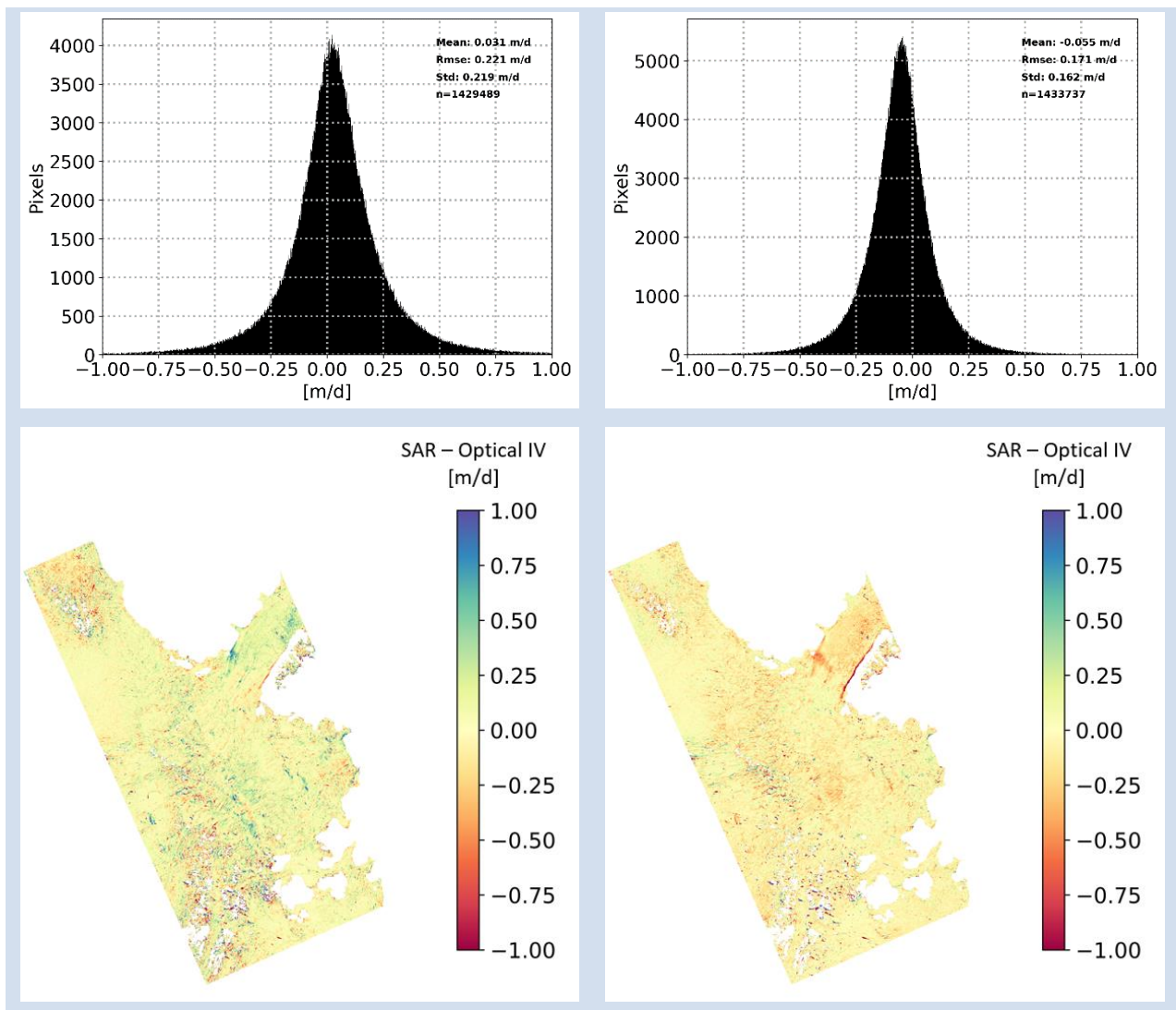


**Figure 3-15: Top: Histograms of Vx (left) and Vy (right) residuals of the intercomparison between the optical IV product and the SAR IV product for 79-Fjord Glacier. Bottom: associated difference map for easting (left) and northing (right) velocity component.**

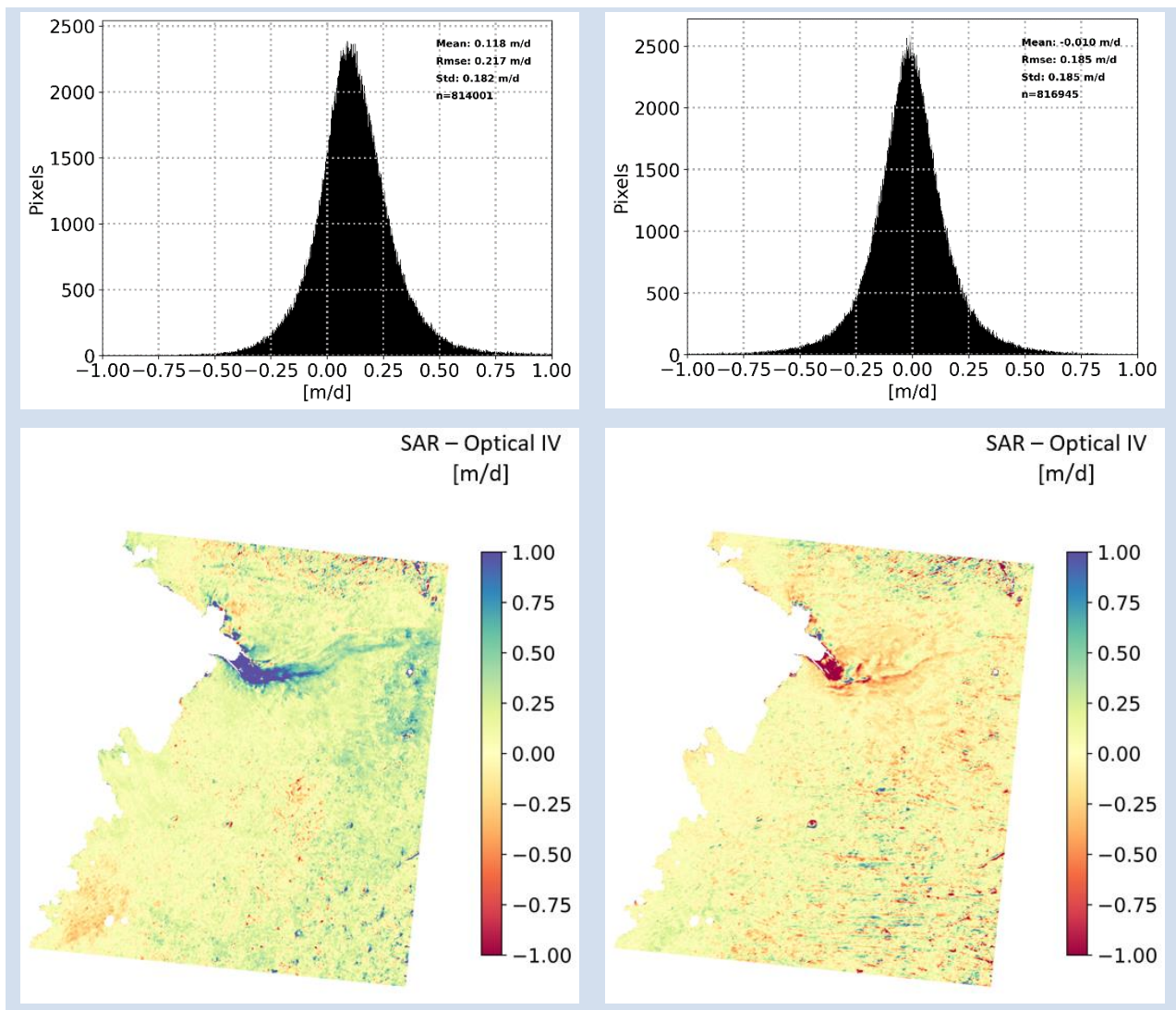


**Figure 3-16: Top: Histograms of Vx (left) and Vy (right) residuals of the intercomparison between the optical ice velocity product and the SAR ice velocity product for Jakobshavn Glacier. Bottom: associated difference map for easting (left) and northing (right) velocity component.**

Figure 3-15 and Figure 3-16 show the intercomparison results of the optical and SAR IV products for 79-Fjord and Jakobshavn glaciers, respectively. For 79-Fjord Glacier, based on a sample size of >1.4 million pixels, the overall mean bias between the two data sets is 3.1 cm/d (RMSE: 22 cm/d) for the x velocity component, and 5.5 cm/d (RMSE: 17 cm/d) for the y velocity component. For Jakobshavn Glacier, based on a sample size of >800k pixels, the overall mean bias between the two data sets is 11.8 cm/d (RMSE: 22 cm/d) for the x velocity component, and 1.0 cm/d (RMSE: 19 cm/d) for the y velocity component. The difference map for Jakobshavn Glacier reveals that larger differences are found on the fast flowing main trunk of the outlet glacier, with better agreement in other areas. Jakobshavn Glacier is among the fastest flowing outlet glaciers in Greenland and well known to have large velocity fluctuations during the year. Velocities near the calving front show a doubling during summer months, reaching up to 40 m/d. Larger differences found here can be explained by the different temporal coverage of SAR and optical IV maps during the 4-month averaging period (May-August) used for the composite velocity map.

## 4 Gravimetry Mass Balance (GMB)

This chapter gives a summary of the activities carried out to assess the quality of the GMB products.

There has been no direct validation of the GMB products because no independent data sets are available. Instead inter-comparisons have been carried out to assess the variability of these products arising from the use of different methods and data sets.

Previously, several inter-comparison exercises have been carried out. The results of these together with further investigations made on the specific CCI products are presented here.

### 4.1 (Inter-) comparison procedure

There are several (inter-)comparison strategies to follow. We focus on the mass change time series (and the trend in this) product and describe the following:

1. Comparison to other methods for regional and ice sheet mass balance. These are the Input-output method (or mass budget method) and volume change method.
2. Inter-comparison of the results from different methods for deriving mass changes from the same GRACE data
3. Inter-comparison of the results from using the same method but different data sets.

### 4.2 (Inter-) comparison procedure outcome

1. A comparison of GRACE-derived mass changes to other methods for regional and ice sheet mass balance is a major task to undertake, and outside the scope of this document. Several of such studies have been published, and here we highlight a few. The IMBIE (international mass balance inter-comparison experiment, Shepherd et al., 2012, 2018 and 2020) was an ambitious project including numerous methods and data sets.

The overall mass balance for ice sheets from different methods is seen in Fig 4-1. These are the Input-output method (or mass budget method) and volume change method.

It can be seen that the gravimetry method predicts mass balance results that agree with the two other methods within the error bars. Both methods, i.e. the point mass inversion and the tailored sensitivity kernel approach, which are used for generating the GIS CCI GMB products (see AD5) were also provided to the IMBIE study (Shepherd et al., 2018 and 2020).

2. A detailed inter-comparison of the results from different methods for deriving mass changes applied on the same GRACE data was undertaken in the CCI GMB Round Robin Exercise (RRE). The procedure and the results are described in detail in Groh et al. (2019). Both methods used in the GIS CCI GMB production were included in the RRE and showed good agreement with other submissions.

The RRE participants were anonymized, but Fig. 4-2 shows the good agreement between the GIS CCI GMB products derived by DTU and TUDr (for the entire GIS). Figure 4-3 and 4-4 also shows the other drainage basin mass change time series. The two products show very small differences only in few basins and all the differences are within the error bars.

3. The third strategy is the inter-comparison of results from using the same method but different data sets. Figure 4-5 shows the mass change time series based on two data sets: CSR05 and ITSG2016. From this comparison no significant differences are seen between the two data sets.

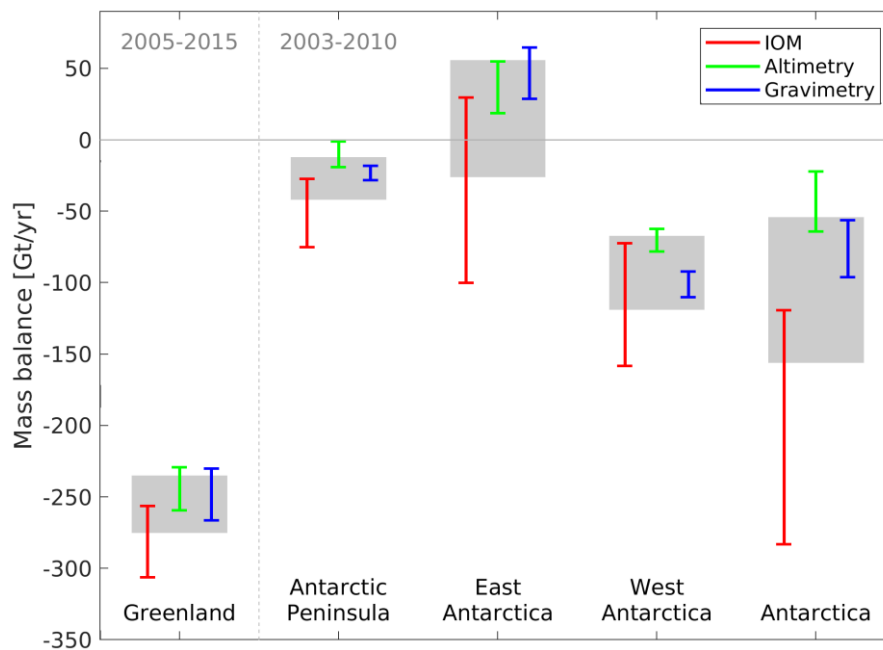


Figure 4-1: Mass balance of the ice sheets from different methods (Shepherd et al., 2018,2020).

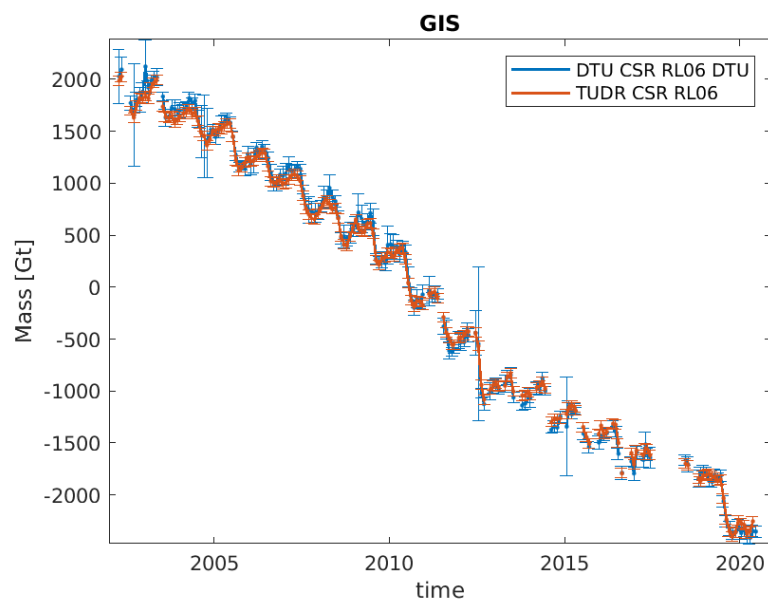
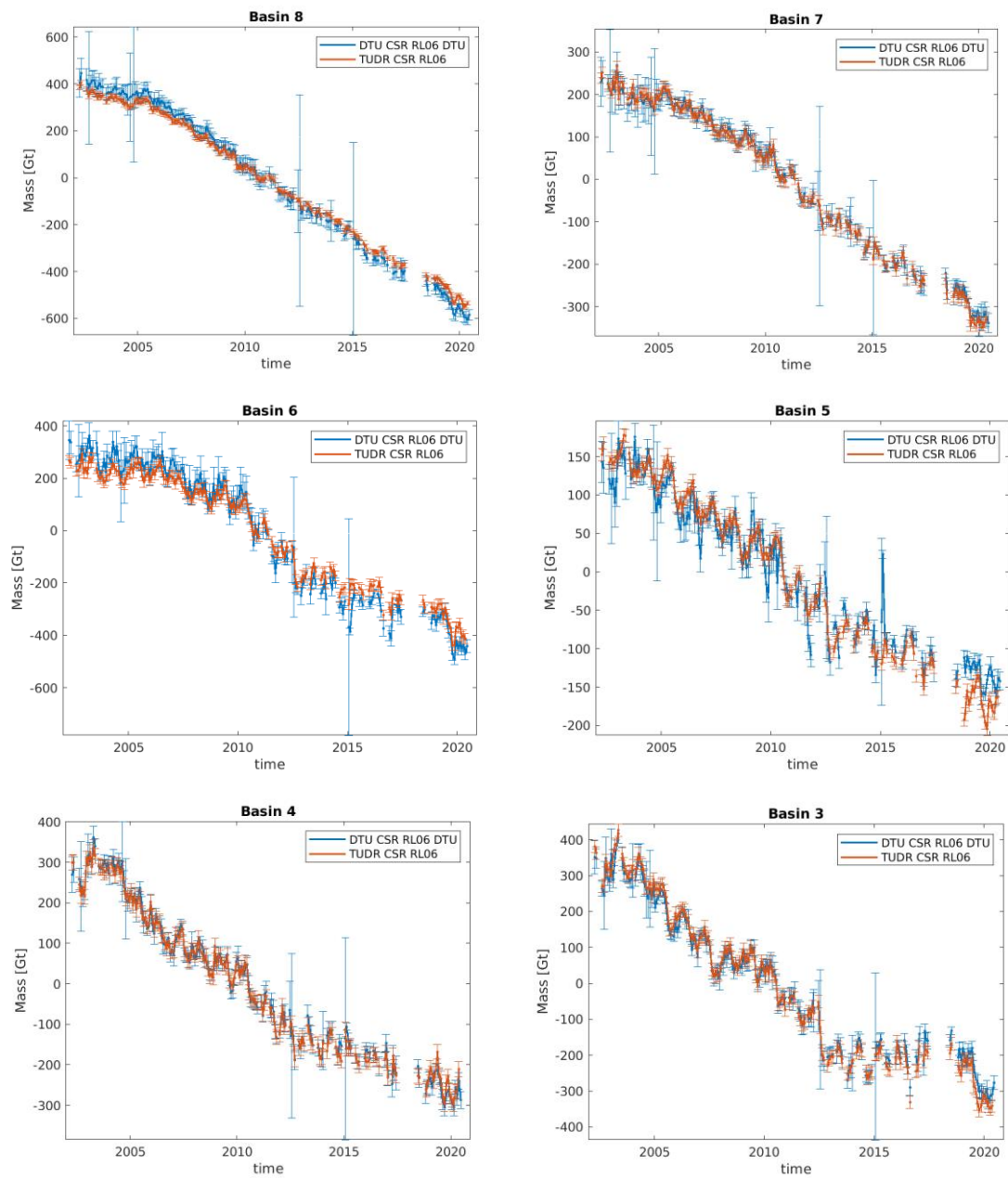
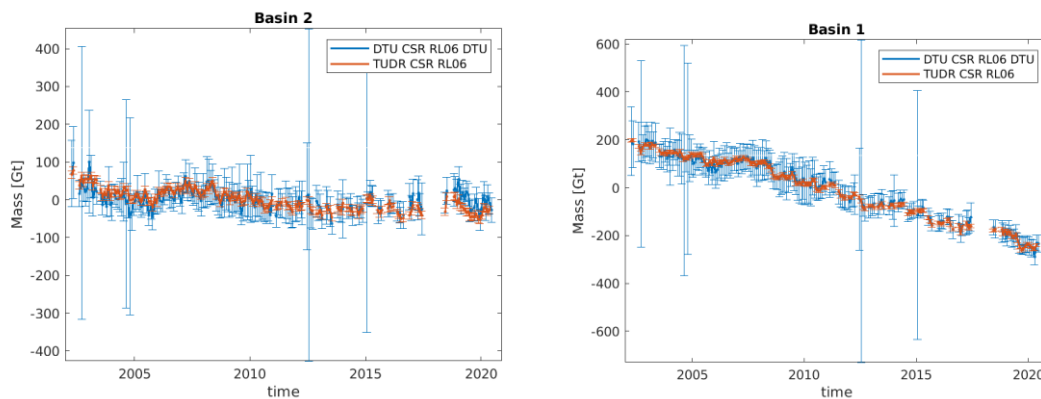


Figure 4-2: Mass change time series of the entire GIS, from the GIS CCI GMB products derived by DTU (blue) and TUDr (red).



**Figure 4-3: Mass change time series of basin 8 to 3 from the GIS CCI GMB products derived by DTU (blue) and TUDr (red).**





**Figure 4-4: Mass change time series of basin 1 and 2 from the GIS CCI GMB products derived by DTU (blue) and TUDr (red).**

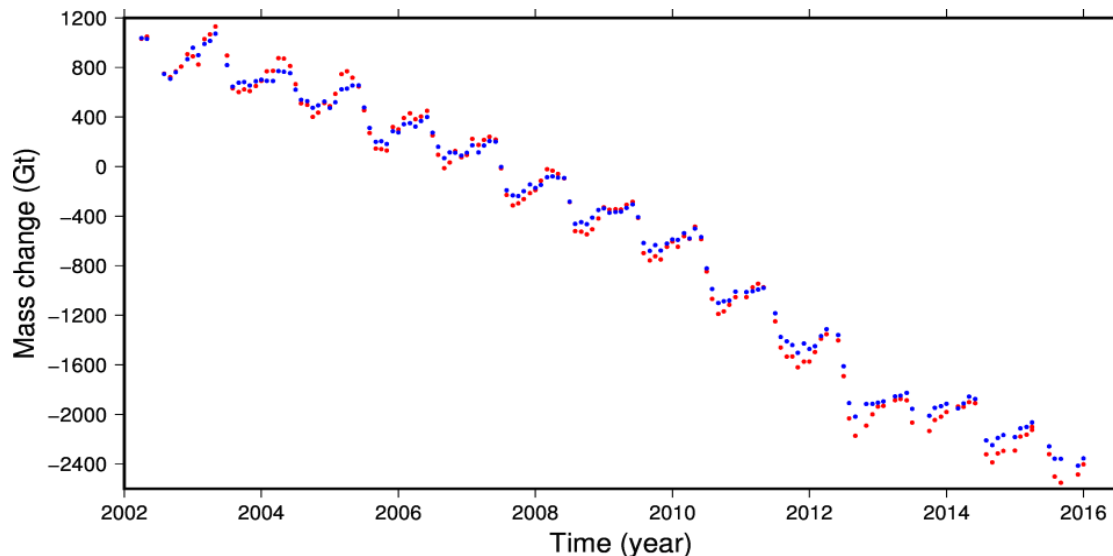


**Figure 4-5: Mass change time series derived from CSR05 data (red) and ITSG2016 (blue)**

### 4.3 Recommendations for products improvement

Better models for GIA, degree one, and ocean model correction will lead to future improvement in the products. Studies targeted on these corrections could lead to improvements in the products.

#### Integrated CryoSat, GRACE and Sentinel-1 data.

One issue with the GRACE-only products is the low spatial resolution and therefore one recommendation is to produce products with increased resolution. This could be done from integrated CryoSat, GRACE and Sentinel-1 data, combined with firn compaction and snow surface density meteorological models.

The mass changes of the Greenland ice sheet are measured directly with GRACE, but only with limited spatial resolution, and relatively large errors associated with leakage from oceans, land, and other ice caps. Combining CryoSat and GRACE data, supplemented with a firn density and compaction model, an integrated mass solution can be obtained with high spatial resolution. Noting that rapid temporal changes of the ice sheet is primarily driven by rapid changes in velocities of outlet glaciers, which can now be monitored at

weekly resolution by Sentinel-1, the combination of all three EO data sources – GRACE, CryoSat altimetry and Sentinel-1 ice velocities – into a unified mass product, will give a new enhanced experimental ECV product, superior to the existing CCI SEC, IV and GMB products. This enhanced product will represent an operational product following the IMBIE principles and can easily be extended to Antarctica as well at a later stage. The first concept demonstration results of such activities, for both Greenland and Antarctica, has been published in Forsberg et al. 2017.

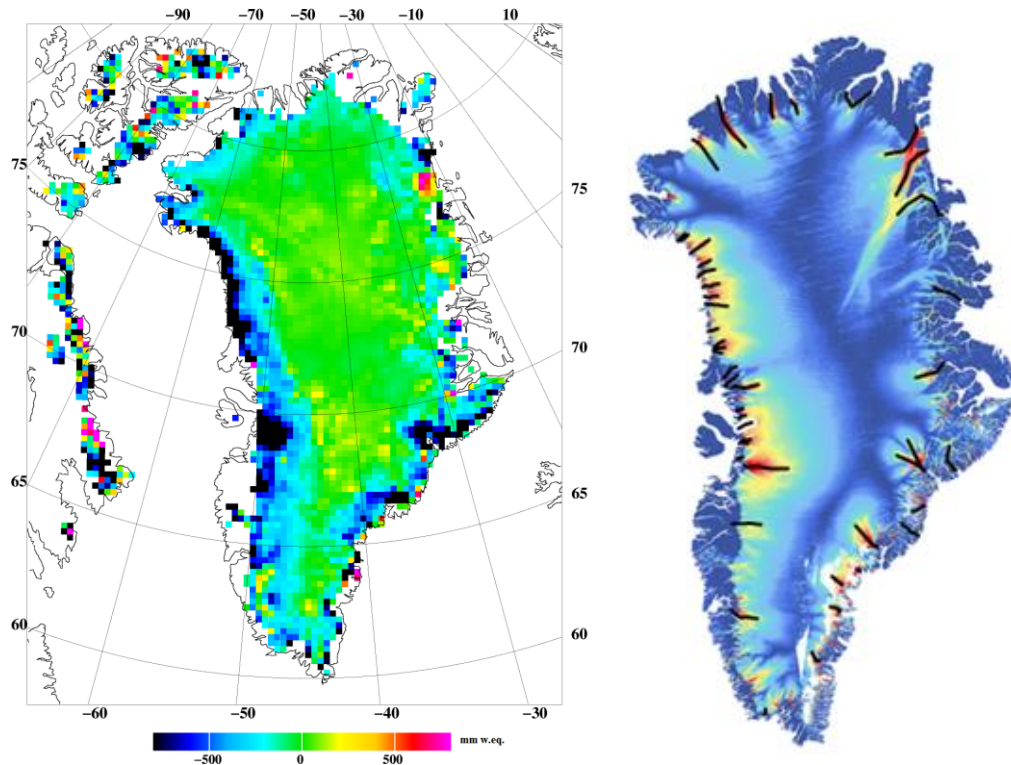


**Fig. 4-6. GRACE/CryoSat mass balance grid of Greenland (left, low-resolution demonstration product) will be combined with Sentinel 1-A (and later -B) ice velocities from the Greenland ice sheet (right) in the proposed CCN/CCI+ action. Current S-1 acquisition scheme allow sub-monthly estimation of essentially all Greenland outlet glaciers.**

## 5 Mass Flow Rate and Ice Discharge (MFID)

The MFID product is validated against all known estimates of ice discharge that are available at the spatial (sector, Zwally *et al.* (2012)) and at least annual resolution. This includes two completely independent plus one different dataset of ice discharge. The independent estimates come from external parties while the “different” dataset is produced by Ken Mankoff (producer of these CCI+ data), using a similar algorithm, but tuned differently. That is, the Mankoff *et al.* (2020) validation data set is generated with gates in different locations and using a different cutoff velocity than this CCI+ work.

### 5.1 Sources and selection of independent validation data

Independent data comes from King *et al.* (2020), Mouginot *et al.* (2019), and Mankoff *et al.* (2020). King *et al.* (2020) provides discharge estimates at monthly temporal and glacier spatial resolution. Mouginot *et al.* (2019) provides discharge estimates at *annual* temporal and sector spatial resolution. Mankoff *et al.* (2020) provides discharge at ~12-day temporal and glacier spatial resolution. Although Mouginot *et al.* (2019) is only annual resolution, this should not significantly impact results which according to King *et al.* (2018) only vary by ~6 % seasonally.

### 5.2 Validation procedure

We downsample the Mankoff *et al.* (2020) and King *et al.* (2020) data to monthly temporal and basin spatial resolution, by averaging in time and summing in space, and then compare to this product that already exists at that resolution. The Mouginot *et al.* (2019) product remains at annual temporal resolution. We then graphically display this product (CCI+), with all of the other products, in individual plots per sector (Zwally *et al.* (2012)). We then visually compare the lines in the graphics.

### 5.3 Validation procedure outcome

The lines all overlap within the uncertainty estimates. Some sectors do have outliers, but the CCI+ product is never the outlier. Therefore, the CCI+ product always falls within the uncertainty estimates of the majority of the other comparable discharge products.

### 5.4 Recommendations for products improvement

No recommendations at this time.

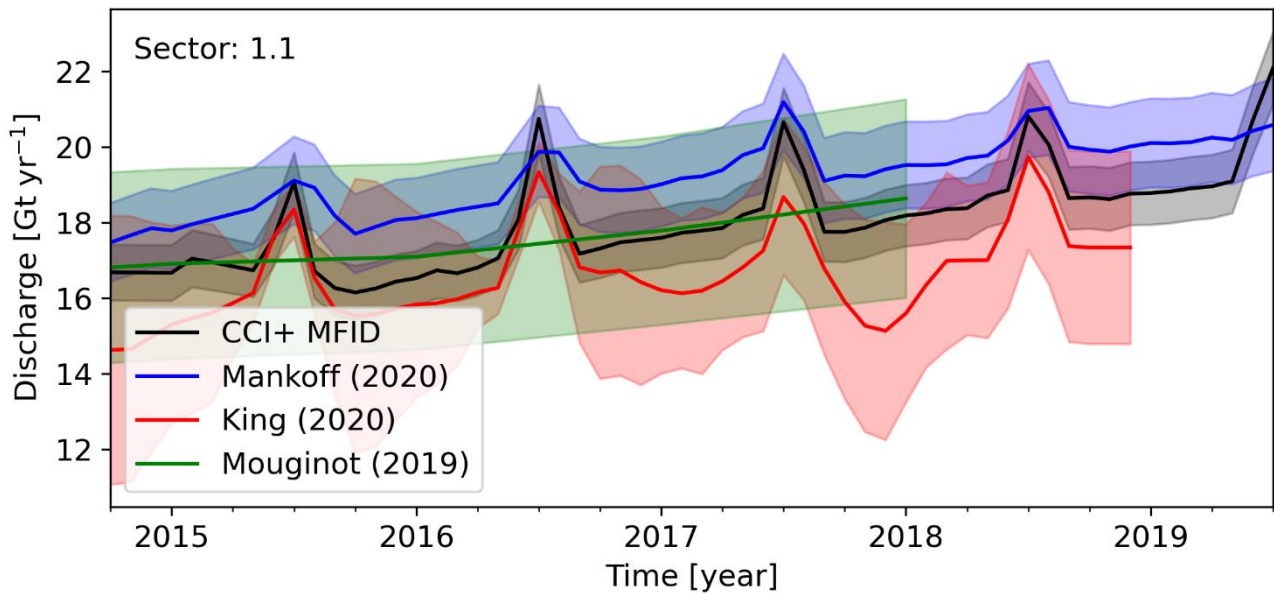


Figure 5-1: Comparison between this product (CCI+ MFD; black), Mankoff et al. (2020) (blue), King et al. (2020) (red), and Mouginitot et al. (2019) (green). Uncertainty estimates come from the respective published products or described in the ATBD and uncertainty documentation for the CCI+ product. Sector label from Zwally et al. (2012) is printed in top-left corner of graphic.

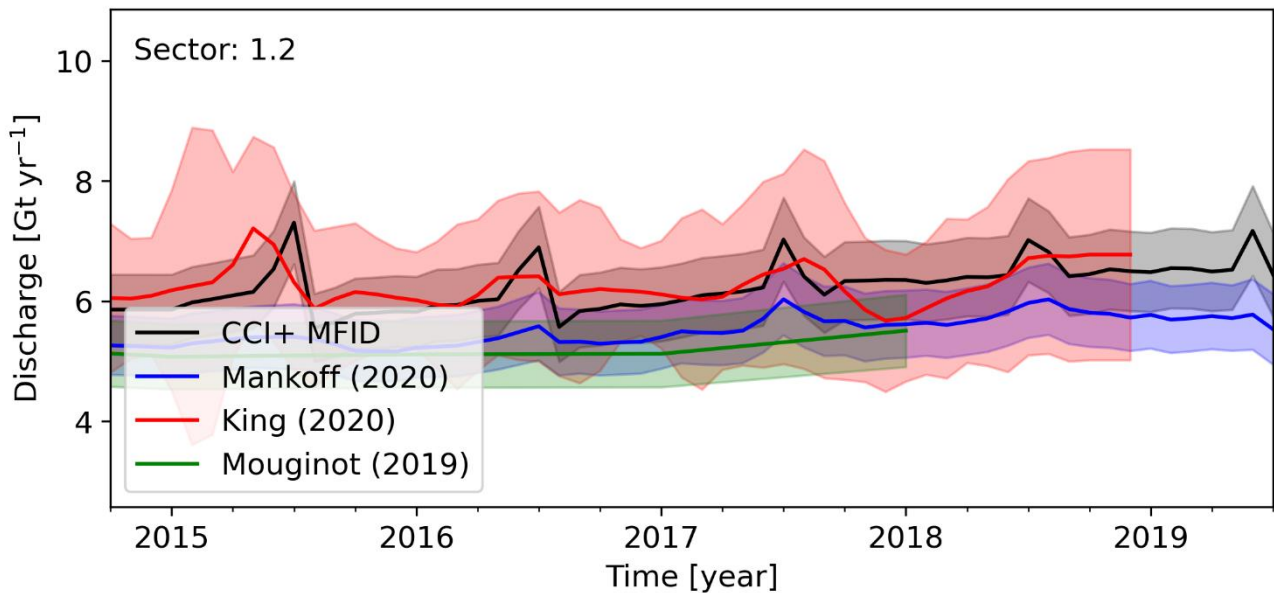


Figure 5-2: Same as Figure 5-1 caption.

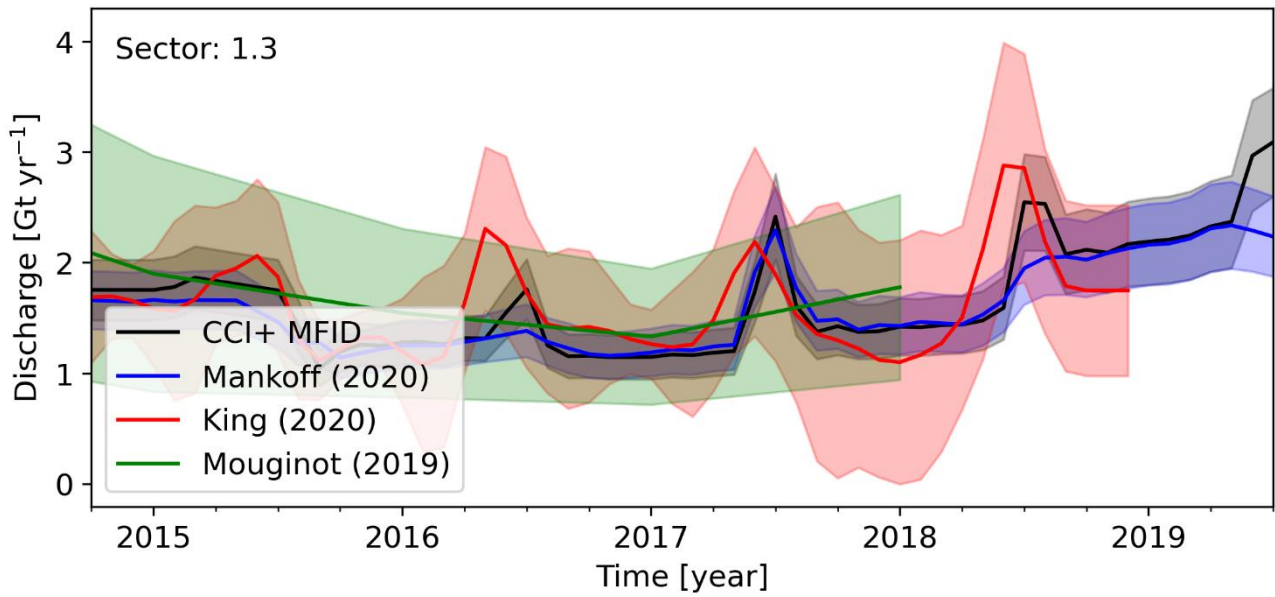


Figure 5-3: Same as Figure 5-1 caption.

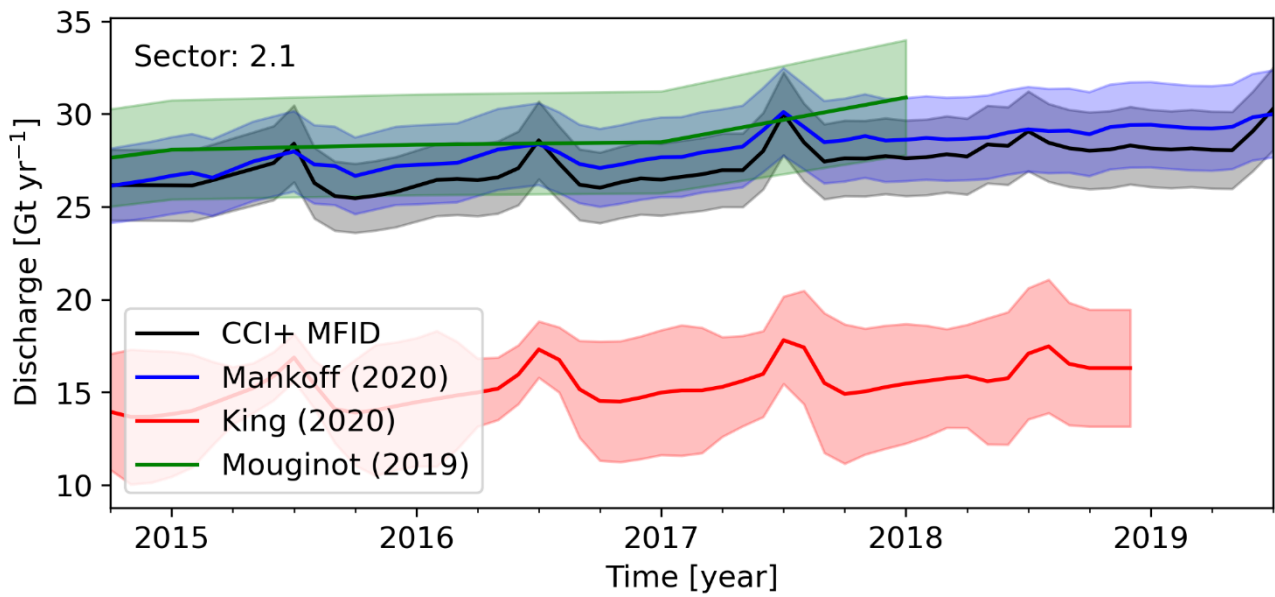


Figure 5-4: Same as Figure 5-1 caption.



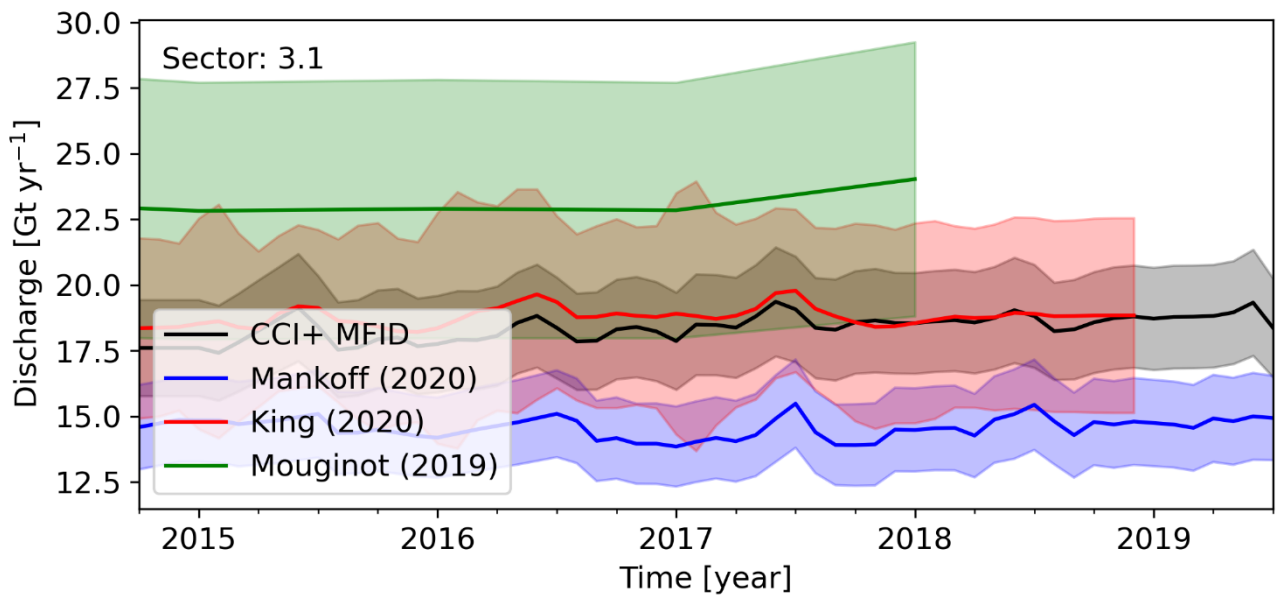


Figure 5-5: Same as Figure 5-1 caption.

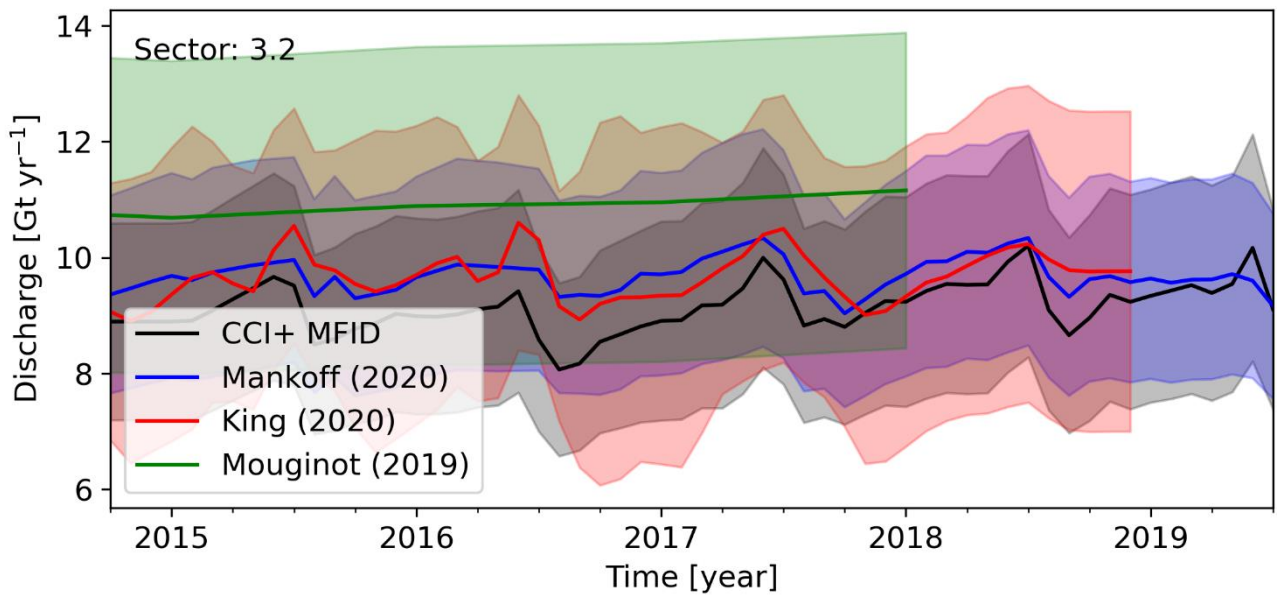


Figure 5-6: Same as Figure 5-1 caption.

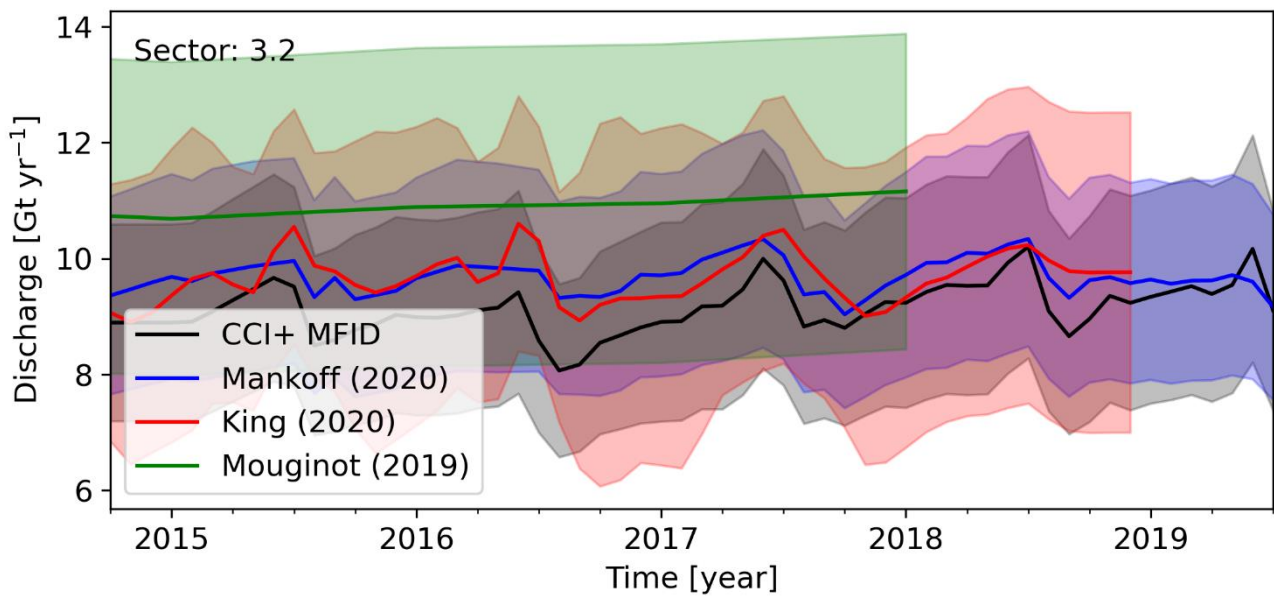


Figure 5-7: Same as Figure 5-1 caption.

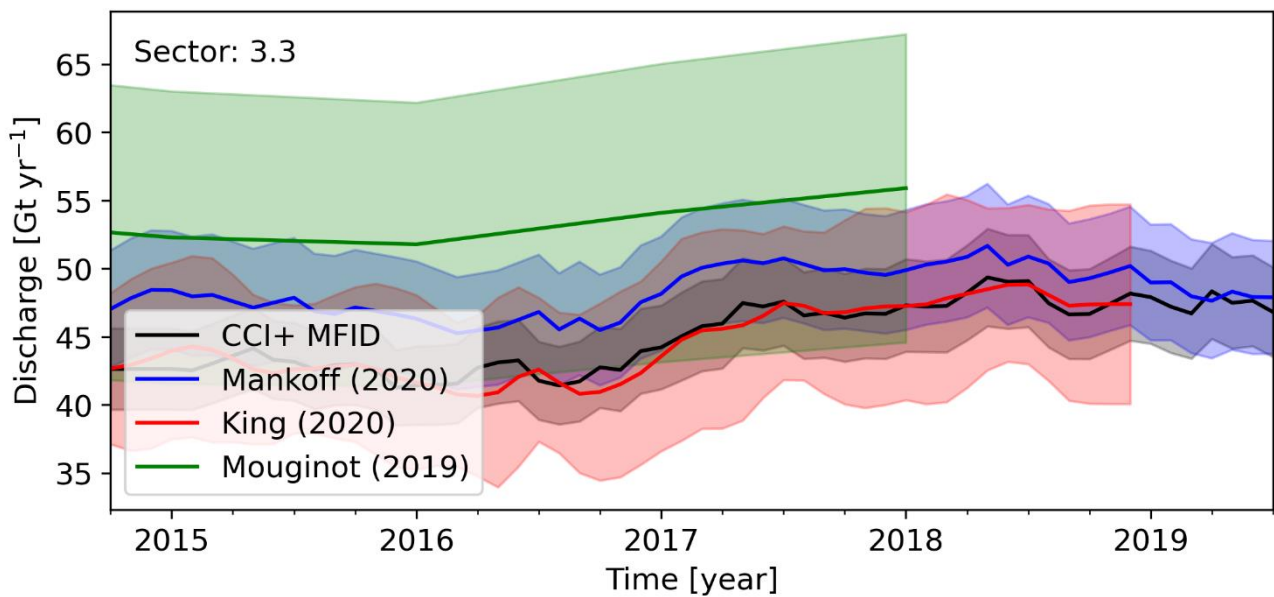


Figure 5-8: Same as Figure 5-1 caption.

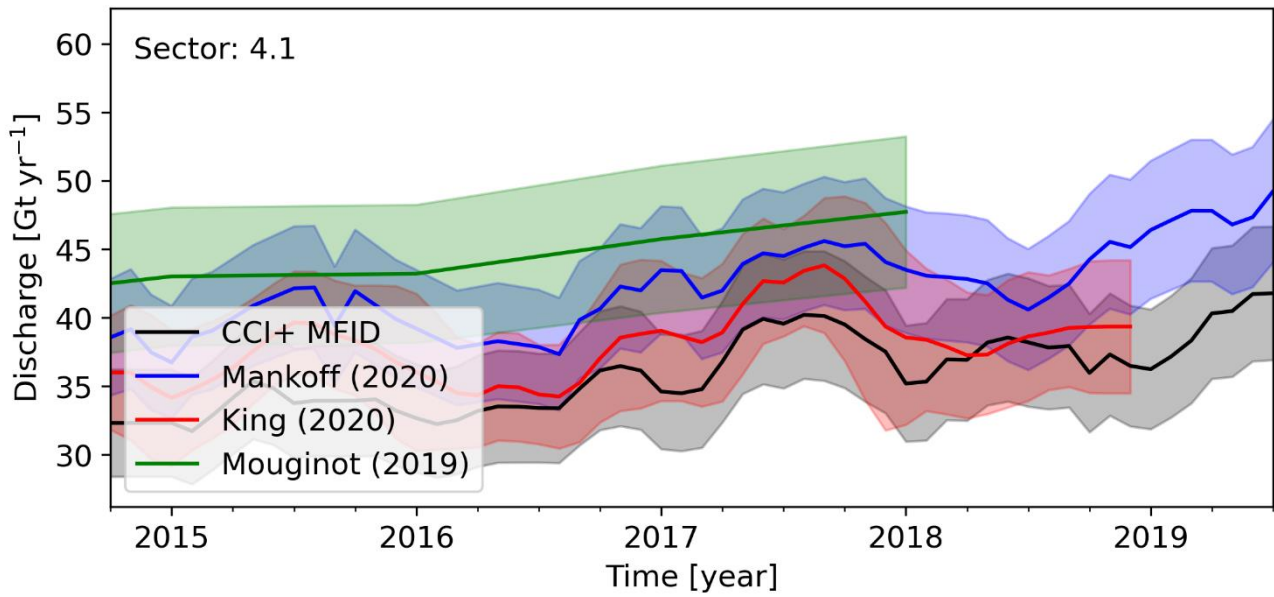


Figure 5-9: Same as Figure 5-1 caption.

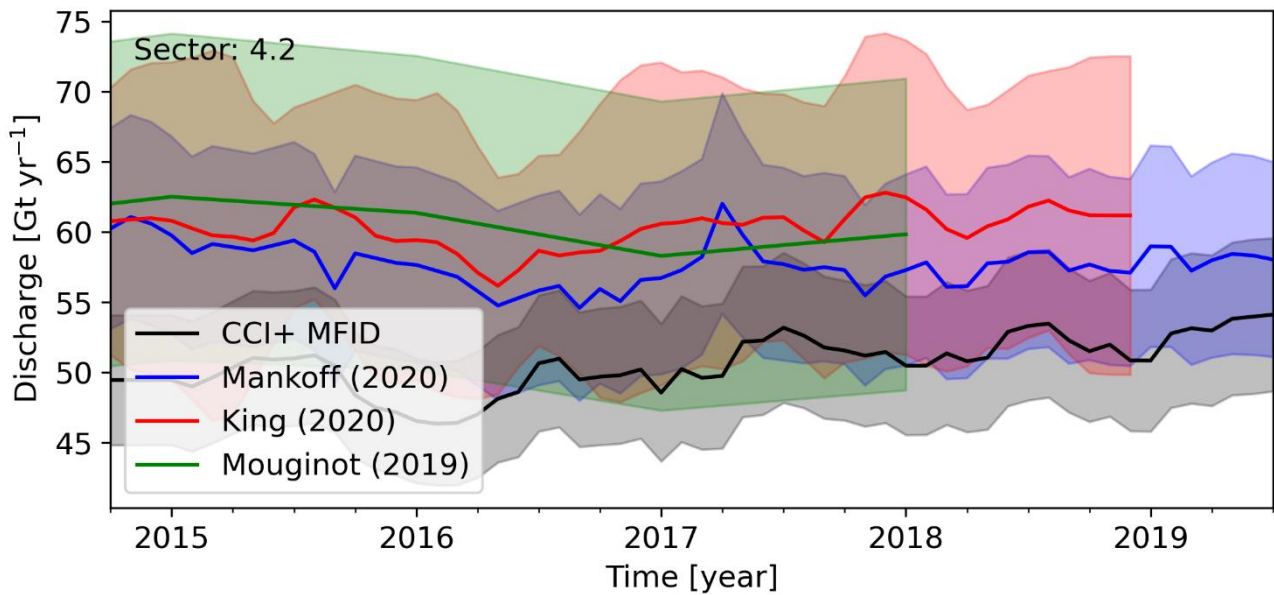


Figure 5-10: Same as Figure 5-1 caption.



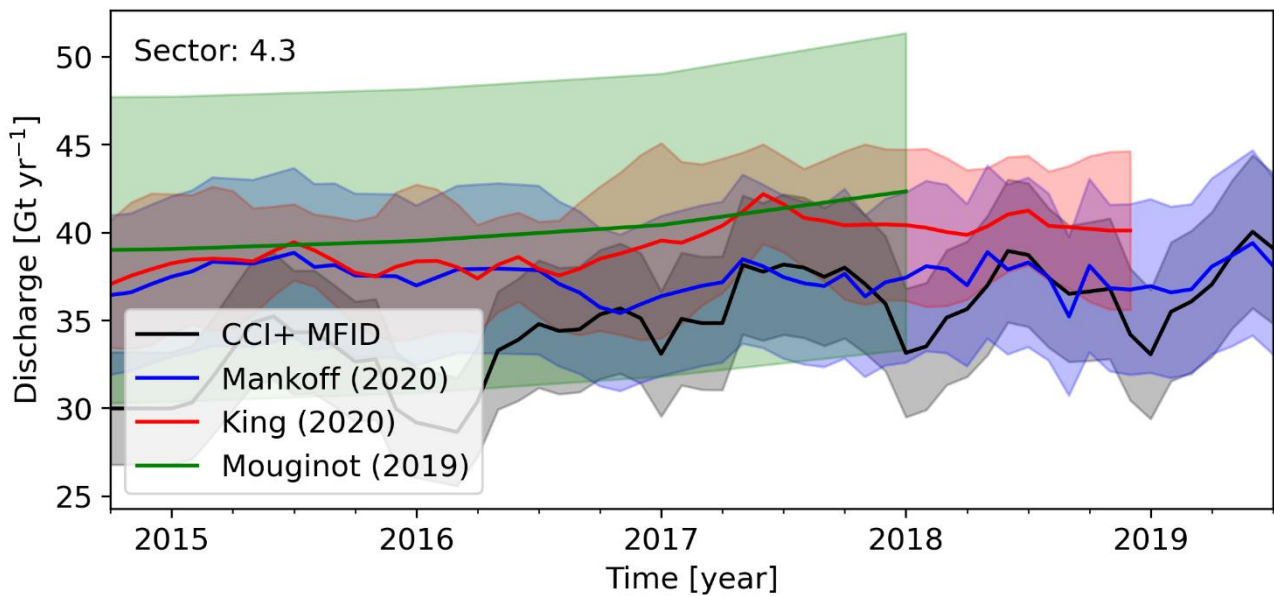


Figure 5-11: Same as Figure 5-1 caption.

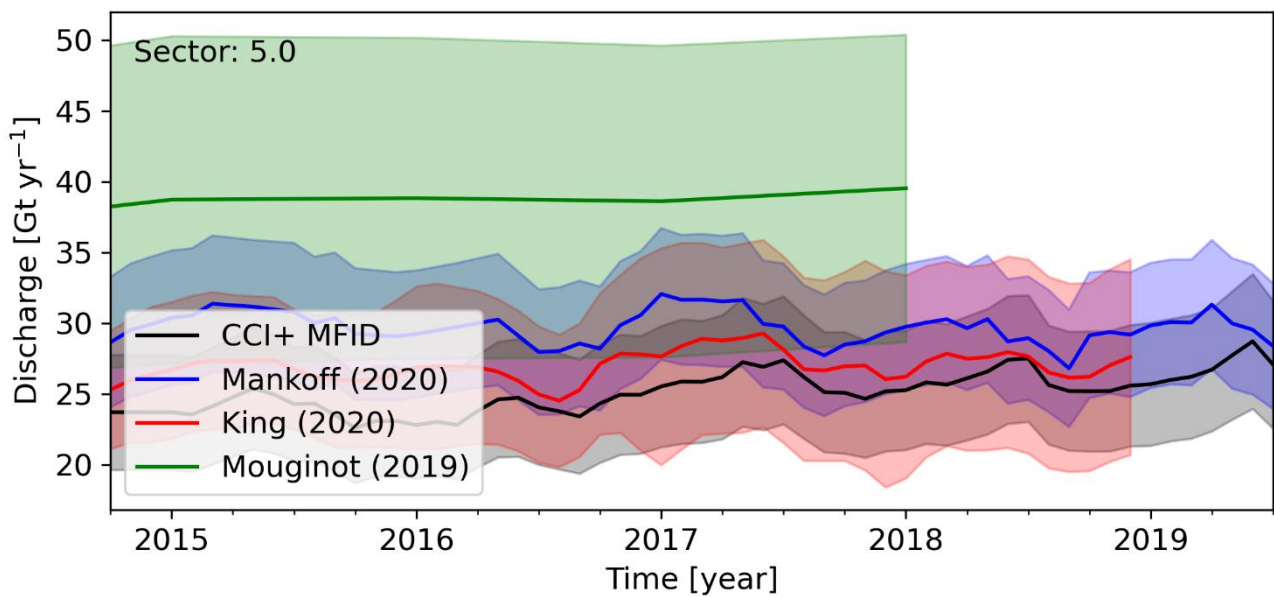


Figure 5-12: Same as Figure 5-1 caption.

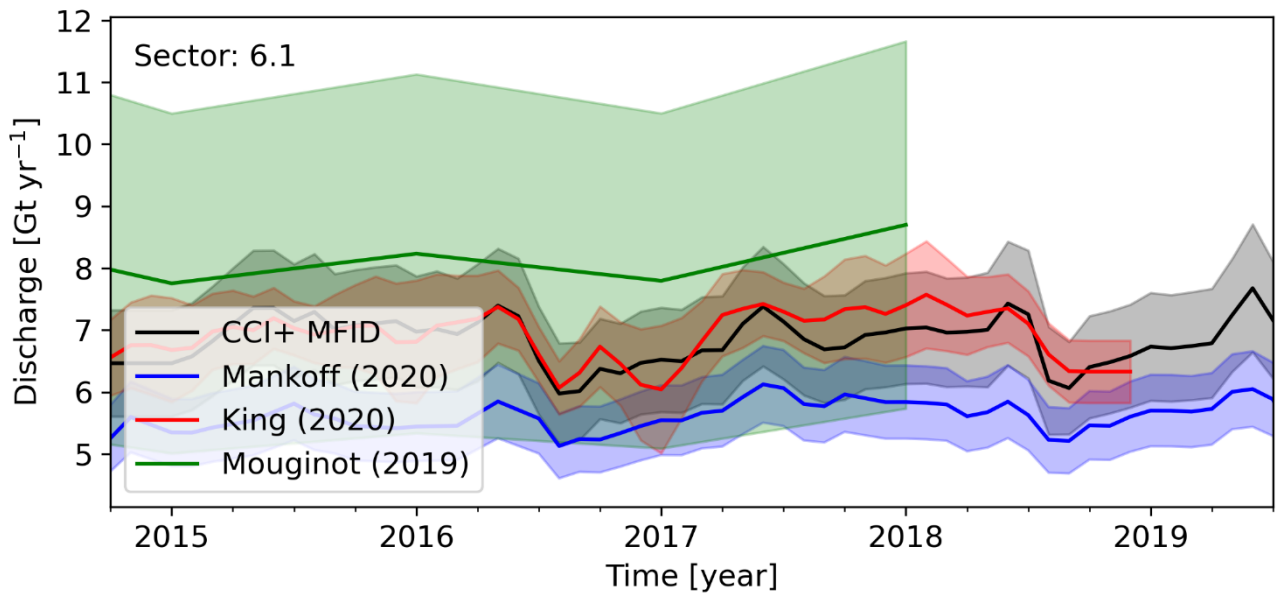


Figure 5-13: Same as Figure 5-1 caption.

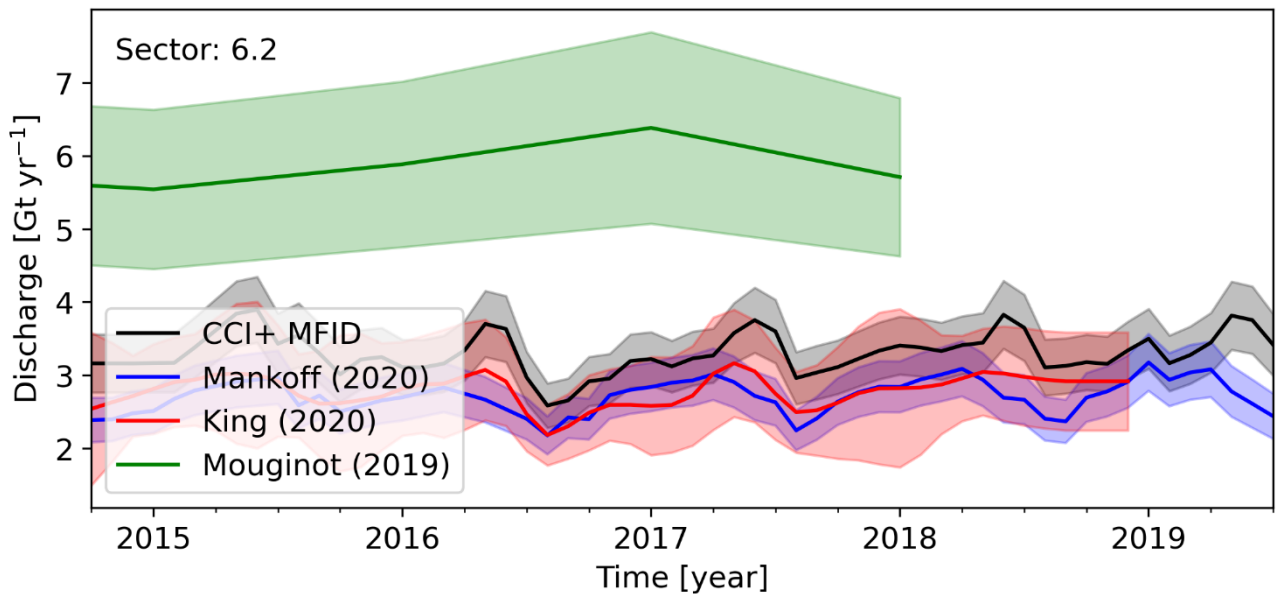


Figure 5-14: Same as Figure 5-1 caption.

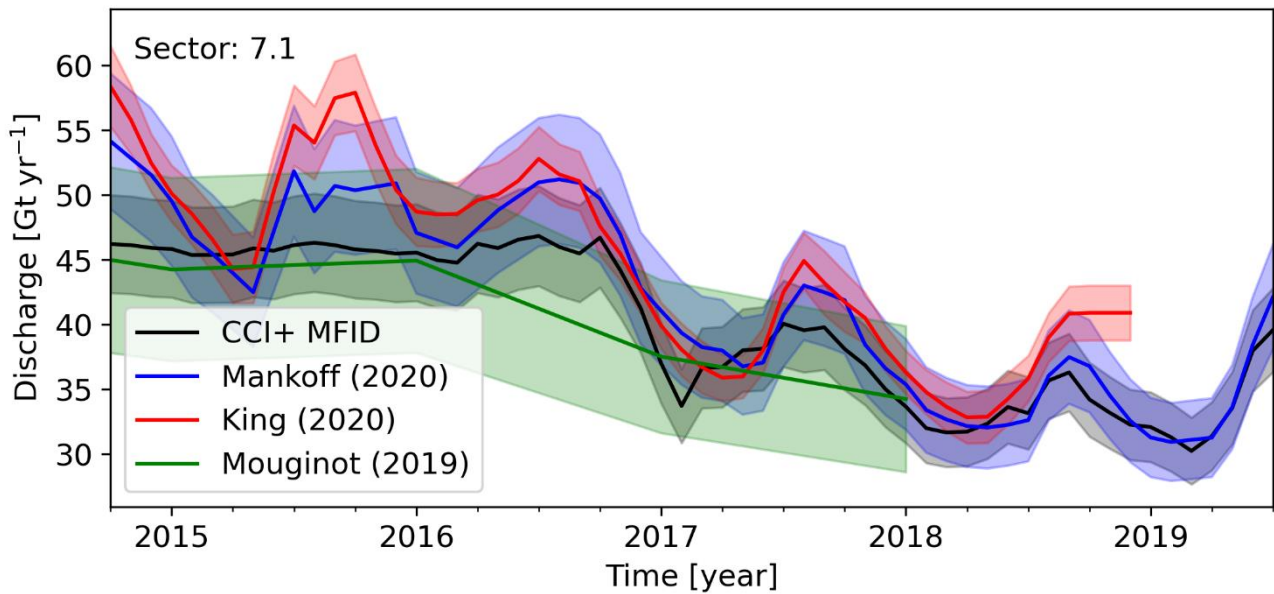


Figure 5-15: Same as Figure 5-1 caption.

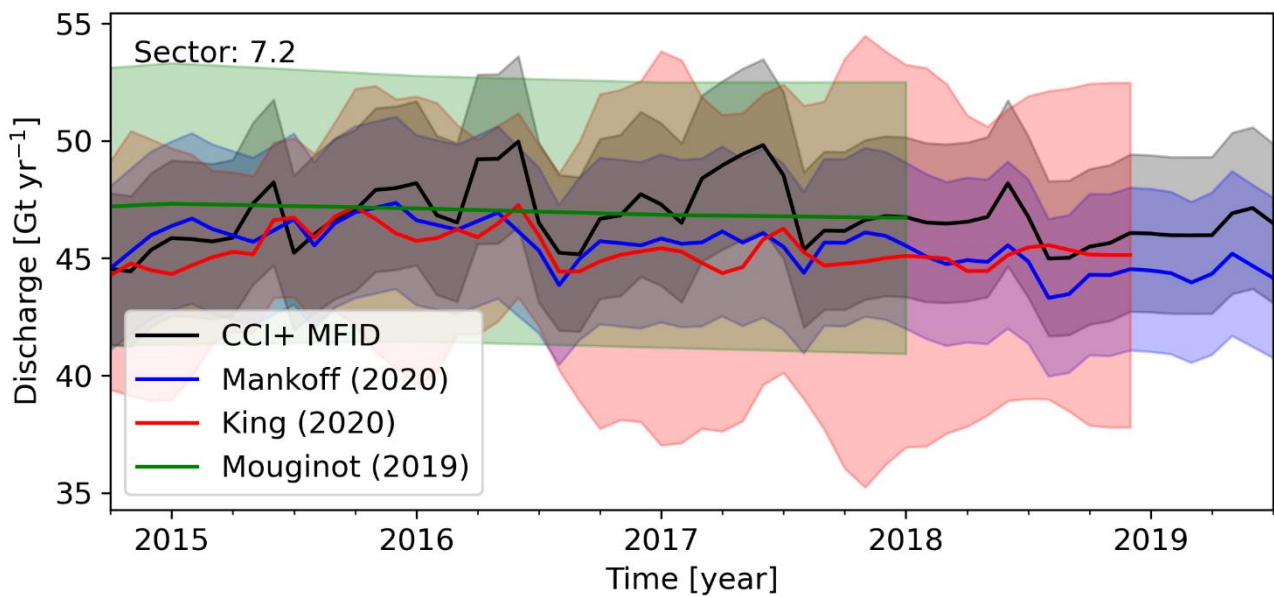


Figure 5-16: Same as Figure 5-1 caption.

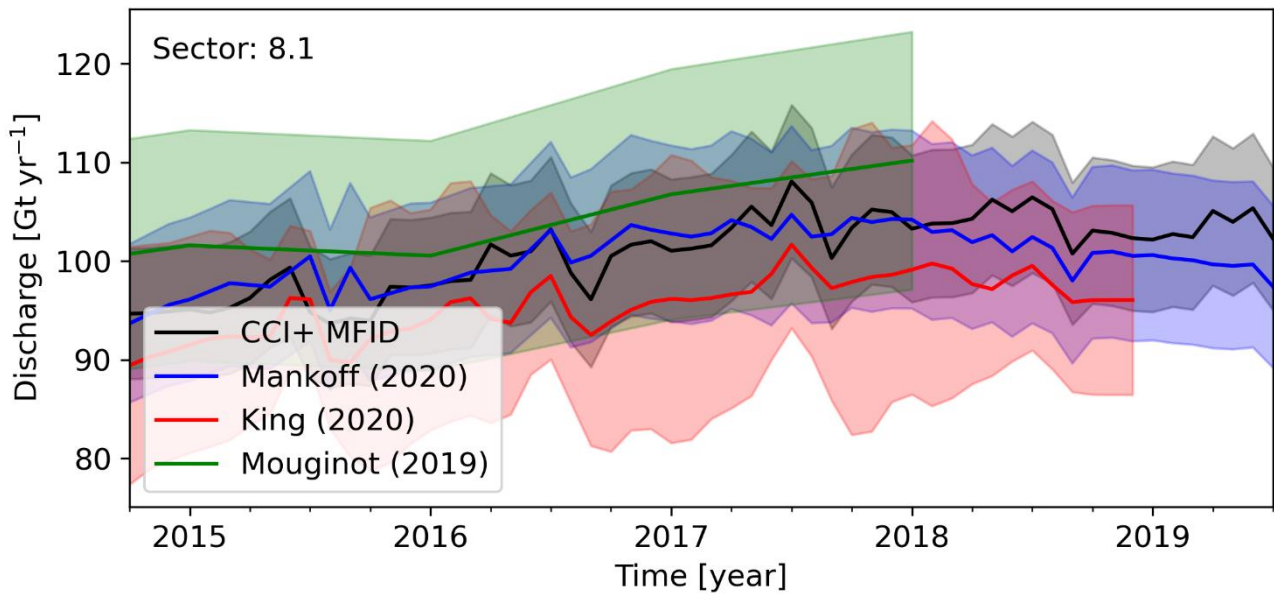


Figure 5-17: Same as Figure 5-1 caption.

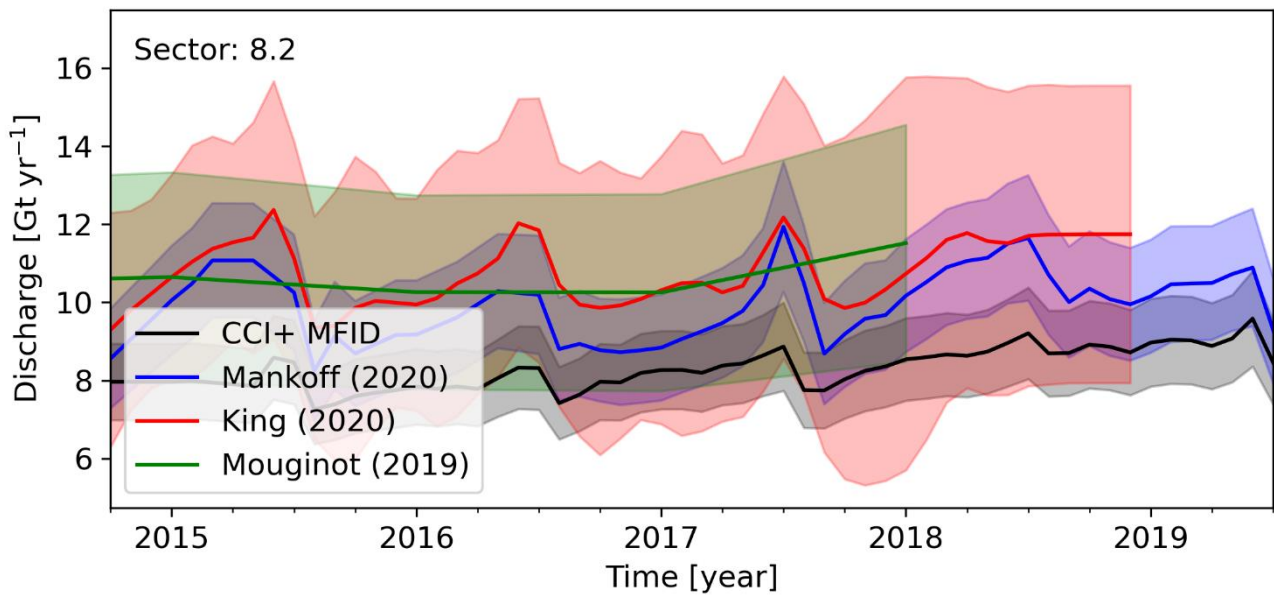


Figure 5-18: Same as Figure 5-1 caption.



## 6 Supraglacial Lakes

Supraglacial lakes (SGLs) have been identified in the catchment of Sermeq Kujalleq (SK, also known as Jakobshavn Isbræ) for the melt season of 2019. The selected catchment area covers 160,039.11 km<sup>2</sup>, approximately 22% of SK's catchment. Supraglacial lakes were detected in this area for each available time step, subject to data availability and cloud cover. Over 6000 ( $\pm 15\%$ ) lake features were identified over the melt season, with an average lake area of 0.4 km<sup>2</sup> ( $\pm 22\%$ ). As expected, a high majority of these lakes were identified in the lower part of the SK catchment (3190 lakes in total), with the maximum number of lakes evident during the peak of the melt season in August.

Although SGL is not a standard data product in the Greenland Ice Sheet CCI+ project, it is recognised that it is an important R&D product because glacier dynamics are understood to be inherently linked to supraglacial lake extent and drainage (e.g. Das et al., 2008; Andrews et al., 2018). As a result, validation analysis of the SGLs is essential to this work.

The validation analysis could be conducted under two approaches:

1. Through inter-comparison with available independent datasets for the same study area
2. Through inter-comparison with alternative sensors for the same time period; hereafter referred to as the sensor inter-comparison

Many remote sensing studies have previously been conducted at SK to derive supraglacial lakes, including those derived from MODIS, Landsat, Sentinel-2, and WorldView imagery (Hoffman et al., 2011; Liang et al. 2012; Williamson et al., 2017; Rowley et al., 2019). However, no ideal supraglacial lake dataset was found that was suitable for comparison to the dataset derived here, either due to spatial (e.g. Rowley et al., 2019) or temporal (Liang et al., 2012) mismatches. For this reason, we focus on the latter approach for our validation analysis – sensor inter-comparison.

### 6.1 Sources and selection of independent validation data

Landsat-8 imagery is used for the sensor inter-comparison, adopting the detection method used for the SGL product to derive supraglacial water bodies from coinciding Landsat-8 scenes. Scenes were selected based on three key criteria: 1) cloud cover (less than 60%); 2) spatial coverage (across the entire monitoring area used for the SGL product); and 3) corresponding with Sentinel-2 image acquisitions (less than 24 hours). The selected scenes are outlined in Table 6-1.

**Table 6-1: Selected Landsat-8 scenes as validation data.**

Scene IDs	Acquisition date	Cloud cover	Corresponding SGL time step for comparison
LC08_L1TP_008011_20190507_20190521_01_T1 LC08_L1TP_008012_20190507_20190521_01_T1	07/05/2019	10% 17%	06/05/2019
LC08_L1TP_008011_20190523_20190604_01_T1 LC08_L1TP_008012_20190523_20190604_01_T1	23/05/2019	0% 21%	22/05/2019 & 24/05/2019 (average)
LC08_L1TP_082233_20190530_20190605_01_T1 LC08_L1TP_009011_20190530_20190605_01_T1	30/05/2019	3% 3%	30/05/2019
LC08_L1TP_008011_20190608_20190619_01_T1 LC08_L1TP_008012_20190608_20190619_01_T1	08/06/2019	1% 55%	08/06/2019
LC08_L1TP_008011_20190811_20190820_01_T1 LC08_L1TP_008012_20190811_20190820_01_T1	11/08/2019	2% 7%	11/08/2019



LC08_L1TP_008011_20190827_20190903_01_T1	27/08/2019	3%	27/08/2019
LC08_L1TP_008012_20190827_20190903_01_T1		23%	

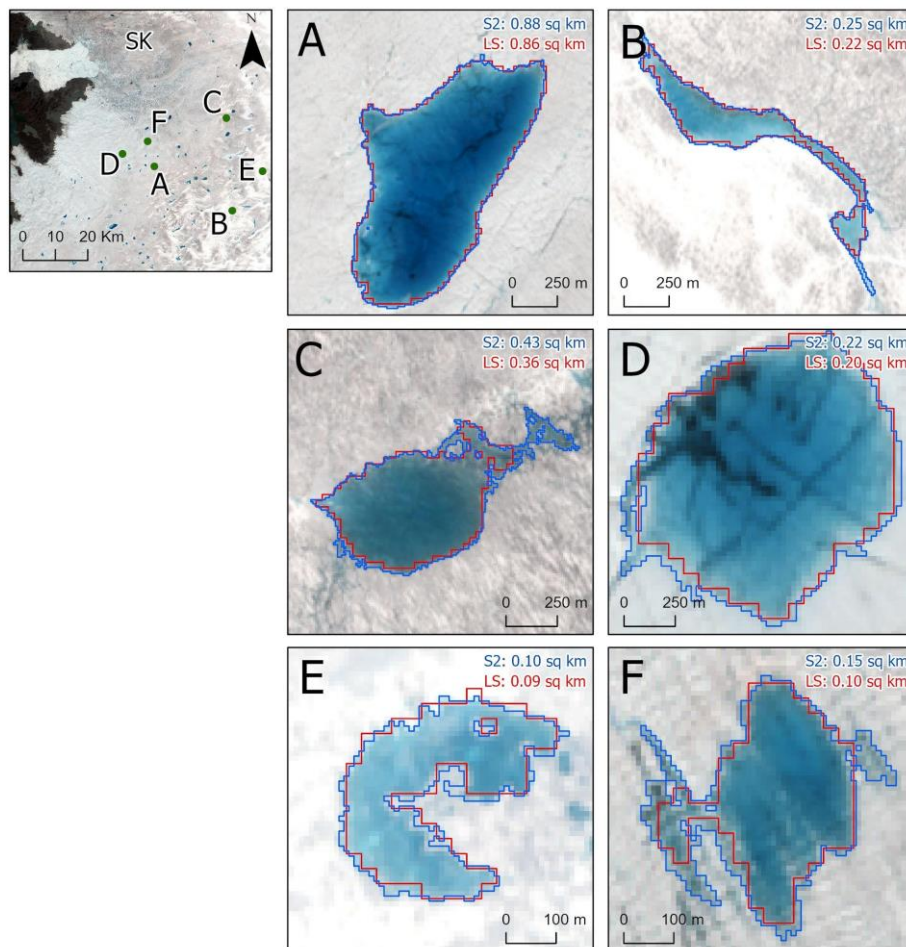
## 6.2 Validation procedure


The Landsat-8 scenes outlined in Table 6-1 were processed in the same manner as described for the SGL product – a dual threshold was applied to create binary rasters from NDWI images, which were subsequently vectorised and filtered using a DEM mask denoting sinks in the ice surface. This method is adopted from those provided by Yang and Smith (2013) and Yang (2019), modified for batch processing and specific file handling procedures compatible with the ESA CCI+ product specifications.

Statistics were generated from the resulting supraglacial water bodies, including lake abundance, total lake area and average lake area. These statistics were compared to those determined from the SGL product. Additionally, individual examples of supraglacial lakes were selected and compared to provide further insight into the sensor inter-comparison.

## 6.3 Validation procedure outcome

Generally, Sentinel-2 detected more lakes than Landsat-8, with an average difference of 34 lakes per time step. This is likely due to differing coverage due to scene cover and cloud cover but could also be linked to the difference in spatial resolution which is commonly observed in inter-comparison studies (Williamson et al., 2018).



	<p style="text-align: center;">Greenland_Ice_Sheet_cci+ Product Validation and Intercomparison Report (PVIR) for CCI+ Phase 1</p>	<p>Reference: ST-DTU-ESA-GISCCI+-PVIR-001 Version : 3.0 page Date : 05 May 2022 47/62</p>
---	---	---

**Figure 6-1: Selected lakes from the sensor inter-comparison analysis. Lakes are taken from the supraglacial lake datasets derived from Sentinel-2 and Landsat-8 scenes acquired on 08/06/2019. Zoom-ins of the Sentinel-2 subset (left) shown examples of lake delineation with unconstrained lake forms (A, D, F), intricate or constrained forms (B, E, F) and more challenging forms that include saturated snow (C).**

Comparison between the SGL and the Landsat-derived supraglacial water bodies indicate slight discrepancies in individual lake form, with an average difference in lake size of 0.03 km<sup>2</sup> (8%). This forms an RMSE of 0.159 km<sup>2</sup>. The examples in Fig. 6-1 demonstrate differences in form between supraglacial water bodies derived from Sentinel-2 and Landsat-8 imagery acquired 30/05/2019, with both closely corresponding delineations (e.g. A, D) and relatively poor delineations (e.g. C, F). Discrepancies in lake area appear to generally stem from the difference in spatial resolution, where lake areas are under-estimated from the 30-m resolution Landsat-8 imagery compared to the 10-m resolution Sentinel-2 imagery. This is especially evident when lake forms have intricate forms or include areas of saturated snow, which are not as distinguished in the Landsat-8 imagery (e.g. E and F).

## 6.4 Recommendations for products improvement

Overall, the sensor inter-comparison validation shows good correspondence between the SGL and lakes derived from Landsat-8 imagery, with an average difference in lake size of 0.03 km<sup>2</sup> (8%) and an RMSE of 0.159 km<sup>2</sup>. Selected examples demonstrate that this difference largely reflects the difference in spatial resolution between Sentinel-2 and Landsat-8.

A recommendation to improve the SGL in future work would be to detect supraglacial water bodies from both sensors, and other available optical imagery, to form a multi-sensor approach. By doing this, the temporal resolution of the SGL dataset could be improved, and coinciding scene acquisitions could be used to form a robust validation approach as demonstrated in this report.

Through undertaking this validation analysis, the processing chain for generating the SGL dataset was easily modified to incorporate the inclusion of Landsat-8 imagery alongside Sentinel-2, proving that this recommendation is an achievable goal that is already implemented in processing chains for future work.

## 7 Calving Front Location (CFL)

This chapter gives an overview of the activities carried out to assess the quality of the CFL products produced in CCN Option-2: "Enhancement of machine learning-based methodology for calving front line (CFL) detection". In this option shapefiles of the calving front location (CFL) were generated for selected Greenland outlet glaciers (Figure 7-1) based on a machine learning methodology using Sentinel-2 optical imagery acquired in August 2019 and 2020.

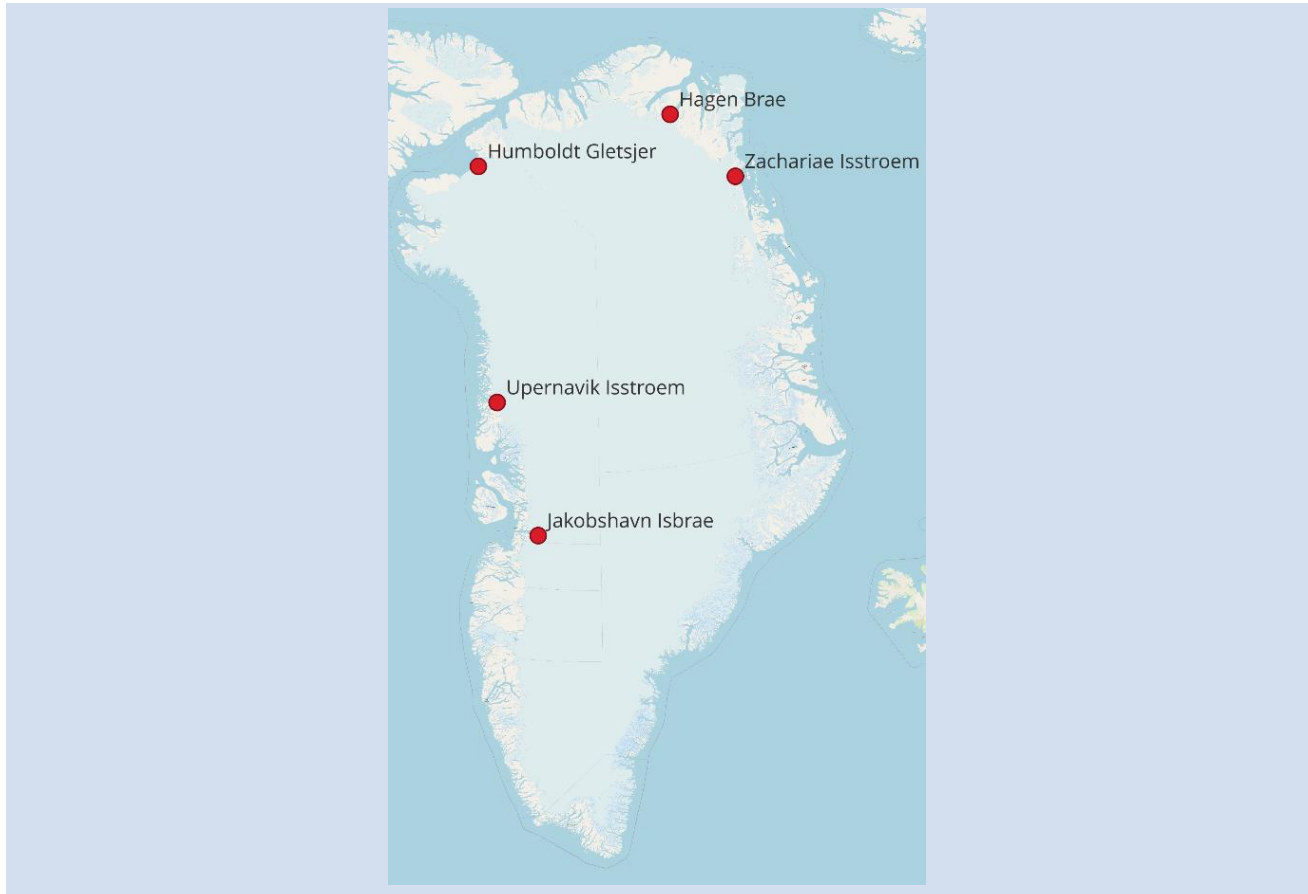


**Figure 7-1: Locations of the calving front locations mapped in CCN Option-2.**

### 7.1 Sources and selection of independent validation data

For quality assessment the generated CFLs were intercompared with CFLs that were manually delineated by an expert operator and based on the same source imagery (Sentinel-2). Therefore there is no difference in resolution or time-lag between the two data sets, ensuring the conditions and calving front position are the same. The Sentinel-2 data products used to delineate the CFLs are listed in Table 7-1. All products were acquired from the Copernicus Open Access Hub (<https://scihub.copernicus.eu/>). For CFL delineation Band 8 (NIR) was used which has a resolution of 10m.

**Table 7-1: Validation source imagery**


Glacier	Sentinel-2 Product	Date
Hagen Brae	S2B_MSIL1C_20190826T171859_N0208_R012_T25XEL_20190826T205126	2019/08/26

Hagen Brae	S2A_MSIL1C_20200801T173911_N0209_R098_T26XMR_20200801T211154	2020/08/01
Humboldt Gletsjer	S2A_MSIL1C_20190816T180921_N0208_R084_T20XMN_20190816T21444 6	2019/08/16
Humboldt Gletsjer	S2A_MSIL1C_20190816T180921_N0208_R084_T20XMP_20190816T214446	2019/08/16
Humboldt Gletsjer	S2B_MSIL1C_20200815T180919_N0209_R084_T20XMN_20200815T20184 2	2020/08/15
Humboldt Gletsjer	S2B_MSIL1C_20200815T180919_N0209_R084_T20XMP_20200815T201842	2020/08/15
Jakobshavn Isbrae	S2A_MSIL1C_20190802T150921_N0208_R025_T22WEB_20190802T170710	2019/08/02
Jakobshavn Isbrae	S2A_MSIL1C_20200816T150921_N0209_R025_T22WEB_20200816T171850	2019/08/02
Upernavik-A/E/F	S2B_MSIL1C_20190802T155829_N0208_R097_T21XWB_20190802T193545	2019/08/02
Upernavik-A/E/F	S2A_MSIL1C_20200801T155911_N0209_R097_T21XWB_20200801T19211 8	2019/08/01
Zachariae Isstroem	S2B_MSIL1C_20190820T151809_N0208_R068_T27XWH_20190820T18560 5	2019/08/20
Zachariae Isstroem	S2B_MSIL1C_20190820T151809_N0208_R068_T27XVH_20190820T185605	2019/08/20
Zachariae Isstroem	S2B_MSIL1C_20200824T151809_N0209_R068_T27XWH_20200824T18443 3	2020/08/24
Zachariae Isstroem	S2B_MSIL1C_20200824T151809_N0209_R068_T27XVH_20200824T184433	2020/08/24

## 7.2 Validation procedure

The validation procedure is based on the procedure developed for CFL validation in Greenland Ice Sheet CCI (AD4) and involves several steps that were performed for each of the (14) generated CFL products:

- 1) Manual delineation of CFL using same Sentinel-2 source data (no time lag). The delineation was done in QGIS in the native map projection of the Sentinel-2 image and CFL product (local UTM zone) by an expert operator.
- 2) The distance from the CFL to the nearest point of the validation dataset was measured every 5 m across the entire length of the calving front ( $D_n$ ).
- 3) Next, the following statistics are calculated and reported based on  $D_n$ :
  - Mean: Mean Distance [m]
  - RMSE: Root Mean Square Error [m]
  - Std: Standard Deviation [m]
  - Med: Median Distance [m]
  - Mad: Mean Absolute Deviation [m]
  - Fr100: Fraction of distances within 100 m band [-]
  - n: Sample Size [#]
- 4) In addition, the following figures are generated:
  - CFL map showing both lines and distances

	<p style="text-align: center;">Greenland_Ice_Sheet_cci+ Product Validation and Intercomparison Report (PVIR) for CCI+ Phase 1</p>	<p>Reference: ST-DTU-ESA-GISCCI+-PVIR-001 Version : 3.0 page Date : 05 May 2022 50/62</p>
---	---	---

- Distance profile along the ice front (100m band indicated)
- Histogram

### 7.3 Validation procedure outcome

This section provides the generated figures (CFL location maps, distance profiles and histograms) for each glacier separately, followed by an overview of the calculated statistics and a summary of the validation procedure outcome.



### 7.3.1 Hagen Brae

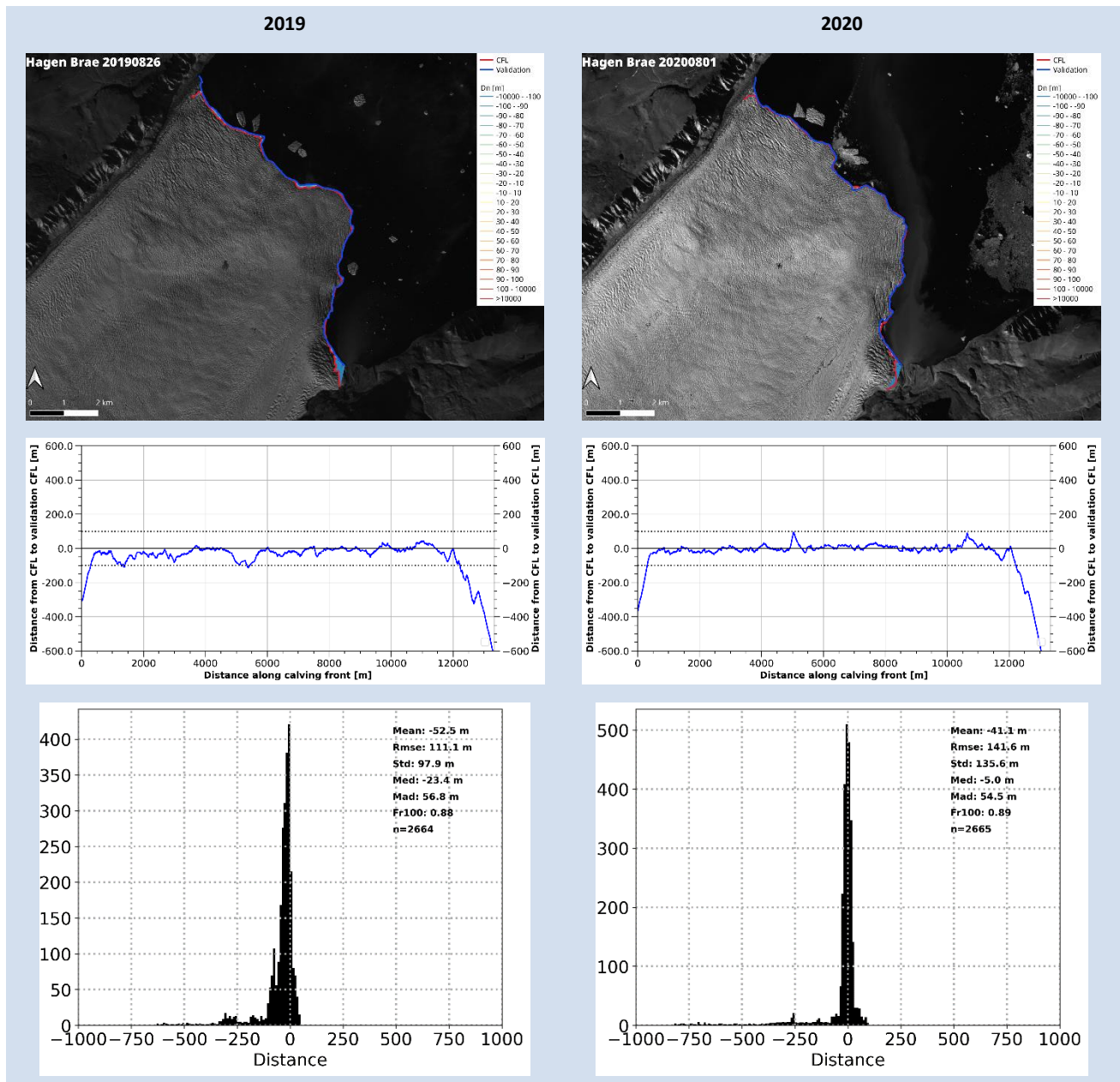


Figure 7-2: For 2019 (left column) and 2020 (right column): (top) Sentinel-2 image of Hagen Brae showing the CFL (red) and validation CFL (blue) and distances ( $D_n$ ); (middle) graph showing the distance between both CFL and validation data set along the length of the calving front. Positive distances indicate the ice front is more advanced than the validation dataset, negative distance vice versa; (bottom) histogram of  $D_n$ .

### 7.3.2 Humboldt Gletsjer

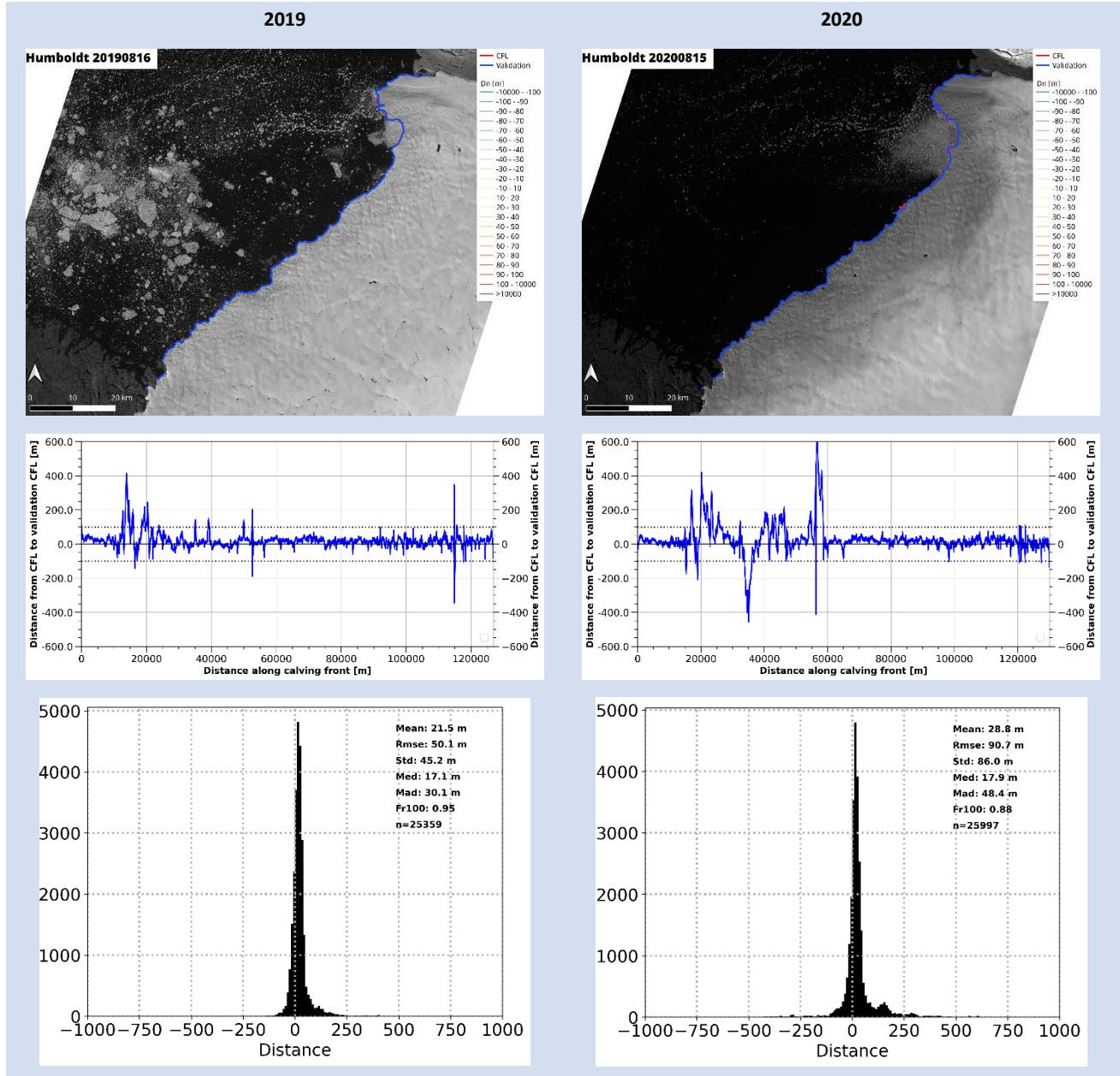


Figure 7-3: For 2019 (left column) and 2020 (right column): (top) Sentinel-2 image of Hagen Brae showing the CFL (red) and validation CFL (blue) and distances ( $D_n$ ); (middle) graph showing the distance between both CFL and validation data set along the length of the calving front. Positive distances indicate the ice front is more advanced than the validation dataset, negative distance vice versa; (bottom) histogram of  $D_n$

### 7.3.3 Jakobshavn Isbrae

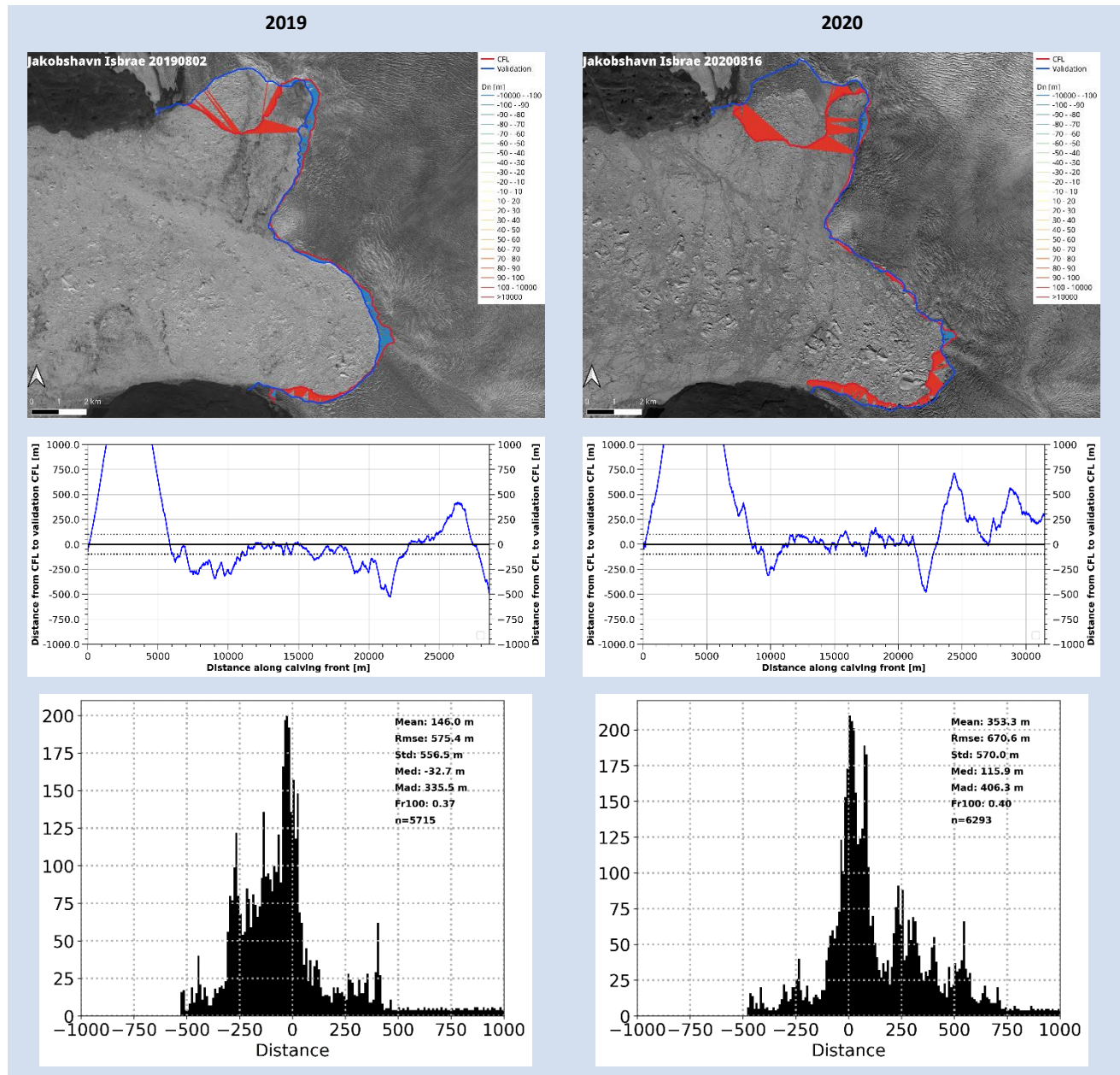


Figure 7-4: For 2019 (left column) and 2020 (right column): (top) Sentinel-2 image of Hagen Brae showing the CFL (red) and validation CFL (blue) and distances ( $D_n$ ); (middle) graph showing the distance between both CFL and validation data set along the length of the calving front. Positive distances indicate the ice front is more advanced than the validation dataset, negative distance vice versa; (bottom) histogram of  $D_n$



### 7.3.4 Upernavik A

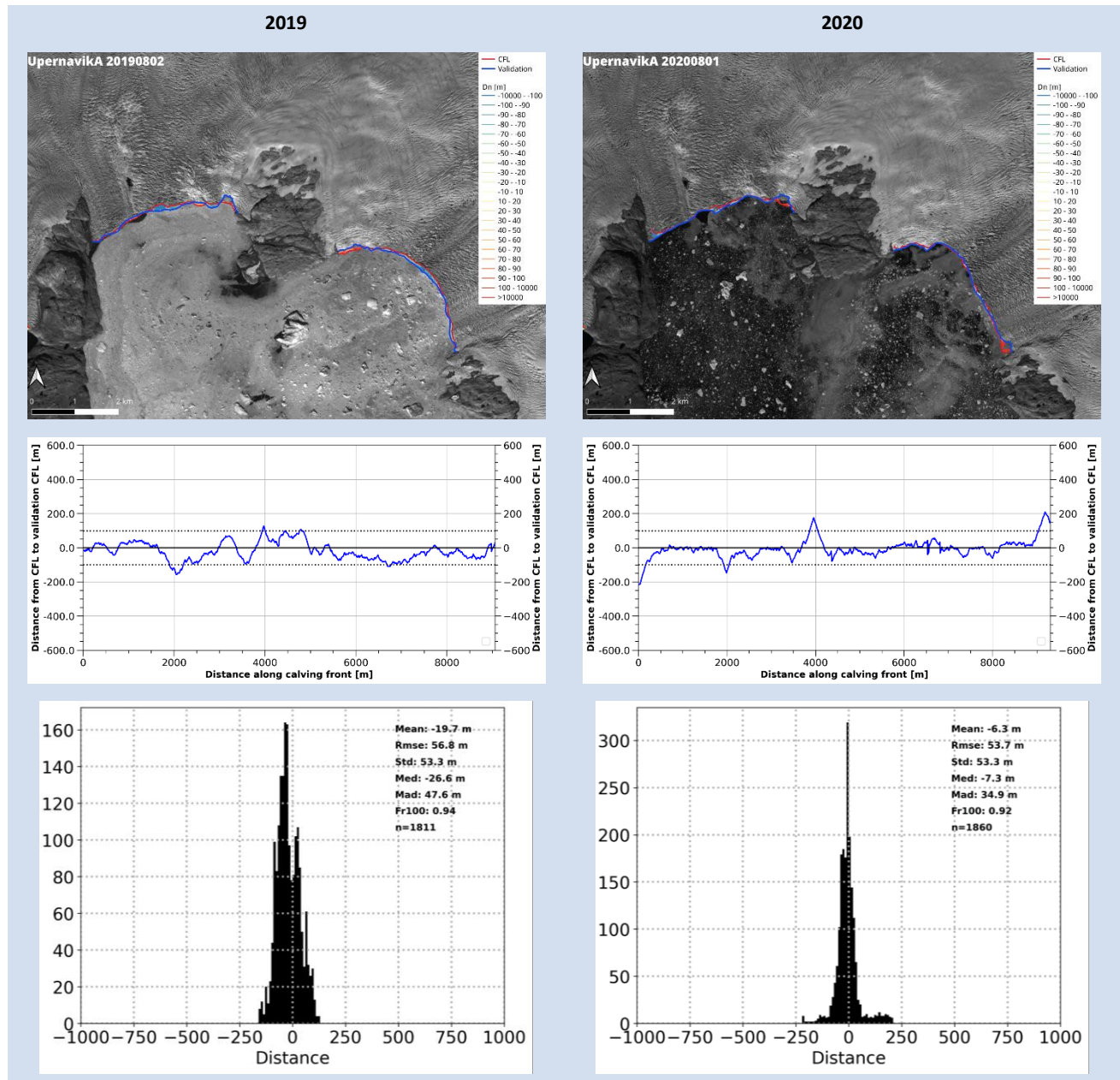


Figure 7-5: For 2019 (left column) and 2020 (right column): (top) Sentinel-2 image of Hagen Brae showing the CFL (red) and validation CFL (blue) and distances ( $D_n$ ); (middle) graph showing the distance between both CFL and validation data set along the length of the calving front. Positive distances indicate the ice front is more advanced than the validation dataset, negative distance vice versa; (bottom) histogram of  $D_n$

### 7.3.5 Upernavik E

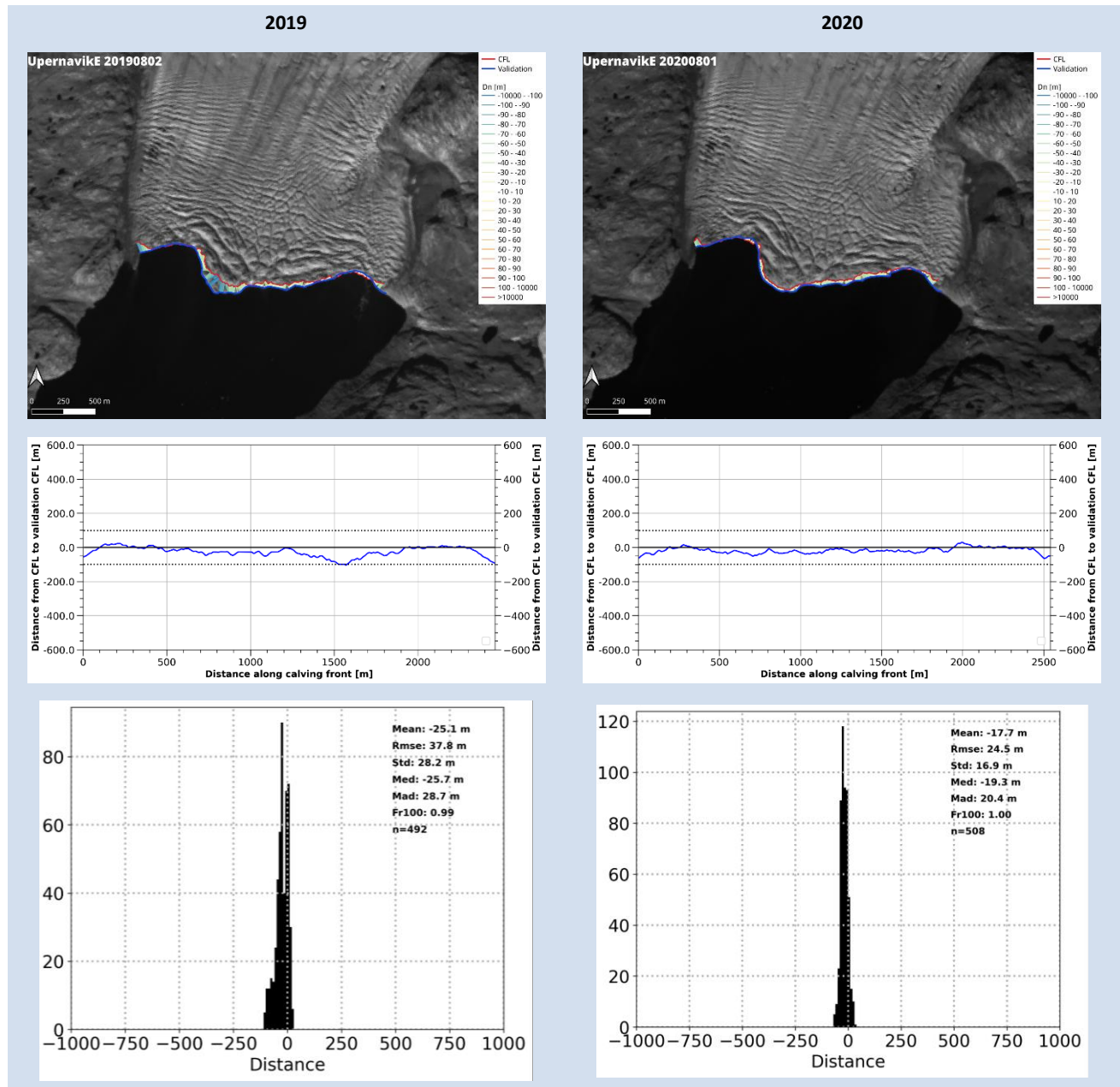


Figure 7-6: For 2019 (left column) and 2020 (right column): (top) Sentinel-2 image of Hagen Brae showing the CFL (red) and validation CFL (blue) and distances ( $D_n$ ); (middle) graph showing the distance between both CFL and validation data set along the length of the calving front. Positive distances indicate the ice front is more advanced than the validation dataset, negative distance vice versa; (bottom) histogram of  $D_n$



### 7.3.6 Upernavik F

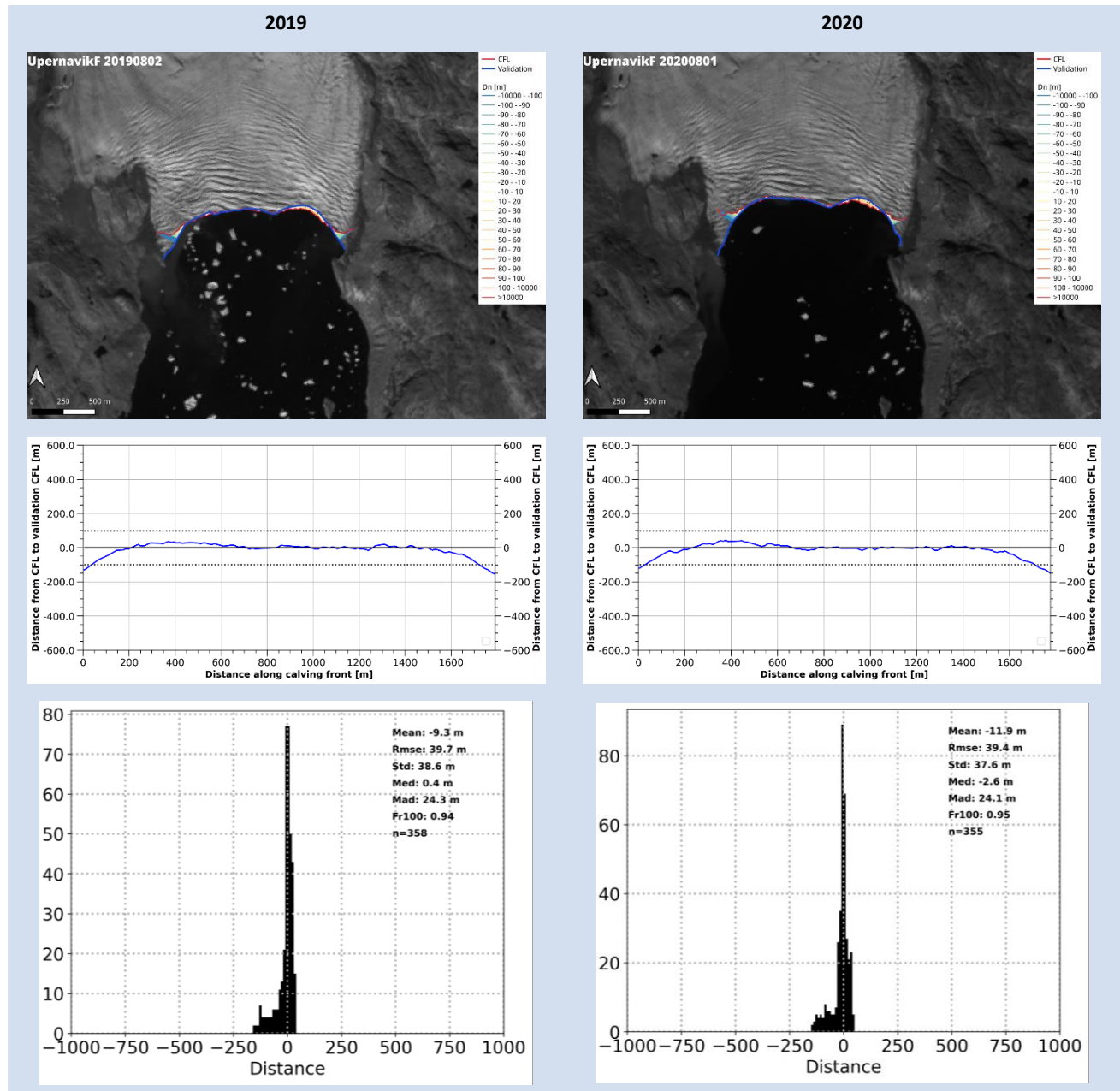


Figure 7-7: For 2019 (left column) and 2020 (right column): (top) Sentinel-2 image of Hagen Brae showing the CFL (red) and validation CFL (blue) and distances ( $D_n$ ); (middle) graph showing the distance between both CFL and validation data set along the length of the calving front. Positive distances indicate the ice front is more advanced than the validation dataset, negative distance vice versa; (bottom) histogram of  $D_n$

### 7.3.7 Zachariae Isstroem

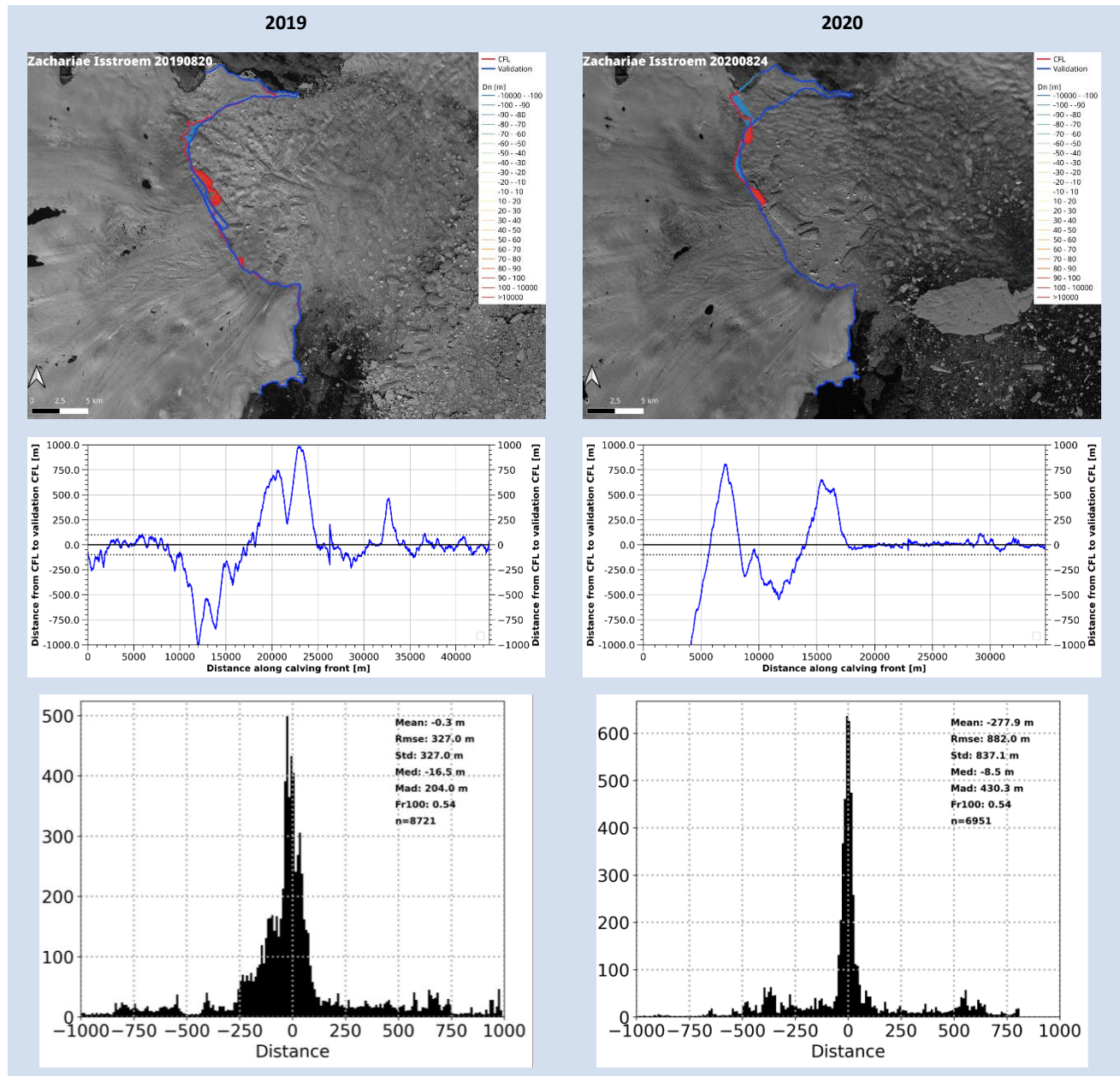


Figure 7-8: For 2019 (left column) and 2020 (right column): (top) Sentinel-2 image of Hagen Brae showing the CFL (red) and validation CFL (blue) and distances ( $D_n$ ); (middle) graph showing the distance between both CFL and validation data set along the length of the calving front. Positive distances indicate the ice front is more advanced than the validation dataset, negative distance vice versa; (bottom) histogram of  $D_n$


### 7.3.8 Overview and summary

Table 7-2 provides an overview of the calculated statistics for each of the assessed CFLs. The ensemble of figures and statistics clearly indicate that the CFLs for Jakobshavn Isbrae and Zachariae Isstroem clearly stand out in terms of agreement, with relatively large mean and absolute deviations and RMSEs. The fraction of the calving front that falls within a 100-m band is for Jakobshavn Isbrae 0.37 for 2019 and 0.40 for 2020, for Zachariae Isstroem this number is 0.54 for both 2019 and 2020. For both glaciers there are several factors that complicate the identification of the calving front. The fjord in front of Jakobshavn Isbræ has a very dense and coarse chaotic ice melange in direct contact with the terminus. This causes, in particular for the northern section very large differences with the validation data set. The fjord in front of Zachariae Isstroem is also characterised by an ice melange with many large floating ice bergs. In 2019 large ice bergs are about to calve at the ice front, showing long and narrow rifts running parallel to the ice front. However, close investigation shows that these parts are still connected with the main glacier through narrow ice bridges. The algorithm is not capable of capturing these features, thus explaining the large differences between the CFL and validation data set. In 2020, the northern section also shows large differences, the likely explanation being that this section is partly obscured by a veil of clouds in the image.

Much better agreement is found for the CFLs of the other glaciers: Humboldt, Hagen Brae and Upernavik-A, E and F. The mean absolute deviations between the CFLs and validation data sets are in the order of 20-55 m and the fraction of measured distances falling within the 100-m band are much higher (0.88 to 1.00). For these glaciers the ice front is generally well pronounced, with only little to no ice melange in front of the outlet glaciers, making the boundary between open water and glacier ice relatively easy to distinguish. In most cases the largest differences are found at the glacier margins, with better agreement in the central parts. The largest differences for the long ice front (>125 km) of Humboldt Gletsjer, visible in the distance profiles, coincide with the most active part of the glacier, which does have an ice melange with many ice bergs, that are sometimes still connected, in front of it.

**Table 7-2: Overview of statistics for CFL quality assessment.**

<i>Glacier</i>	<i>CFL date</i>	<i>n</i>	<i>Mean</i>	<i>RMSE</i>	<i>Std</i>	<i>Med</i>	<i>Mad</i>	<i>Fr100</i>
Jakobshavn Isbrae	20190802	5715	146.0	575.4	556.5	-32.7	335.5	0.37
Jakobshavn Isbrae	20200816	6293	353.3	670.6	570.0	115.9	406.3	0.40
Humboldt Gletsjer	20190816	25359	21.5	50.1	45.2	17.1	30.1	0.95
Humboldt Gletsjer	20200815	25997	28.8	90.7	86.0	17.9	48.4	0.88
Hagen Brae	20190826	2664	-52.5	111.1	97.9	-23.4	56.8	0.88
Hagen Brae	20200801	2665	-41.1	141.6	135.6	-5.0	54.5	0.89
Upernavik A	20190802	1811	-19.7	56.8	53.3	-26.6	47.6	0.94
Upernavik A	20200801	1860	-6.3	53.7	53.3	-7.3	34.9	0.92
Upernavik E	20190802	492	-25.1	37.8	28.2	-25.7	28.7	0.99
Upernavik E	20200801	508	-17.7	24.5	16.9	-19.3	20.4	1.00
Upernavik F	20190802	358	-9.3	39.7	38.6	0.4	24.3	0.94
Upernavik F	20200801	355	-11.9	39.4	37.6	-2.6	24.1	0.95

	<p style="text-align: center;">Greenland_Ice_Sheet_cci+ Product Validation and Intercomparison Report (PVIR) for CCI+ Phase 1</p>	<p>Reference: ST-DTU-ESA-GISCCI+-PVIR-001 Version : 3.0 page Date : 05 May 2022 59/62</p>
---	---	---

Zachariae Isstroem	20190820	8721	-0.3	327.0	327.0	-16.5	204.0	0.54
Zachariae Isstroem	20200824	6951	-277.9	882.0	837.1	-8.5	430.3	0.54

## 7.4 Recommendations for products improvement

The quality assessment described in this chapter has indicated stronger and weaker aspects of the currently implemented CFL detection algorithm. While the CFL detection performs generally good for well-defined calving fronts with no ice melange in front, it performs poorly for more complicated cases. Future development should therefore focus on CFL delineation for these cases, in particular for outlet glaciers with an ice melange at the ice front or which are (partly obscured) by a thin veil of clouds. A more extensive training data set for these types of conditions will therefore be required. It is further recommended to focus on improving the identification of the calving front at the glacier margins, where currently the largest discrepancies are found.

A strong aspect of machine-learning based approaches, is the ability to replace time-consuming manual delineated fronts by automatically extracting dense glacier front time series. Future products should therefore further exploit the increasingly extensive archive and availability of satellite EO data and include more extensive calving front time series.



## 8 References

- Andrews, L. C. et al. (2018) Seasonal evolution of the subglacial hydrologic system modified by supraglacial lake drainage in Western Greenland. *Journal of Geophysical Research: Earth Surface* **123**, 1479-1496. 10.1029/2017JF004585
- Blair, B. and Hofton, M.: IceBridge LVIS L2 Geolocated Surface Elevation Product. Boulder, Colorado USA: NASA DAAC at the National Snow and Ice Data Center. <http://nsidc.org/data/docs/daac/icebridge/ilvis2/>, 2012.
- Brenner, A. C., Bindschadler, R. A., Thomas, R. H. and Zwally, H. J.: Slope-induced errors in radar altimetry over continental ice sheets, *J. Geophys. Res. - Oceans*, vol. 88, no.C3, pp. 1617–1623, 1983.
- Das, S.B. et al. (2008) Fracture propagation to the base of the Greenland Ice Sheet during supraglacial lake drainage. *Science* **320**, 778-781. 10.1126/science.1153360
- Fausto, R.S. and van As, D. 2019. Programme for monitoring of the Greenland ice sheet (PROMICE): Automatic weather station data. Version: v03, Dataset published via Geological Survey of Denmark and Greenland. doi: <https://doi.org/10.22008/promice/data/aws>
- Fausto, R. S., van As, D., Mankoff, K. D., Vandecrux, B., Citterio, M., Ahlstrøm, A. P., Andersen, S. B., Colgan, W., Karlsson, N. B., Kjeldsen, K. K., Korsgaard, N. J., Larsen, S. H., Nielsen, S., Pedersen, A. Ø., Shields, C. L., Solgaard, A. M., and Box, J. E.: Programme for Monitoring of the Greenland Ice Sheet (PROMICE) automatic weather station data, *Earth Syst. Sci. Data*, 13, 3819–3845, <https://doi.org/10.5194/essd-13-3819-2021>, 2021.
- Forsberg, R., Sørensen, L. & Simonsen, S: Greenland and Antarctica Ice Sheet Mass Changes and Effects on Global Sea Level. *Surveys in Geophysics* (2017) 38: 89. doi:10.1007/s10712-016-9398-7
- Geological Survey of Denmark and Greenland: PROMICE, Programme for Monitoring of the Greenland Ice Sheet. <http://www.promice.org/home.html>, 2015.
- Groh, A.; Horwath, M.; Horwath, A.; Meister, R.; Sørensen, L.S.; Barletta, V.R.; Forsberg, R.; Wouters, B.; Ditmar, P.; Ran, J.; Klees, R.; Su, X.; Shang, K.; Guo, J.; Shum, C.K.; Schrama, E.; Shepherd, A. Evaluating GRACE Mass Change Time Series for the Antarctic and Greenland Ice Sheet—Methods and Results. *Geosciences* (2019), 9, 415. doi:10.3390/geosciences9100415.
- Hoffman, M.J. et al. (2011) Links between acceleration, melting, and supraglacial lake drainage of the western Greenland Ice Sheet. *Journal of Geophysical Research: Earth Surface* **116**, F4, F04035. 10.1029/2010JF001934
- Hvidberg, C.S., et al., User Requirements Document for the Ice\_Sheets\_cci project of ESA's Climate Change Initiative, version 1.5, 03 Aug 2012. Available from: <http://www.esa-icesheets-cci.org/>
- Hvidberg, C. S., Grinsted, A., Dahl-Jensen, D., Khan, S. A., Kusk, A., Andersen, J. K., Neckel, N., Solgaard, A., Karlsson, N. B., Kjær, H. A., and Vallenga, P., "Surface velocity of the Northeast Greenland Ice Stream (NEGIS): assessment of interior velocities derived from satellite data by GPS", *The Cryosphere*, 14, 3487–3502, <https://doi.org/10.5194/tc-14-3487-2020>, 2020.
- Joughin, I. 2002. Ice-sheet velocity mapping: a combined interferometric and speckle-tracking approach. *Annals of Glaciology*, 34, 195–201. <https://doi.org/10.3189/172756402781817978>
- Joughin, I., B. Smith, I. Howat, and T. Scambos. 2015, updated 2018. MEaSUREs Greenland Ice Sheet Velocity Map from InSAR Data, Version 2. [Indicate subset used]. Boulder, Colorado USA. NASA National Snow and Ice Data Center Distributed Active Archive Center. doi: <https://doi.org/10.5067/OC7B04ZM9G6Q> [Date Accessed: Date accessed: August 2020]
- Joughin, I., I. Howat, B. Smith, and T. Scambos. 2020. MEaSUREs Greenland Ice Velocity: Selected Glacier Site Velocity Maps from InSAR, Version 3. [Indicate subset used]. Boulder, Colorado USA. NASA National Snow and Ice Data Center Distributed Active Archive Center. doi: <https://doi.org/10.5067/YXMJRM5OUNC> [Date accessed: August 2020]



- Khvorostovsky, K.: Merging and analysis of elevation time series over Greenland ice sheet from satellite radar altimetry, *IEEE Trans. Geosc. Remote Sens.*, 50, 1:23–36. doi: 10.1109/TGRS.2011.2160071, 2012.
- King, Michalea D., Howat, Ian M., Jeong, Seongsu, Noh, Myoung J., Wouters, Bert, Noël, Brice, van den Broeke, Michiel R.: Seasonal to decadal variability in ice discharge from the Greenland Ice Sheet, *The Cryosphere* 12(12), Copernicus GmbH, 3813–3825, 12 2018
- King, Michalea D., Howat, Ian M., Candela, Salvatore G., Noh, Myoung J., Jeong, Seongsu, Noël, Brice P. Y., van den Broeke, Michiel R., Wouters, Bert, Negrete, Adelaide: Dynamic ice loss from the Greenland Ice Sheet driven by sustained glacier retreat, *Communications Earth & Environment* 1(1), Springer Science and Business Media LLC, 8 2020
- Krabill, W. B.: IceBridge Level-4 ATM Surface Elevation Rate of Change. Boulder, Colorado USA: NASA DAAC at the National Snow and Ice Data Center. <http://nsidc.org/data/idhdt4.html>, 2014.
- Krabill, W. B.: IceBridge ATM L1B Elevation and Return Strength. Boulder, Colorado USA: NASA DAAC at the National Snow and Ice Data Center. <http://nsidc.org/data/ilatm1b.html>, 2010.
- Krabill, W. B., Abdalati, W., Frederick, E., Manizade, S., Martin, C., Sonntag, J., Swift, R., Thomas, R. and J. Yungel, J.: Aircraft laser altimetry measurement of elevation changes of the Greenland Ice Sheet: technique and accuracy assessment, *J. Geodyn.*, 34:357–376. doi: 10.1016/S0264-3707(02)00040-6, 2002.
- Legresy, B., Papa, F., Remy, F., Vinay, G., van den Bosch, M. and Zanife, O.-Z.: ENVISAT radar altimeter measurements over continental surfaces and ice caps using the ICE-2 retracking algorithm, *Remote Sens. Environ.*, 95(2):150–163. doi: 10.1016/j.rse.2004.11.018, 2005.
- Liang, Y.-L. et al. (2012) A decadal investigation of supraglacial lakes in West Greenland using a fully automatic detection and tracking algorithm. *Remote Sensing of Environment* **123**, 127–138. doi: 10.1016/j.rse.2012.03.020
- McMillan, M., Muir, A., Shepherd, A., Escolà, R., Roca, M., Aublanc, J., Thibaut, P., Restano, M., Ambrozio, A., and Benveniste, J.: Sentinel-3 Delay-Doppler altimetry over Antarctica, *The Cryosphere*, 13, 709–722, <https://doi.org/10.5194/tc-13-709-2019>, 2019.
- Mankoff, Kenneth D., Solgaard, Anne, Colgan, William, Ahlstrøm, Andreas P., Khan, Shfaqat Abbas, Fausto, Robert S.: Greenland Ice Sheet solid ice discharge from 1986 through March 2020, *Earth System Science Data* 12(2), Copernicus GmbH, 1367–1383, 6 2020
- Mouginot, Jérémie, Rignot, Eric, Bjørk, Anders A., van den Broeke, Michiel, Millan, Romain, Morlighem, Mathieu, Noël, Brice, Scheuchl, Bernd, Wood, Michael: Forty-six years of Greenland Ice Sheet mass balance from 1972 to 2018, *Proceedings of the National Academy of Sciences*, *Proceedings of the National Academy of Sciences*, 201904242, 4 2019
- Rastner, P., Bolch, T., Mölg, N., Machguth, H., Le Bris, R., Paul, F. 2012, updated 2018. The first complete inventory of the local glaciers and ice caps on Greenland. *The Cryosphere*, 6, 1483–1495. doi:10.5194/tc-6-1483-2012
- Roemer, S., Legresy, B., Horwath, M., and Dietrich, R.: Refined analysis of radar altimetry data applied to the region of the subglacial Lake Vostok/Antarctica, *Remote Sens. Environ.*, vol. 106, no. 3, pp. 269–284, 2007.
- Rowley, N.A. & Fegyveresi, J.M. (2019) Generating a supraglacial melt-lake inventory near Jakobshavn, West Greenland, using a new semi-automated lake-mapping technique. *Polar Geography* **42:2**, 89–108. doi: 10.1080/1088937X.2019.1578289
- Shepherd, A., Ivins, E. R., Geruo, A., Barletta, V. R., Bentley, M. J., Bettadpur, S., ... & Horwath, M. (2012). A reconciled estimate of ice-sheet mass balance. *Science*, 338(6111), 1183–1189.
- Shepherd, A., Ivins, E., Rignot, E. et al. Mass balance of the Antarctic Ice Sheet from 1992 to 2017. *Nature* 558, 219–222 (2018). <https://doi.org/10.1038/s41586-018-0179-y>

Shepherd, A., Ivins, E., Rignot, E. et al. Mass balance of the Greenland Ice Sheet from 1992 to 2018. *Nature* 579, 233–239 (2020). <https://doi.org/10.1038/s41586-019-1855-2>

Simonsen, S. B. and Sørensen, L. S. (2017): Implications of changing scattering properties on Greenland ice sheet volume change from Cryosat-2 altimetry. *Remote Sensing of Environment*, 190, p. 207-216, 2017.

Skourup, H., Barletta, V., Einarsson, I., Forsberg, R., Haas, C., Helm, V., Hendricks, S., Hvidegaard, S. M., and Sørensen, L. S.: ESA CryoVEx 2011: Airborne field campaign with ASIRAS radar, EM induction sounder and laser scanner. DTU Space, National Space Institute, Technical University of Denmark, 1st edition, 2011.

Slater T., A. Shepherd, M. Mcmillan, T. W. K. Armitage, I. Ootosaka and R. J. Arthern, "Compensating Changes in the Penetration Depth of Pulse-Limited Radar Altimetry Over the Greenland Ice Sheet," in *IEEE Transactions on Geoscience and Remote Sensing*, vol. 57, no. 12, pp. 9633-9642, Dec. 2019, doi: 10.1109/TGRS.2019.2928232.

Sørensen, L. S., Simonsen, S. B., Forsberg, R., Stenseng, L., Skourup, H., Kristensen, S. S., & Colgan, W. (2017). Circum-Greenland, ice-thickness measurements collected during PROMICE airborne surveys in 2007, 2011 and 2015. *Geological Survey of Denmark and Greenland Bulletin*, 79-82.

Williamson, A.G. et al. (2017) A Fully Automated Supraglacial lake area and volume Tracking ("FAST") algorithm: Development and application using MODIS imagery of West Greenland. *Remote Sensing of Environment* **196**, 113-133. 10.1016/j.rse.2017.04.032

Yang, K. & Smith, L. (2013) Supraglacial streams on the Greenland Ice Sheet delineated from combined spectral-shape information in high-resolution satellite imagery. *IEEE Geosci. Remote Sens. Lett.*, 10 (4), 801- 805.

Yang, K. (2019) Supraglacial river and lake analysis [software]. *figshare*. 10.6084/m9.figshare.9758051.v1.

Zwally, H. Jay, Giovinetto, Mario B., Beckley, Matthew A., Saba, Jack L.: Antarctic and Greenland Drainage Systems, 2012, GSFC Cryospheric Sciences Laboratory